UNIVERSITY OF CALIFORNIA, SAN DIEGO

The Role of CAMSAPs and Non-Centrosomal Microtubules in Tissue Injury Response in *Caenorhabditis elegans*

A dissertation submitted in partial satisfaction of the requirements for the degree Doctor of Philosophy

in

Biology

by

Marian Chuang

Committee in charge:

Professor Andrew Duncan Chisholm, Chair
Professor Shelley Halpain
Professor Karen Oegema
Professor Emily Troemel
Professor James Wilhelm

2016

The Dissertation of Marian Chuang is approved, and it is acceptable in quality and form for publication on microfilm and electronically:

Chair

University of California, San Diego

2016

TABLE OF CONTENTS

LIST OF TABLES

LIST OF FIGURES

LIST OF SUPPLEMENTAL FILES

All movies are in Quicktime format, played back at 33 fps (8x). Time stamps are mm::ss::msec. Scales, 10 μm.

Movie S1. EBP-GFP dynamics in adult lateral epidermis (P*col-19*).

Movie S2. EBP-GFP dynamics in adult dorsoventral epidermis.

Movie S3. EBP-GFP dynamics in adult lateral epidermis, *dapk-1(ju4)* background.

Movie S4. EBP-GFP dynamics in adult dorsoventral epidermis, *dapk-1(ju4)* background.

Movie S5. GFP::DAPK-1 dynamics in larval epidermis. Lateral seam cells are in the center of the movie.

Movie S6. GFP::DAPK-1 dynamics in adult lateral epidermis. Lateral seam in center.

Movie S7. GFP::DAPK-1 dynamics in adult dorsoventral epidermis. Dorsal midline is at bottom of movie.

Movie S8. P*dpy-7*-GFP::RAB-5 dynamics.

ACKNOWLEDGEMENTS

I would like to acknowledge Professor Andrew D. Chisholm for his guidance and support as a mentor. He has helped me become a better scientist. I thank my thesis committee members for their advice and support. I am grateful to all past and present members of the Jin and Chisholm labs, who have contributed to the friendly, collaborative, and stimulating environment, and helped me grow intellectually and emotionally over the last several years—arduous years that yet disappeared in the blink of an eye. Lastly, I want to thank, first, my parents and brother, and second, my new family—my husband and my beautiful baby.

Chapter 2 is a reformatted reprint in full of Chuang M and Chisholm A. Insights into the functions of the death associated protein kinases from C. elegans and other invertebrates. *Apoptosis*. 2014 Feb;19(2):392-7 with permission of all authors. The dissertation author was the primary author of this paper.

Chapter 3 is a reformatted reprint in full of Chuang M, Goncharov A, Wang S, Oegema K, Jin Y, Chisholm AD. The microtubule minus-end-binding protein Patronin/PTRN-1 is required for axon regeneration in *C. elegans. Cell Reports.* Volume 9, Issue 3, p874–883, 6 November 2014. The dissertation author was the primary researcher and author of this paper.

Chapter 4, in part, has been submitted for publication of the material as it may appear in eLife, 2016, Chuang M, Hsiao, TI, Tong A, Xu S, Chisholm AD. DAPK interacts with Patronin and the microtubule cytoskeleton in epidermal development and

wound repair. The dissertation author was the primary researcher and author of this paper.

VITA

2010	Bachelor of Arts in Molecular and Cellular Biology, University of California, Berkeley
2009-2011	Research Assistant for Dr. David A. Weisblat, University of California, Berkeley
2012-2016	Research Assistant for Dr. Andrew D. Chisholm, University of California, San Diego
2016	Doctor of Philosophy in Biology, University of California, San Diego

PUBLICATIONS

1. Chuang, M., Chisholm, A.D. (2014). Insights into the functions of the death associated protein kinases from C. elegans and other invertebrates. Apoptosis 19, 392-7.

2. Chuang, M., Goncharov, A., Wang, S., Oegema, K., Jin, Y., Chisholm, A.D. (2014). The microtubule minus-end-binding protein patronin/PTRN-1is required for axon regeneration in C. elegans. Cell Rep. 9, 874-83.

3. Chen, L., Chuang, M., Koorman, T., Boxem, M., Jin, Y., Chisholm, A.D. (2015). Axon injury triggers EFA-6 mediated destabilization of axonal microtubules via TACC and doublecortin like kinase. eLife. 4:e08695

4. Liu J., EMBS Member, Chuang, M., Chisholm, A.D., Cosman, P. Fellow, IEEE (2015) Image Registration Robust to Sparse Large Errors. Submitted as presentation/paper for 37th Annual International Conference of IEEE Engineering in Medicine and Biology Society. Milan, Italy.

5. Chuang, M., Hsiao, T.I., Tong, A., Xu, S., Chisholm, A.D. DAPK interacts with Patronin and the microtubule cytoskeleton in epidermal development and wound repair. eLife. (in revision)

ABSTRACT OF THE DISSERTATION

The Role of CAMSAPs and Non-Centrosomal Microtubules in Tissue Injury Response in *Caenorhabditis elegans*

by

Marian Chuang

Doctor of Philosophy in Biology

University of California, San Diego, 2016

Professor Andrew Duncan Chisholm, Chair

Microtubule (MT) arrays in mature polarized cells comprise mostly of non-centrosomal MTs; their regulation is poorly understood. Recently, the MT minus end binding proteins CAMSAPs have been shown to be important regulators of non-centrosomal microtubule organization and dynamics. In this dissertation I describe my work on the *C. elegans* member of the CAMSAP family, PTRN-1, and its roles in the injury responses of two types of tissues, the neurons and the epidermis. First, I found that PTRN-1 is required for axon regeneration. Though PTRN-1 is largely dispensable for normal neuronal development, its proper regulation of neuronal microtubule dynamics is

required for axons to regrow after injury. The second part of my work focuses on PTRN-1's role in epidermal development and wound response by regulating epidermal microtubule stability. Mutations in the gene death associated protein kinase 1 (DAPK1/*dapk-1)* results in both hyperactive innate immune response and enhanced wound closure in the epidermis. A genetic suppressor screen of the *dapk-1* mutant identified PTRN-1 as a key player in *dapk-1* mediated wound phenotypes. Further work uncovered DAPK-1 as a potential novel regulator of PTRN-1's function in epidermal MT architecture and dynamics. My thesis work reveals new in vivo roles of PTRN-1 in regulating non-centrosomal MTs for normal tissue damage response.

Chapter 1

Introduction Part One:

Non-centrosomal Microtubules

1.1 Properties and Dynamics of Microtubules

Microtubules (MTs) are one of the main cytoskeletal components of the cell. They are polar polymers consisting of α and β tubulin heterodimer subunits, with β tubulin at the plus end, and α tubulin at the minus end. A unique property of MTs is their dynamic instability, defined as the abrupt switching between phases of rapid depolymerization and sudden renewed growth events, termed catastrophes and rescues, respectively (Mitchison and Kirschner, 1984). The dynamics of these filaments enables their well-known cellular functions, such as the building of highways crucial for directed motor-dependent intracellular trafficking, and forming the spindle apparatus during cell division.

Due to their polar structure, MT filaments exhibit a polarity in dynamics. MTs grown in vitro from purified tubulin are able to polymerize and depolymerize at both ends—however, the plus end undergoes dynamic instability much more frequently, while the minus end is more stable (Desai and Mitchison, 1997; Walker et al., 1988; Tran et al., 1997; Walker et al., 1989). The ends also differ in dynamics in a similar fashion in vivo

as in vitro, with the plus end displaying more dynamics compared to the minus end (Howard and Hyman, 2003). This difference is however more pronounced; MT minus ends in vivo are extremely stable in most types of cells (reviewed in Dammermann et al., 2003). Dynamics of the minus end in vivo have mostly been only observed upon MT severing or breakage, which results in depolymerization or stabilization of the newly formed minus end (Dammermann et al., 2003), and until 2010 the minus end had never been reported to undergo polymerization in vivo (Goodwin and Vale, 2010). This MT minus end stability is due to proteins, such as the γ-tubulin ring complex (γ-TuRC) (Kollman et al., 2011), and the more recently discovered CAMSAPs (see Section 1.4), which bind to the minus end and stabilize it by anchoring the end to a cellular structure and/or protecting it from depolymerizing enzymes (reviewed in Akhmanova and Hoogenraad, 2015). These proteins will be discussed in further detail in later sections. Regulation of the dynamics and orientation of MTs by various plus-end and minus-end binding proteins results in varying but distinctly organized MT arrays in different cell types, which we will describe next.

1.2 Centrosomal MT arrays

What are centrosomal MT arrays? Non-polarized, mitotic cells primarily contain centrosomal MT arrays, which consist of MTs that are nucleated by and attached to the centrosome. The centrosome is an organelle consisting of two centrioles and pericentriolar material, and is the main MT organizing center (MTOC) of these cells. During cell division, multiple MTs emanate radially plus-end out from two centrosomes

to form the mitotic spindle required for proper chromosomal segregation. In cells in interphase, only one centrosome and one associated radial MT array is present.

Formation of Centrosomal MTs**.** Centrosomal MT arrays are attached to the centrosome by the γ tubulin ring complex (γ-TuRC), which is composed of a ring of γ tubulin and γ tubulin complex proteins (GCPs). The γ tubulin ring binds to the α and β tubulin heterodimers, with the α tubulin at the end, and the GCP proteins anchor the γ-TuRC to the pericentriolar material components. The γ-TuRC in the centrosome then acts as a nucleating center, with MTs polymerizing outward from their plus ends (reviewed in Kollman et al., 2011, Oakley et al., 2015). The plus end then associates with various plus-end binding proteins, which regulate their localization and dynamics (reviewed in Akhmanova and Steinmetz, 2015). MTs which fail to attach to the centrosome depolymerize from their minus ends, so that only centrosomal MTs remain in the array.

1.3 Non-centrosomal MT arrays

In contrast to mitotic cells, non-radial, non-centrosomal MTs predominate in polarized, terminally differentiated cells (reviewed in Keating and Borisy, 1999). These non-centrosomal MTs are often oriented linearly in a polarized fashion. In addition, while MTs in dividing cells are very dynamic, MTs in differentiated cells are mostly stabilized (Bartolini and Gundersen, 2006). We will describe below the organization and function of non-centrosomal MT arrays in several different cell types (for more details, read review Bartolini and Gundersen, 2006 and book chapter Dyachuk et al., 2016).

Epithelial cells. Epithelial cells are polarized cells with apical and basal surfaces. In early cells, MTs are nucleated from the centrosome; later in development, centrosomes are inactivated and MTs detach, leaving few remaining centrosomal MTs. The newly formed non-centrosomal MTs become polarized, with their plus ends localizing at the basal surface, and minus ends at the apical surface (Mogensen et al., 1989; Meads and Schroer, 1995; Mogensen et al., 1993; Brodu et al., 2010). Polar non-centrosomal MT arrays have been shown to play many important roles in intracellular sorting and cellular organization. Disruption of MT array polarity leads to mis-sorting of apical and basal components (Musch, 2004; Rodriguez-Boulan et al., 2005). Non-centrosomal MTs have also been shown to be required for proper recycling of endosomes in HeLa cells (Chi et al., 2015; Delevoye et al., 2014), as well as nuclear positioning in vivo, in the *C. elegans* skin and intestine models (Wang et al., 2015; Feldman and Priess, 2012), reviewed in Quintin et al., 2016.

Neurons. Though centrosomal MTs do reside in the soma, the neuron contains primarily non-centrosomal MTs, located mostly in the axonal and dendritic processes, reviewed in Conde and Caceres, 2009, and in Kapitein and Hoogenraad, 2015. In the axons, MTs form uniformly oriented bundles, with the plus ends facing away from the soma (Heidemann et al., 1981). These bundles overlap each other all along the axon, serving as tracks for motor proteins to carry cargo between the cell body and the distal tip of the axon. The shorter, dendritic MTs, on the other hand, often display mixed polarity (Baas et al., 1988; Burton, 1988).

Muscle cells. Like early epithelial cells, myoblasts initially contain a centrosomal MT array (Tassin et al, 1985). After differentiating into multinucleate myotubes, the MT

array then becomes non-centrosomal. These MTs are orientated parallel to the long axis of the myotube. As the myotubes fuse into a larger syncytium, the centriolar material cluster around the nucleus, and in old myotubes, the centrosomes completely disappear (Tassin et al., 1985).

Plant cells. Plants entirely lack centrosomes or any distinct MTOC. However, plant cells contain linear MT arrays at the cortex, and these arrays can switch from transverse to a longitudinal orientation depending on the presence of blue light (Lindeboom et al., 2013).

Generation and regulation of non-centrosomal MT arrays. The formation and organization of both centrosomal and non-centrosomal MTs arrays are similar in three aspects: (1) γ-TuRC is required for MT nucleation (Petry and Vale, 2015) (2) After nucleation, free minus ends are capped and anchored by γ-TuRC or some other minus-end targeting proteins (-TIPs) (reviewed in Akhmanova and Hoogenraad, 2015) (3) Plus end dynamics are regulated by their binding to plus-end targeting proteins (+TIPs) (reviewed in Akhmanova and Steinmetz, 2010). However, non-centrosomal MTs differ from centrosomal MTs in aspects 1 and 2 in the types of MT-associated proteins involved and the cellular location where the nucleation or organization events occur.

Though summarized below, the reader can learn more about the generation of non-centrosomal MT networks from the review (Bartolini and Gundersen, 2006).

Formation. There are two main mechanisms underlying the formation of non-centrosomal MTs. By the first mechanism, non-centrosomal MTs are originally nucleated at the centrosome, but then are released by MT severing proteins. In hypocotyl cells, exposure to blue light triggers MT severing protein katanin to break cortical MTs to

produce a new MT array, which re-orients orthogonally to the original array to aid in bending of the hypocotyl towards the light source (Lindeboom et al., 2013). Katanin-mediated release of MTs nucleated at the centrosome is also seen in neurons (Yu et al., 1993) to promote axonal growth (Ahmad et al., 1999; Karabay et al., 2004; Yu et al., 2005). MT release has also been observed in epithelial cell lines (Keating et al., 1997).

The second mechanism for the production of non-centrosomal MTs is nucleation from non-centrosomal sites. As mentioned earlier, nucleation requires γ-TuRC, but the complex is not always localized to the centrosome—often, γ-tubulin and PCM re-localize away from the centrosome during the swap from centrosomal to noncentrosomal MT arrays in the cell (reviewed in Petry and Vale, 2015), though the mechanism of relocalization is unclear. Relocalization of γ-TuRC has been observed in various cell lines (reviewed in Petry and Vale, 2015), as well as in vivo, such as in the *C. elegans* epidermis, intestine, and germline (Feldman and Priess, 2012; Wang et al., 2015). In plants, γ-tuRC is recruited to pre-existing cortical MTs to nucleate new MTs (Murata et al., 2005). In dendrites of *Drosophila* sensory neurons, MTs are nucleated by γ-tuRC localized at the Golgi (Ori-McKenney et al., 2012). γ-tubulin dependent non-centrosomal MT nucleation has also been observed at the nuclear membrane (Bugnard et al., 2005; Stoppin et al., 1994; Seltzer et al., 2007), and in plants, from existing MTs at the cell cortex (Lindeboom et al., 2013). For more information on non-centrosomal MT nucleation, refer to review (Petry and Vale, 2015).

Organization. Once MTs are generated, either by nucleation or severing from existing MTs, they are assembled into a polarized linear array, sometimes in specific compartments of the cell. Some MTs are formed in the correct region of the cell in which

the array is to reside, such as the MTs nucleated at the Golgi in the dendrites of Drosophila sensory neurons (Ori-McKenney et al., 2012). Other MTs, such as axonal, which are traditionally thought to be generated in the soma, must be transported to the correct location before being incorporated into an array. Evidence shows that cytoplasmic dynein is required for the translocation of MTs from the soma into the axon (Ahmad et al., 1998; He et al., 2005), as well as kinesin motor proteins for developing neurites and dendrites (Sharp et al., 1997; Yu et al., 2000). More recently, kinesin-1 has been shown to mediate MT sliding in axons, and this sliding is important for initiating the formation of protrusions required for neurite outgrowth (Lu et al., 2013) and axon regeneration in *Drosophila* (Lu et al., 2015). Another method for repositioning MTs to proper sites is MT treadmilling. This seems to be the predominant mechanism in plants to move non-centrosomal MTs to the cortex (Shaw et al., 2003).

At the correct sites, MTs are then stabilized and assembled into specific arrays. The stabilization of MTs is achieved through several mechanisms at different parts of the MT filament. The plus ends of MTs are captured by various +TIPs, which are reviewed in Akhmanova and Steinmetz, 2010. In neurons, MTs are thought to be stabilized along their filaments and bundled by MAP2 and tau in dendrites and axons, respectively (Farah and Leclerc, 2008; Qiang et al., 2006). It is not entirely clear whether tau and MAP2 are definitive MT bundling proteins, since over-expression of many +TIPs and MAPs in general causes ectopic MT bundling. Extremely critical for MT stabilization is the stabilization of the minus end. Especially if non-centrosomal MTs are formed from centrosomal release, the newly generated free minus end must immediately be stabilized by –TIPs to prevent depolymerization of the entire filament. γ-TuRC plays such a role in

capping (reviewed in Petry and Vale, 2015), as well as the protein Ninein (Mogensen et al., 2000). Recently, a new family of MT minus end binding proteins, CAMSAPs, has been shown to stabilize non-centrosomal MT minus ends as well.

1.4 CAMSAPs

CAMSAPs, or Calmodulin And Spectrin Associated Proteins, are a family of MT minus end-associated proteins present in the Metazoan kingdom. The CAMSAP protein family is characterized by a unique CKK (CAMSAP1, KIAA1078 and KIAA1543) domain, which has the ability to bind directly along the length of the MT (Baines et al., 2009; Goodwin and Vale, 2010, Jiang et al., 2014; Yau et al., 2014; Wang et al., 2015). All homologs contain two other conserved regions: the Calponin Homology (CH) domain, and a region with three coiled-coil motifs (CC domain) (Akhmanova and Hoogenraad, 2015). Importantly, the family of CAMSAPs is the second group of proteins after γ-tubulin to bind directly to MT minus ends (Goodwin and Vale, 2010; Jiang et al., 2014).

Role of CAMSAPs in MT binding and stabilization. CAMSAPs have been shown to play a role in promoting MT stability in multiple in vitro and in vivo systems. The three mammalian homologs, CAMSAPs 1-3, all associate with MT minus ends, but have subtle differences in MT binding and the control of MT dynamics. CAMSAP1 only transiently binds to the minus ends, and tracks the growth of the minus ends, whereas CAMSAP2 and CAMSAP3 are stably localized as long stretches along the MT lattice from the minus end, preventing filament depolymerization (Yau et al., 2014; Hendershott

and Vale, 2014). In vitro laser microsurgery assays show that this deposition of CAMSAPs occurs only on growing MT minus ends, suggesting CAMSAPs bind to free MT minus-ends, uncapped by other factors (Yau et al., 2014). Depletions of CAMSAP2/CAMSAP3 strongly decreased the density of noncentrosomal MTs in cell culture, and led to rapid MT minus end depolymerization in laser MT severing assays, suggesting CAMSAPs play important roles in MT stabilization. These two functions, minus end tracking and stabilization, seem to be achieved by different domains in the mammalian CAMSAP protein. The C-terminal CKK domain enables the tracking activity, though activity is more robust with the addition of the third coil-coil domain, whereas different sub-regions of the coiled-coil (CC) domain are required for MT stabilization (Yau et al., 2014).

Studies on the invertebrate members of the CAMSAP family also suggest CAMSAP functions in stabilizing MT minus ends, though the mechanism of function seems to be slightly different. In S2 cells, the Drosophila homolog Patronin forms puncta, which co-localize with MT minus end-associated factors such as Sas-4 (Goodwin and Vale, 2010). Furthermore, in vitro MT gliding assays reveal Patronin forms puncta specifically at the MT minus end. Unlike mammalian CAMSAPs, the CC domain by itself had the same localization patterns as full length Patronin, suggesting that unlike mammalian CAMSAPs, Patronin's CC domain is sufficient for MT minus end tracking (Goodwin and Vale, 2010). PTRN-1, the sole *C. elegans* ortholog, also has been shown to promote stability of MT foci in neuronal processes and in body wall muscle (Richardson et al., 2014).

How do CAMSAPs stabilize MTs? In flies Patronin by itself protects the minus ends from kinesin-13 Klp10A mediated depolymerization. In S2 cells, knockdown of Patronin led to free MTs treadmilling, and sometimes even minus end growth (Goodwin and Vale, 2010), while in *Drosophila* embryos inhibition of Patronin resulted in a short spindle phenotype due to a reduction in poleward flux caused by KLP10A activity (Wang et al., 2013). Another MT associated protein that acts antagonistically with CAMSAPs is the MT-severing protein katanin. Katanin shortens the length of CAMSAP2 stretches at the MT minus end, and in this way may promote destabilization of the CAMSAP bound MT (Jiang et al., 2014).

Though CAMSAPs are similar to γ-tubulin in that they can bind directly to MT minus ends, there is no hard evidence implicating CAMSAPs in MT nucleation. CAMSAPs localize at nucleation sites in various cell types and animal systems (Goodwin and Vale, 2010; Meng et al., 2008; Tanaka et al., 2012). However, in the dendrites of cultured hippocampal neurons, γ-tubulin depletion does not alter CAMSAP2 dynamics, but changes the number of CAMSAP stretches, indicating CAMSAP2 acts independent but downstream of γ-tubulin (Yau et al, 2014). In addition, CAMSAP2 is recruited to MT minus ends a few minutes after washout of the MT depolymerizing drug nocodazole in hippocampal neurons and after MTs re-polymerize (Jiang et al., 2014). Altogether, evidence supports CAMSAPs primarily act to stabilize, instead of generate, MTs at the minus ends.

CAMSAPs in Neurons. CAMSAPs may play important roles in brain development. In cultured hippocampal neurons, depletion of CAMSAP2 resulted in a reduction in MT density, a decrease in dendritic branching, lack of neuronal polarization,

failure of neuronal migration, and impaired axon specification (Yau et al., 2014). Depletion of CAMSAP1 in PC12 cells and primary cerebellar granule cells inhibited neurite outgrowth (King et al., 2014). CAMSAP1's function in neurite outgrowth is dependent on its binding to spectrin and calmodulin. Additionally, variants in the CAMSAP2 locus have been associated with epilepsy (Guo et al., 2012; Zhang et al., 2013).

PTRN-1 in the worm does not seem to play such an essential role in neuronal development as CAMSAPs in mammals. Loss of PTRN-1 function causes slight defects in neurite morphology (Marcette et al., 2014) and localization of synaptic components (Richardson et al., 2014). Despite these neuronal defects, *ptrn-1* mutants are grossly wild type (WT) in development and behavior. However, the mutants possess a striking phenotype. For WT mechanosensory neurons, treatment with high concentration of MT depolymerizing drug colchicine causes ectopic branching (Richardson et al., 2014). *ptrn-1* mutants are even more susceptible to this treatment compared to WT. However, the phenotype is almost completely suppressed with the additional loss of function in *dlk-1*, a MAPKKK. These results suggest that there may be other MT-associated proteins sharing redundant functions with PTRN-1—however, PTRN-1 is necessary for proper development in the presence of certain stresses or perturbations in MT dynamics. Furthermore, DLK-1, which has been shown to control the activity of downstream MT-associated proteins in neurons (Ghosh-Roy et al., 2012), may regulate PTRN-1's function in MT stability, or is required for PTRN-1 to detect MT defects.

Though CAMSAPs are required for normal MT stability and subsequent neurite morphology, neither knockdown of CAMSAP2 or mutation in PTRN-1 had any effect on MT orientation in neurons (Yau et al., 2014; Richardson et al., 2014).

CAMSAPs in Epithelial Cells. As in neurons, in epithelial cells, CAMSAPs have been shown to be involved in intracellular sorting. Fly Patronin functions together with the spectraplakin protein Shot/Shortstop to direct Rab11 vesicles to the apical cortex of microvilli in Drosophila follicle cells (Khanal et al., 2016). Unlike in neuronal processes however, Patronin achieves this by regulating the MT orientation, polarizing MTs along the apical-basal axis (Nashchekin et al., 2016). This role in directing MT dynamics is also seen in mammalian cells. CAMSAP3/Nezha accumulates at the apical cortex in mouse intestinal cells, and tethers MTs to the cortex (Toya et al., 2016). Loss of CAMSAP3 function in human intestinal Caco-2 cell line leads to random MT orientation and perturbs nuclei and Golgi positioning. Studies also show that CAMSAP3, in conjunction with membrane-associated protein PLEKHA, tethers MT minus ends to the zonula adherens, a cadherin-based cell-cell junction, and is required for normal cell-cell contact (Meng et al., 2008).

This function in maintaining epithelial integrity is supported by in vivo data. In nematodes, although *ptrn-1* mutants are superficially wild type, loss of another MT minus end-associated gene, *noca-1*, together with loss of *ptrn-1* leads to severe disintegration of epidermal tissue and eventual larval lethality (Wang et al., 2015). The number of MT bundles in the larval anterior epidermis is strongly reduced in double mutants, while largely unchanged in the single mutants. These results suggest *ptrn-1* and *noca-1* act

redundantly to stabilize and maintain the normal MT architecture in the *C. elegans* epidermis, and this MT array is crucial for larval development (Wang et al., 2015).

1.5 Role of MTs in injury response and tissue repair

Living organisms encounter a multitude of environmental stresses, resulting in damage to various tissues. The inability to recover from such traumatic events leads to a failure in homeostasis and health, and can eventually impact survival. Thus, animals have evolved an array of methods to defend and heal various types of tissues from different types of trauma. This section will focus on how tissues repair themselves after physical injury, and will discuss how the regulation of MTs has been implicated in injury response in two types of tissues systems: the nervous and the epithelial.

Axon injury and regeneration. Axon regrowth requires the formation of a growth cone, followed by extension of the proximal portion of the axon until it reaches its target site. In most vertebrates, nerve regeneration is more feasible in the peripheral nervous system (PNS), while nerves in the central nervous system (CNS) fail to regrow. This discrepancy in the ability to repair has historically been explained by the differences in the extracellular environment in the two nervous systems, with the CNS enriched with specific myelin associated proteins that inhibit regeneration (reviewed in Filbin, 2003). However, there has recently been a renewed focus on the intrinsic factors regulating the neuronal response to injury.

Much progress has been seen in the research on the neuronal MT cytoskeleton and its regulators. As mentioned in Section 1.3, axons are particularly enriched in highly

stable polarized MTs, oriented plus-end out. Upon axonal breakage, this stable MT network is disrupted, resulting in rapid depolymerization at the injury site (Erez et al., 2007; Chen et al., 2015). Soon after insult, a pool of growing MTs begins to form at the injury site (Erez et al., 2007; Song et al., 2012; Ghosh-Roy et al., 2012), and this polymerization and at least partial stabilization of MTs is required for remodeling the axon into a motile growth cone (Erez et al., 2007; Ghosh-Roy et al., 2012). Stabilization of MTs seems to be key in successful axonal regrowth. In injured CNS axons, MTs depolymerize and remain disorganized at the axon stump, while injured PNS axons retain MT integrity and bundling (Erturk et al., 2007). Indeed, treating neurons with the MT stabilizing drugs taxol/paclitaxel and epithilone D promoted axon regeneration in the CNS (Hellal et al., 2011; Baas and Ahmad, 2013; Brunden et al., 2010; Zhang et al., 2012). In fact, epithilone D is currently in clinical trials for patients with mild Alzheimer's disease (ClinicalTrals.gov Identifier: NCT01492374) (Baas and Ahmad, 2013). This MT stability may be important in forming the tracks to transport material essential for membrane repair and growth cone formation to the injury site (reviewed in Bradke et al., 2012). For more information on how MTs function in axon regeneration, readers are directed to (Chisholm, 2013) for review.

Epithelial wound healing

Innate immunity. One of the main roles of epithelial tissue is to line cavities and surfaces, acting as physical barriers against the outside world. In contrast to neuronal injury, breach of the epithelia exposes the organism to the external environment (in the case of the epidermis) and the lumen, which often contains foreign, non-self substances (as in the intestine). Pathogen invasion is a large threat that comes with epithelial

wounds, and the organism must mount a defense mechanism to fight against infection. The innate immune system, which includes the barrier function of epithelia, the initial recognition of non-self signals, and inflammation, acts as a first line of defense against these dangers. Much is known about the cytokines, cell types, and signaling pathways involved in innate immunity; however, the specific roles of intracellular components, especially that of the MT cytoskeleton, is unclear.

The roles of MTs in immunity have mostly been investigated through pharmacological experiments. In one *C. elegans* immunity model, fungal infection or sterile wounding induces high expression of antimicrobial peptides (AMPs) such as NLP-29 (Couillault et al., 2004; Pujol et al., 2008). In one study looking at which cytoskeletal component of the epidermal architecture was important for innate immunity, the researchers showed that chronic treatment of the MT destabilizing drug nocodazole to the worms did not affect *nlp-29* expression (Zhang et al., 2015). In fact, out of all single cytoskeletal components tested, only disruption of the hemi-desmosomes triggered AMP induction, suggesting that though MTs play a strong role in epidermal structure and integrity (Wang et al., 2015), overall collapse of the epidermal architecture, such as from MT impairment, was not sufficient to trigger at least the specific *nlp-29* AMP expression. Whether MTs can affect other innate immune pathways in the worm remains to be seen.

In another drug experiment, scientists examined how MT function was important in the inflammasome, or the multiprotein complex of caspases that assembles when activated by antigens, and whose assembly leads to cytokine maturation (reviewed in Guo et al., 2015). One component of the inflammasome is the pathogen recognition receptor NLRP3. The addition of MT destabilizing drugs colchicine, nocodazole, and

podophyllotoxin abolished NLRP3-dependent caspase 1 activity (Misawa et al., 2013; reviewed in Mostowy and Shenoy, 2015). It is still unclear how MTs enable inflammasome activity—the authors hypothesize that MT-dependent trafficking of mitochondria may be involved in NLRP3-mediated inflammasome activity--but the pharmacology results may explain how colchicine alleviates the symptoms of gout, a medical condition associated with NLRP3 activation (Kingsbury et al., 2011).

An additional study showed the role of MTs in mounting antiviral host defenses. GEF-H1, a MT regulated Rho-GEF, is required to signal to the macrophage to induce production of interferon regulatory factors upon the sensing of viral RNA. Normally, the MT network sequesters GEF-H1, and only releases GEF-H1 after its activation to mediate a defense response. Application of nocodazole prevented GEF-H1 activation, and GEF-H1 mutant mice could not produce an immune response against influenza A and encephalomyocarditis (Chiang et al., 2013). This result suggested an active regulatory function of MTs, instead of its usual role in intracellular sorting, is at play in the downstream innate immunity signaling after viral nucleic acid recognition.

The innate immune system encompasses a wide variety of pathogen detection methods, signaling pathways and immune response output. Which defense mechanism is dependent on MT function, and how MTs function in each one, have yet to be addressed. Furthermore, more research on which MT associated proteins and regulatory factors are involved, instead of simple pharmacological tests, should be done to elucidate fully how MT architecture and dynamics are controlled for effective innate immunity.

Wound closure. Wound repair undergoes similar steps in all complex organisms: the ruptured membrane of the wound is quickly sealed, the injury site is rebuilt, and

finally the area is remodeled to restore normal function. An important player in wound healing is the cytoskeleton. Much work has been done studying the roles of polymerizing actin in single cell lamellopodia and *C. elegans* epidermis (Henson et al., 2002; Xu and Chisholm, 2011) or actomyosin contractile ring in *Xenopus* oocyte, *Drosophila* embryos, and intestinal epithelial monolayers (Mandato and Bement, 2001; Mandato and Bement, 2003; Abreu-Blanco et al., 2011; Wood et al., 2002; Russo et al., 2005). Actin alone or actin in conjunction with myosin is the driving force of wound closure in these wound models. However, the interaction of MTs with actin has also been shown to be crucial in healing. In the *Xenopus* oocyte model, F-actin and myosin concentrate at the wound border due to local assembly and cortical flow, and close the wound via a "purse string" mechanism (Mandato and Bement, 2001). During this process, MTs are pulled towards the wound site as a radial array by the flowing F-actin, buckling and breaking as they are translocated (Mandato and Bement, 2003). This zone of MT disassembly is similar to that seen in migrating cells and growth cones in neurons (see Section 1.5 on axon injury). At the same time, the MT distal ends polymerize continuously as they move towards the site of injury, again as seen at the leading edge of migrating cells and growth cones. The transport of MTs is important for proper organization of actomyosin array around the wound; disruption of the MT network before or after wounding can disrupt or accelerate the purse-string contraction, respectively (Mandato and Bement, 2003). In the *Drosophila* embryo, after wounding, no rearrangement of MTs into a radial array was observed; however, disruption of the MT network by colchicine resulted in defective actin formation (Abreu-Blanco et al., 2011).

Besides their function in actomyosin contractile ring formation, drug experiments suggest MTs are required to mobilize lipids to reseal the wound. Lack of plasma membrane delivery after wounding was seen after colchicine treatment on Drosophila embryos (Abreu-Blanco et al., 2011). Nocodazole inhibits the recruitment of Golgi-derived lipids to the wound site in PtK2 epithelial kidney cells (Togo, 2006). Furthermore, inhibition of kinesin by antibody injection blocked resealing after wounding in sea urchin eggs and Swiss 3T3 fibroblasts (Steinhardt et al., 1994), suggesting MTs are most likely enabling resealing by mediating motor-dependent transport of vesicles to the site of membrane rupture.

The studies mentioned so far all used single cell models of wound healing to probe MT function. In complex mature organisms, repair of damaged tissues requires directed migration of cells to the wound site. Loss of normal MT regulation has been shown to lead to a lack of or misdirected migration. The depletion of CAMSAPs (see Section 1.4) inhibited directed cell migration in monolayer scratch wound assays. CAMSAPs are required to maintain correctly oriented MT arrays in epithelial cells; without functional CAMSAPs present, improper polarization of MTs may cause defective Golgi reorientation toward the wound site (Jiang et al., 2014). To learn more about MTs and their roles in cell migration, irrespective of wound context, the reader is referred to the following reviews (Etienne-Manneville, 2013; Ganguly et al., 2012). MTs are important in forming cell protrusions, controlling cell polarity and regulating cell adhesion in migrating cells—further work is needed to show how relevant these functions are in wound healing. For more information on the known cytoskeletal dynamics in wound repair, the reader is directed to Abreu-Blanco et al., 2012 for review.

1.6 References

Abreu-Blanco, M.T., Verboon, J.M., and Parkhurst, S.M. (2011). Cell wound repair in Drosophila occurs through three distinct phases of membrane and cytoskeletal remodeling. J Cell Biol *193*, 455-464.

Abreu-Blanco, M.T., Watts, J.J., Verboon, J.M., and Parkhurst, S.M. (2012). Cytoskeleton responses in wound repair. Cell Mol Life Sci *69*, 2469-2483.

Ahmad, F.J., Echeverri, C.J., Vallee, R.B., and Baas, P.W. (1998). Cytoplasmic dynein and dynactin are required for the transport of microtubules into the axon. J Cell Biol *140*, 391-401.

Ahmad, F.J., Yu, W., McNally, F.J., and Baas, P.W. (1999). An essential role for katanin in severing microtubules in the neuron. J Cell Biol *145*, 305-315.

Akhmanova, A., and Hoogenraad, C.C. (2015). Microtubule minus-end-targeting proteins. Curr Biol *25*, R162-171.

Akhmanova, A., and Steinmetz, M.O. (2008). Tracking the ends: a dynamic protein network controls the fate of microtubule tips. Nat Rev Mol Cell Biol *9*, 309-322.

Akhmanova, A., and Steinmetz, M.O. (2010). Microtubule +TIPs at a glance. J Cell Sci *123*, 3415-3419.

Akhmanova, A., and Steinmetz, M.O. (2015). Control of microtubule organization and dynamics: two ends in the limelight. Nat Rev Mol Cell Biol *16*, 711-726.

Baas, P.W., and Ahmad, F.J. (2013). Beyond taxol: microtubule-based treatment of disease and injury of the nervous system. Brain *136*, 2937-2951.

Baas, P.W., Deitch, J.S., Black, M.M., and Banker, G.A. (1988). Polarity orientation of microtubules in hippocampal neurons: uniformity in the axon and nonuniformity in the dendrite. Proc Natl Acad Sci U S A *85*, 8335-8339.

Baines, A.J., Bignone, P.A., King, M.D., Maggs, A.M., Bennett, P.M., Pinder, J.C., and Phillips, G.W. (2009). The CKK domain (DUF1781) binds microtubules and defines the CAMSAP/ssp4 family of animal proteins. Mol Biol Evol *26*, 2005-2014.

Bartolini, F., and Gundersen, G.G. (2006). Generation of noncentrosomal microtubule arrays. J Cell Sci *119*, 4155-4163.

Bradke, F., Fawcett, J.W., and Spira, M.E. (2012). Assembly of a new growth cone after axotomy: the precursor to axon regeneration. Nat Rev Neurosci *13*, 183-193.

Brodu, V., Baffet, A.D., Le Droguen, P.M., Casanova, J., and Guichet, A. (2010). A developmentally regulated two-step process generates a noncentrosomal microtubule network in Drosophila tracheal cells. Dev Cell *18*, 790-801.

Brunden, K.R., Zhang, B., Carroll, J., Yao, Y., Potuzak, J.S., Hogan, A.M., Iba, M., James, M.J., Xie, S.X., Ballatore, C., Smith, A.B., Lee, V.M., Trojanowski, J.Q. (2010). Epothilone D improves microtubule density, axonal integrity, and cognition in a transgenic mouse model of tauopathy. J Neurosci *30*, 13861-13866.

Bugnard, E., Zaal, K.J., and Ralston, E. (2005). Reorganization of microtubule nucleation during muscle differentiation. Cell Motil Cytoskeleton *60*, 1-13.

Burton, P.R. (1988). Dendrites of mitral cell neurons contain microtubules of opposite polarity. Brain Res *473*, 107-115.

Chen, L., Chuang, M., Koorman, T., Boxem, M., Jin, Y., and Chisholm, A.D. (2015). Axon injury triggers EFA-6 mediated destabilization of axonal microtubules via TACC and doublecortin like kinase. Elife *4*.

Chi, R.J., Harrison, M.S., and Burd, C.G. (2015). Biogenesis of endosome-derived transport carriers. Cell Mol Life Sci *72*, 3441-3455.

Chiang, H.S., Zhao, Y., Song, J.H., Liu, S., Wang, N., Terhorst, C., Sharpe, A.H., Basavappa, M., Jeffrey, K.L., and Reinecker, H.C. (2013). GEF-H1 controls microtubule-dependent sensing of nucleic acids for antiviral host defenses. Nat Immunol *15*, 63-71.

Chisholm, A.D. (2013). Cytoskeletal dynamics in Caenorhabditis elegans axon regeneration. Annu Rev Cell Dev Biol *29*, 271-297.

Conde, C., and Caceres, A. (2009). Microtubule assembly, organization and dynamics in axons and dendrites. Nat Rev Neurosci *10*, 319-332.

Couillault, C., Pujol, N., Reboul, J., Sabatier, L., Guichou, J.F., Kohara, Y., and Ewbank, J.J. (2004). TLR-independent control of innate immunity in Caenorhabditis elegans by the TIR domain adaptor protein TIR-1, an ortholog of human SARM. Nat Immunol *5*, 488-494.

Dammermann, A., Desai, A., and Oegema, K. (2003). The minus end in sight. Curr Biol *13*, R614-624.

Delevoye, C., Miserey-Lenkei, S., Montagnac, G., Gilles-Marsens, F., Paul-Gilloteaux, P., Giordano, F., Waharte, F., Marks, M.S., Goud, B., and Raposo, G. (2014). Recycling endosome tubule morphogenesis from sorting endosomes requires the kinesin motor KIF13A. Cell Rep *6*, 445-454.

Desai, A., and Mitchison, T.J. (1997). Microtubule polymerization dynamics. Annu Rev Cell Dev Biol *13*, 83-117.

Dyachuk, V., Bierkamp, C., and Merdes, A. (2016). Non-centrosomal Microtubule Organization in Differentiated Cells. The Microtubule Cytoskeleton, 27-41.

Erez, H., Malkinson, G., Prager-Khoutorsky, M., De Zeeuw, C.I., Hoogenraad, C.C., and Spira, M.E. (2007). Formation of microtubule-based traps controls the sorting and concentration of vesicles to restricted sites of regenerating neurons after axotomy. J Cell Biol *176*, 497-507.

Erturk, A., Hellal, F., Enes, J., and Bradke, F. (2007). Disorganized microtubules underlie the formation of retraction bulbs and the failure of axonal regeneration. J Neurosci *27*, 9169-9180.

Etienne-Manneville, S. (2013). Microtubules in cell migration. Annu Rev Cell Dev Biol *29*, 471-499.

Farah, C.A., and Leclerc, N. (2008). HMWMAP2: new perspectives on a pathway to dendritic identity. Cell Motil Cytoskeleton *65*, 515-527.

Feldman, J.L., and Priess, J.R. (2012). A role for the centrosome and PAR-3 in the hand-off of MTOC function during epithelial polarization. Curr Biol *22*, 575-582.

Filbin, M.T. (2003). Myelin-associated inhibitors of axonal regeneration in the adult mammalian CNS. Nat Rev Neurosci *4*, 703-713.

Ganguly, A., Yang, H., Sharma, R., Patel, K.D., and Cabral, F. (2012). The role of microtubules and their dynamics in cell migration. J Biol Chem *287*, 43359-43369.

Ghosh-Roy, A., Goncharov, A., Jin, Y., and Chisholm, A.D. (2012). Kinesin-13 and tubulin posttranslational modifications regulate microtubule growth in axon regeneration. Dev Cell *23*, 716-728.

Goodwin, S.S., and Vale, R.D. (2010). Patronin regulates the microtubule network by protecting microtubule minus ends. Cell *143*, 263-274.

Guo, H., Callaway, J.B., and Ting, J.P. (2015). Inflammasomes: mechanism of action, role in disease, and therapeutics. Nat Med *21*, 677-687.

Guo, Y., Baum, L.W., Sham, P.C., Wong, V., Ng, P.W., Lui, C.H., Sin, N.C., Tsoi, T.H., Tang, C.S., Kwan, J.S., Yip, B.H., Xiao, S.M., Thomas, G.N., Lau, YL., Yang, W., Cherny, S.S., Kwan, P. (2012). Two-stage genome-wide association study identifies variants in CAMSAP1L1 as susceptibility loci for epilepsy in Chinese. Hum Mol Genet

21, 1184-1189.

He, Y., Francis, F., Myers, K.A., Yu, W., Black, M.M., and Baas, P.W. (2005). Role of cytoplasmic dynein in the axonal transport of microtubules and neurofilaments. J Cell Biol *168*, 697-703.

Heidemann, S.R., Landers, J.M., and Hamborg, M.A. (1981). Polarity orientation of axonal microtubules. J Cell Biol *91*, 661-665.

Hellal, F., Hurtado, A., Ruschel, J., Flynn, K.C., Laskowski, C.J., Umlauf, M., Kapitein, L.C., Strikis, D., Lemmon, V., Bixby, J., Hoogenraad, C.C., Bradke, F. (2011). Microtubule stabilization reduces scarring and causes axon regeneration after spinal cord injury. Science *331*, 928-931.

Hendershott, M.C., and Vale, R.D. (2014). Regulation of microtubule minus-end dynamics by CAMSAPs and Patronin. Proc Natl Acad Sci U S A *111*, 5860-5865.

Henson, J.H., Nazarian, R., Schulberg, K.L., Trabosh, V.A., Kolnik, S.E., Burns, A.R., and McPartland, K.J. (2002). Wound closure in the lamellipodia of single cells: mediation by actin polymerization in the absence of an actomyosin purse string. Mol Biol Cell *13*, 1001-1014.

Howard, J., and Hyman, A.A. (2003). Dynamics and mechanics of the microtubule plus end. Nature *422*, 753-758.

Jiang, K., Hua, S., Mohan, R., Grigoriev, I., Yau, K.W., Liu, Q., Katrukha, E.A., Altelaar, A.F., Heck, A.J., Hoogenraad, C.C., Akhmanova, A. (2014). Microtubule minus-end stabilization by polymerization-driven CAMSAP deposition. Dev Cell *28*, 295-309.

Kapitein, L.C., and Hoogenraad, C.C. (2015). Building the Neuronal Microtubule Cytoskeleton. Neuron *87*, 492-506.

Karabay, A., Yu, W., Solowska, J.M., Baird, D.H., and Baas, P.W. (2004). Axonal growth is sensitive to the levels of katanin, a protein that severs microtubules. J Neurosci *24*, 5778-5788.

Keating, T.J., and Borisy, G.G. (1999). Centrosomal and non-centrosomal microtubules. Biol Cell *91*, 321-329.

Keating, T.J., Peloquin, J.G., Rodionov, V.I., Momcilovic, D., and Borisy, G.G. (1997). Microtubule release from the centrosome. Proc Natl Acad Sci U S A *94*, 5078-5083.

Khanal, I., Elbediwy, A., Diaz de la Loza Mdel, C., Fletcher, G.C., and Thompson, B.J. (2016). Shot and Patronin polarise microtubules to direct membrane traffic and biogenesis of microvilli in epithelia. J Cell Sci *129*, 2651-2659.

King, M.D., Phillips, G.W., Bignone, P.A., Hayes, N.V., Pinder, J.C., and Baines, A.J. (2014). A conserved sequence in calmodulin regulated spectrin-associated protein 1 links its interaction with spectrin and calmodulin to neurite outgrowth. J Neurochem *128*, 391-402.

Kingsbury, S.R., Conaghan, P.G., and McDermott, M.F. (2011). The role of the NLRP3 inflammasome in gout. J Inflamm Res *4*, 39-49.

Kollman, J.M., Merdes, A., Mourey, L., and Agard, D.A. (2011). Microtubule nucleation by gamma-tubulin complexes. Nat Rev Mol Cell Biol *12*, 709-721.

Lindeboom, J.J., Nakamura, M., Hibbel, A., Shundyak, K., Gutierrez, R., Ketelaar, T., Emons, A.M., Mulder, B.M., Kirik, V., and Ehrhardt, D.W. (2013). A mechanism for reorientation of cortical microtubule arrays driven by microtubule severing. Science *342*, 1245533.

Lu, W., Fox, P., Lakonishok, M., Davidson, M.W., and Gelfand, V.I. (2013). Initial neurite outgrowth in Drosophila neurons is driven by kinesin-powered microtubule sliding. Curr Biol *23*, 1018-1023.

Lu, W., Lakonishok, M., and Gelfand, V.I. (2015). Kinesin-1-powered microtubule sliding initiates axonal regeneration in Drosophila cultured neurons. Mol Biol Cell *26*, 1296-1307.

Mandato, C.A., and Bement, W.M. (2001). Contraction and polymerization cooperate to assemble and close actomyosin rings around Xenopus oocyte wounds. J Cell Biol *154*, 785-797.

Mandato, C.A., and Bement, W.M. (2003). Actomyosin transports microtubules and microtubules control actomyosin recruitment during Xenopus oocyte wound healing. Curr Biol *13*, 1096-1105.

Marcette, J.D., Chen, J.J., and Nonet, M.L. (2014). The Caenorhabditis elegans microtubule minus-end binding homolog PTRN-1 stabilizes synapses and neurites. Elife *3*, e01637.

Meads, T., and Schroer, T.A. (1995). Polarity and nucleation of microtubules in polarized epithelial cells. Cell Motil Cytoskeleton *32*, 273-288.

Meng, W., Mushika, Y., Ichii, T., and Takeichi, M. (2008). Anchorage of microtubule minus ends to adherens junctions regulates epithelial cell-cell contacts. Cell *135*, 948-959.

Misawa, T., Takahama, M., Kozaki, T., Lee, H., Zou, J., Saitoh, T., and Akira, S. (2013). Microtubule-driven spatial arrangement of mitochondria promotes activation of the NLRP3 inflammasome. Nat Immunol *14*, 454-460.

Mitchison, T., and Kirschner, M. (1984). Dynamic instability of microtubule growth. Nature *312*, 237-242.

Mogensen, M.M., Malik, A., Piel, M., Bouckson-Castaing, V., and Bornens, M. (2000). Microtubule minus-end anchorage at centrosomal and non-centrosomal sites: the role of ninein. J Cell Sci *113 (Pt 17)*, 3013-3023.

Mogensen, M.M., Tucker, J.B., and Baggaley, T.B. (1993). Multiple plasma membrane-associated MTOC systems in the acentrosomal cone cells of Drosophila ommatidia. Eur J Cell Biol *60*, 67-75.

Mogensen, M.M., Tucker, J.B., and Stebbings, H. (1989). Microtubule polarities indicate that nucleation and capture of microtubules occurs at cell surfaces in Drosophila. J Cell Biol *108*, 1445-1452.

Mostowy, S., and Shenoy, A.R. (2015). The cytoskeleton in cell-autonomous immunity: structural determinants of host defence. Nat Rev Immunol *15*, 559-573.

Murata, T., Sonobe, S., Baskin, T.I., Hyodo, S., Hasezawa, S., Nagata, T., Horio, T., and Hasebe, M. (2005). Microtubule-dependent microtubule nucleation based on recruitment of gamma-tubulin in higher plants. Nat Cell Biol *7*, 961-968.

Musch, A. (2004). Microtubule organization and function in epithelial cells. Traffic *5*, 1-9.

Nashchekin, D., Fernandes, A.R., and St Johnston, D. (2016). Patronin/Shot Cortical Foci Assemble the Noncentrosomal Microtubule Array that Specifies the Drosophila Anterior-Posterior Axis. Dev Cell *38*, 61-72.

Oakley, B.R., Paolillo, V., and Zheng, Y. (2015). gamma-Tubulin complexes in microtubule nucleation and beyond. Mol Biol Cell *26*, 2957-2962.

Ori-McKenney, K.M., Jan, L.Y., and Jan, Y.N. (2012). Golgi outposts shape dendrite morphology by functioning as sites of acentrosomal microtubule nucleation in neurons. Neuron *76*, 921-930.

Petry, S., and Vale, R.D. (2015). Microtubule nucleation at the centrosome and beyond. Nat Cell Biol *17*, 1089-1093.

Pujol, N., Cypowyj, S., Ziegler, K., Millet, A., Astrain, A., Goncharov, A., Jin, Y., Chisholm, A.D., and Ewbank, J.J. (2008). Distinct innate immune responses to infection and wounding in the C. elegans epidermis. Curr Biol *18*, 481-489.

Qiang, L., Yu, W., Andreadis, A., Luo, M., and Baas, P.W. (2006). Tau protects microtubules in the axon from severing by katanin. J Neurosci *26*, 3120-3129.

Quintin, S., Gally, C., and Labouesse, M. (2016). Noncentrosomal microtubules in C. elegans epithelia. Genesis *54*, 229-242.

Richardson, C.E., Spilker, K.A., Cueva, J.G., Perrino, J., Goodman, M.B., and Shen, K. (2014). PTRN-1, a microtubule minus end-binding CAMSAP homolog, promotes microtubule function in Caenorhabditis elegans neurons. Elife *3*, e01498.

Rodriguez-Boulan, E., Kreitzer, G., and Musch, A. (2005). Organization of vesicular trafficking in epithelia. Nat Rev Mol Cell Biol *6*, 233-247.

Russo, J.M., Florian, P., Shen, L., Graham, W.V., Tretiakova, M.S., Gitter, A.H., Mrsny, R.J., and Turner, J.R. (2005). Distinct temporal-spatial roles for rho kinase and myosin light chain kinase in epithelial purse-string wound closure. Gastroenterology *128*, 987-1001.

Seltzer, V., Janski, N., Canaday, J., Herzog, E., Erhardt, M., Evrard, J.L., and Schmit, A.C. (2007). Arabidopsis GCP2 and GCP3 are part of a soluble gamma-tubulin complex and have nuclear envelope targeting domains. Plant J *52*, 322-331.

Sharp, D.J., Yu, W., Ferhat, L., Kuriyama, R., Rueger, D.C., and Baas, P.W. (1997). Identification of a microtubule-associated motor protein essential for dendritic differentiation. J Cell Biol *138*, 833-843.

Shaw, S.L., Kamyar, R., and Ehrhardt, D.W. (2003). Sustained microtubule treadmilling in Arabidopsis cortical arrays. Science *300*, 1715-1718.

Song, Y., Ori-McKenney, K.M., Zheng, Y., Han, C., Jan, L.Y., and Jan, Y.N. (2012). Regeneration of Drosophila sensory neuron axons and dendrites is regulated by the Akt pathway involving Pten and microRNA bantam. Genes Dev *26*, 1612-1625.

Steinhardt, R.A., Bi, G., and Alderton, J.M. (1994). Cell membrane resealing by a vesicular mechanism similar to neurotransmitter release. Science *263*, 390-393.

Stoppin, V., Vantard, M., Schmit, A.C., and Lambert, A.M. (1994). Isolated Plant Nuclei Nucleate Microtubule Assembly: The Nuclear Surface in Higher Plants Has Centrosome-like Activity. Plant Cell *6*, 1099-1106.

Tanaka, N., Meng, W., Nagae, S., and Takeichi, M. (2012). Nezha/CAMSAP3 and CAMSAP2 cooperate in epithelial-specific organization of noncentrosomal microtubules. Proc Natl Acad Sci U S A *109*, 20029-20034.

Tassin, A.M., Maro, B., and Bornens, M. (1985a). Fate of microtubule-organizing centers during myogenesis in vitro. J Cell Biol *100*, 35-46.

Togo, T. (2006). Disruption of the plasma membrane stimulates rearrangement of microtubules and lipid traffic toward the wound site. J Cell Sci *119*, 2780-2786.

Toya, M., Kobayashi, S., Kawasaki, M., Shioi, G., Kaneko, M., Ishiuchi, T., Misaki, K., Meng, W., and Takeichi, M. (2016). CAMSAP3 orients the apical-to-basal polarity of microtubule arrays in epithelial cells. Proc Natl Acad Sci U S A *113*, 332-337.

Tran, P.T., Walker, R.A., and Salmon, E.D. (1997). A metastable intermediate state of microtubule dynamic instability that differs significantly between plus and minus ends. J Cell Biol *138*, 105-117.

Walker, R.A., Inoue, S., and Salmon, E.D. (1989). Asymmetric behavior of severed microtubule ends after ultraviolet-microbeam irradiation of individual microtubules in vitro. J Cell Biol *108*, 931-937.

Walker, R.A., O'Brien, E.T., Pryer, N.K., Soboeiro, M.F., Voter, W.A., Erickson, H.P., and Salmon, E.D. (1988). Dynamic instability of individual microtubules analyzed by video light microscopy: rate constants and transition frequencies. J Cell Biol *107*, 1437-1448.

Wang, H., Brust-Mascher, I., Civelekoglu-Scholey, G., and Scholey, J.M. (2013). Patronin mediates a switch from kinesin-13-dependent poleward flux to anaphase B spindle elongation. J Cell Biol *203*, 35-46.

Wang, S., Wu, D., Quintin, S., Green, R.A., Cheerambathur, D.K., Ochoa, S.D., Desai, A., and Oegema, K. (2015). NOCA-1 functions with gamma-tubulin and in parallel to Patronin to assemble non-centrosomal microtubule arrays in C. elegans. Elife *4*, e08649.

Wood, W., Jacinto, A., Grose, R., Woolner, S., Gale, J., Wilson, C., and Martin, P. (2002). Wound healing recapitulates morphogenesis in Drosophila embryos. Nat Cell Biol *4*, 907-912.

Xu, S., and Chisholm, A.D. (2011). A Galphaq-Ca(2)(+) signaling pathway promotes actin-mediated epidermal wound closure in C. elegans. Curr Biol *21*, 1960-1967.

Yau, K.W., van Beuningen, S.F., Cunha-Ferreira, I., Cloin, B.M., van Battum, E.Y., Will, L., Schatzle, P., Tas, R.P., van Krugten, J., Katrukha, E.A., khmanova, A.. (2014).

Microtubule minus-end binding protein CAMSAP2 controls axon specification and dendrite development. Neuron *82*, 1058-1073.

Yu, W., Centonze, V.E., Ahmad, F.J., and Baas, P.W. (1993). Microtubule nucleation and release from the neuronal centrosome. J Cell Biol *122*, 349-359.

Yu, W., Cook, C., Sauter, C., Kuriyama, R., Kaplan, P.L., and Baas, P.W. (2000). Depletion of a microtubule-associated motor protein induces the loss of dendritic identity. J Neurosci *20*, 5782-5791.

Yu, W., Solowska, J.M., Qiang, L., Karabay, A., Baird, D., and Baas, P.W. (2005). Regulation of microtubule severing by katanin subunits during neuronal development. J Neurosci *25*, 5573-5583.

Zhang, B., Carroll, J., Trojanowski, J.Q., Yao, Y., Iba, M., Potuzak, J.S., Hogan, A.M., Xie, S.X., Ballatore, C., Smith, A.B., 3rd, khmanova, A.. (2012). The microtubule-stabilizing agent, epothilone D, reduces axonal dysfunction, neurotoxicity, cognitive deficits, and Alzheimer-like pathology in an interventional study with aged tau transgenic mice. J Neurosci *32*, 3601-3611.

Zhang, S., Kwan, P., and Baum, L. (2013). The potential role of CAMSAP1L1 in symptomatic epilepsy. Neurosci Lett *556*, 146-151.

Zhang, Y., Li, W., Li, L., Li, Y., Fu, R., Zhu, Y., Li, J., Zhou, Y., Xiong, S., and Zhang, H. (2015). Structural damage in the C. elegans epidermis causes release of STA-2 and induction of an innate immune response. Immunity *42*, 309-320.

Chapter 2

Introduction Part Two:

Insights into the functions of the Death Associated Protein Kinases from *C. elegans* and other invertebrates

2.1 Abstract

The death associated protein kinases (DAPK) are a phylogenetically widespread family of calcium-regulated serine/threonine kinases, initially identified from their roles in apoptosis. Subsequent studies, principally in vertebrate cells or models, have elucidated the functions of the DAPK family in autophagy and tumor suppression. Invertebrate genetic model organisms such as *Drosophila* and *C. elegans* have revealed additional functions for DAPK and related kinases. In the nematode *C. elegans*, the sole DAPK family member DAPK-1 positively regulates starvation-induced autophagy. Genetic analysis in *C. elegans* has revealed that DAPK-1 also acts as a negative regulator of epithelial innate immune responses in the epidermis. This negative regulatory role for

DAPK in innate immunity may be analogous to the roles of mammalian DAPK in inflammatory responses.

2.2 Introduction

Death associated protein kinase (DAPK) was first discovered from a functional antisense RNA based screen in cell culture for suppressors of interferon (IFN)-induced cell death (Deiss et al., 1995). DAPK is characterized by a conserved Ca^{2+}/Calmodulin (CaM) regulatory domain, a serine/threonine kinase domain, and several other conserved noncatalytic domains (Figure 2.1). DAPK's link to cell death was primarily deduced from *in vitro* experiments, in which over-expression of DAPK in cell culture resulted in cell membrane blebbing and other apoptotic features (Inbal et al., 2002). DAPK is required for induction of cell death by various death signals (Lin et al., 2010). Further investigation showed that the mode of cell death was dependent on cell type. Over-expression of DAPK in certain cells, such as primary fibroblasts, induced caspase-dependent cell death, apoptosis-associated morphological changes (Harrison et al., 2008), and DNA fragmentation (reviewed by (Gozuacik and Kimchi, 2006)). In other cells, such as HeLa and MCF-7, overexpression resulted in the formation of autophagic vesicles and autolysosomes in the cytoplasm (Inbal et al., 2002). Although autophagy can promote cell survival, it can also cause autophagic (type-II) programmed cell death. DAPK and related kinases are now recognized as playing a wide variety of roles in apoptotic and autophagic cell death and other processes in mammals. One challenge in defining the normal functions of DAPK has been the functional redundancy in the mammalian DAPK

family. As *C. elegans* and Drosophila each encode only a single DAPK family member, genetic analyses in these genetic model organisms could provide insights into the functions of DAPK in normal development and physiology. Here we review findings on DAPK and related kinases from *C. elegans* and Drosophila and attempt to draw connections between these results and studies in mammalian models.

2.3 Phylogenetics of the DAPK family

DAPK-like proteins are found throughout the animal kingdom, but are by far best studied in mammals, i.e. mouse and human. Mammalian DAPK (now DAPK1) is a multidomain protein, consisting of a kinase domain, a calcium-calmodulin (Ca^{2+}/CaM) regulatory domain, ankyrin repeats, P-loop motifs, a death domain, and additional conserved motifs (Bialik and Kimchi, 2012). In addition to DAPK, mammals encode a family of 'DAPK related' kinases that share a closely related kinase domain, and in some cases, a Ca^{2+}/CaM regulatory domain. The DAPK protein family consists of DAPK1 itself, DAPK2 (also known as DRP-1) and DAPK3 (previously known as Zipper interacting kinase, ZIPk). More divergent members of the DAPK family are the DAP kinase related apoptosis inducing protein kinases DRAK1 and 2. The DAPK family has been classified as part of the DMT subfamily of Ca^{2+}/CaM-dependent kinases (Temmerman et al., 2013). All members of the DAPK group have been linked to cell death (Murata-Hori et al., 2001, Sanjo et al., 1998). As the extracatalytic domains and biological function of these proteins differ drastically (Lin et al., 2010), suggesting that DAPK1 has unique roles compared to other DAPK-like proteins.

In general, invertebrates express fewer members of the DAPK family; ZIPK and DRP-1 are found only in mammals. Among invertebrates, nematodes, certain arthropods such as bees, ants, arachnids, and sea urchins have encode proteins similar to DAPK1 (that is, containing the noncatalytic domains such as the ankyrin repeats and a C-terminal death domain) (Figure 2.1A). *C. elegans* encodes a single family member, DAPK-1, overall 33% identical in sequence to human DAPK1 (Tong et al., 2009). Interestingly, *Drosophila melanogaster* lacks a canonical DAPK1 ortholog and instead encodes a single DRAK-like protein, Drak (Neubueser and Hipfner, 2010). The silkworm *Bombyx* also encodes a Drak-like protein. Other arthropod genomes, such as those of *Tribolium* (beetles) or arachnids, are predicted to encode proteins resembling truncated versions of DAPK1, lacking the kinase domain and Ca^{2+}/CaM regulatory domains, but containing ankyrin repeats and a DAPK-like death domain (Figure 2.1B). Among the lophotrochozoa, *Aplysia* encodes a similar kinase-less protein. DAPK1-like proteins are evident in the genomes of echinoderms (sea urchin) and of various non-vertebrate chordates (not shown), but their functions remain unstudied.

2.4 *C. elegans* DAPK-1 regulates autophagy

The function of the *C. elegans dapk-1* gene has been addressed by genetic mutations and RNA interference. Animals mutant for *dapk-1* loss-of-function alleles are viable and fertile, with progressive defects in epidermal structure as described below. Developmentally programmed apoptotic cell deaths appear to occur in *dapk-1* mutants, although a detailed analysis has not yet been reported. Thus, a subtle or redundant role

for *C. elegans* DAPK-1 in apoptosis cannot be excluded. In contrast, DAPK-1 has been clearly linked to stress-induced autophagy. In *C. elegans*, starvation activates a MAPK pathway in the pharyngeal muscles via muscarinic acetylcholine receptor signaling, which acts to increase muscle activity (You et al., 2006). In mutants lacking the G protein β subunit GPB-2, starvation induces damage to the pharyngeal muscle via excessive autophagy, due to constitutive active muscarinic signaling (Kang et al., 2007). Autophagy of pharyngeal muscles renders the worms unable to feed, ultimately leading to lethality. Loss of function in the key autophagy factor beclin/*bec-1* rescues the organismal death of *gpb-2* mutants, confirming that elevated autophagy was the cause of death. By screening candidate cell death genes, Kang et al.. showed that *dapk-1* loss of function partly suppressed the starvation-induced autophagy and lethality of *gpb-2* mutants (Kang et al., 2007). As loss of function in the key apoptotic caspase CED-3 did not rescue the starvation-induced death of *gpb-2* mutants, DAPK-1's effect is unlikely to be due to a role in apoptosis. Thus, it seems that *dapk-1* acts downstream of or in parallel to muscarinic signaling to promote starvation-induced autophagy. Interestingly, *DAPK(-/-)* knockout mice are defective in ER stress-induced autophagic and apoptotic cell death (Gozuacik et al., 2008). Thus, the DAPK family may play a conserved role in stress-induced cell death.

2.5 Roles in epidermal morphogenesis, epithelial integrity, and wound healing

C. elegans dapk-1 mutations were also independently identified in forward genetic screens for mutants displaying aberrant epidermal morphogenesis (Tong et al., 2009). *dapk-1* loss of function mutants display progressive defects in the morphology of the epidermis and cuticle (Figure 2.2A). This aberrant morphology involves over-accumulation of collagens and other cuticle components, making the cuticle up to 5–10 times thicker than wild type. The cuticle over-secretion is first apparent in late larval stages and becomes progressively more severe during adult life; defects are also spatially confined to the head, tail, vulva, and interfacial regions of the epidermis. These morphological defects do not seem to result from mis-regulation of apoptosis or autophagy, as loss of function in core apoptosis or autophagy genes neither phenocopied nor suppressed the cuticle defects in *dapk-1* mutants (Tong et al., 2009). The cuticle deposits of *dapk-1* mutants contain autofluorescent aggregates similar to components of scars that form after skin wounding (Pujol et al., 2008), suggesting *dapk-1* might negatively regulate epidermal wound responses.

DAPK-like kinases also play roles in epithelial morphogenesis or integrity in *Drosophila*. Mutants lacking the *Drosophila* Drak are viable and fertile and show normal levels of apoptosis. However *drak* null mutants display shortened and malformed appendages (wings and legs) reminiscent of *rok* mutants defective in Rho-associated protein kinase (Neubueser and Hipfner, 2010). *drak* displays dose-dependent genetic interactions with *rok* mutants, in that *drak(-/-) rok(+/-)* animals display defects in the tracheal and wing disk epithelia. These tissues are thinned and distorted, likely from cell loss due to high levels of apoptosis in the epithelia. Hence, the loss of epithelial integrity in *drak* mutants is mechanistically distinct from the apparently apoptosis-independent

epidermal defects of *C. elegans dapk-1* mutants. Furthermore, *drak-/- rok-/-* mutants displayed fully penetrant defects in head involution, a process in which dorsal and lateral epidermal cells spread to cover the anterior end of the embryo, suggesting Drak is important in epithelial morphogenesis at multiple stages of development. *Drosophila* Drak also functions redundantly with Rok to promote adherens junction remodeling during morphogenesis of ommatidia from the eye disk neuroepithelium (Robertson et al., 2012). In summary, DAPK family members play either subtle or partly redundant roles in the morphology and integrity of epithelia of Drosophila and *C. elegans*.

2.6 DAPK-1 regulation of actin dynamics in epithelial development and wound healing

DAPK has long been known to associate with actin microfilaments (Cohen et al., 1997). DAPK localizes to actin stress fibers in HeLa cells, and when over-expressed, induces extensive membrane protrusions and membrane blebbing (Bialik et al., 2004). These cytoplasmic changes are a result of DAPK mediated phosphorylation of myosin-II regulatory light chain (RLC) and may contribute to DAPK's pro-apoptotic activity. *In vivo*, DAPK family members play important roles in regulating actin dynamics. In *Drosophila*, Drak phosphorylates the fly myosin RLC (Sqh) to promote proper morphogenesis of epithelial tissues during development (Neubueser and Hipfner, 2010). Drak and Rok can each phosphorylate Sqh, explaining their synergistic lethality; expression of a constitutively activated Sqh can strongly rescue the elevated apoptosis and lethality of the *drak rok* double mutant.

The regulation of the actin cytoskeleton by DAPK is important in epidermal wound healing in *C. elegans*. The worm epidermis is a simple barrier epithelium that provides the first line of defense against pathogens and wounds (Ewbank, 2002, Chisholm and Xu, 2012). As the nematode body is under hydrostatic pressure, it is imperative that damage to the epidermis be repaired rapidly for the worm to survive. Wounding causes massive calcium influx into the epidermal cytoplasm, triggering a Gqα signaling cascade that results in actin-mediated wound closure (Xu and Chisholm, 2011). During wound closure, an actin ring forms around the wound site. In *dapk-1* mutants, actin rings closed more rapidly around the wound site compared to wild type. Reduced Ca^{2+} signaling did not suppress *dapk-1* fast wound closure, but loss of *dapk-1* function does suppress the low post-wound survival of Gqα mutants. These results support DAPK-1 acting as a negative regulator of wound closure dynamics in the epidermal epithelium, likely downstream of Ca^{2+} signals. Mammalian DAPK has also been studied in the context of wound repair, using the *in vitro* scratch assay. When NIH3T3 derivatives were assayed for wound-healing migration, over-expression of DAPK caused a significant delay in wound closure (Kuo et al., 2006). Possibly, the impaired wound healing migration in DAPK over-expressing cells reflects misregulation of the actin cytoskeleton.

2.7 DAPK-1 is a negative regulator of epithelial innate immunity in *C. elegans*

In *C. elegans* as in other animals the skin is a barrier epithelium, forming the first line of defense against external pathogens and physical damage (Chisholm and Xu, 2012). *C. elegans* is now known to have a sophisticated and robust epidermal innate immune response that protects animals from infection via the skin. Infection by epidermis-penetrating fungi such as *Drechmeria coniospora* induces expression of numerous antimicrobial peptide (AMP) genes (Couillault et al., 2004). Sterile skin wounding by needles or laser damage induces an overlapping set of responses (Pujol et al., 2008). In *dapk-1* mutants transcription of AMPs such as *nlp-29* is constitutively up-regulated in the epidermis (Tong et al., 2009). This upregulation in *dapk-1* mutants can be rescued by epidermal-driven DAPK-1 expression, suggesting *dapk-1* acts cell autonomously to inhibit the innate immune response. Moreover, transient over-expression of DAPK-1 can suppress the up-regulation of *nlp-29* in response to needle wounding, indicating that DAPK-1 can acutely block innate immune responses to damage.

Induction of the AMP *nlp-29* by infection or wounding requires the SARM protein TIR-1 and a p38 MAPK cascade, acting in the epidermis (Pujol et al., 2008) (Figure 2.2). TIR-1 and the p38 MAPK cascade are required for the constitutive induction of *nlp-29* in *dapk-1* mutants, indicating DAPK-1acts upstream of the TIR-1/p38 signaling pathway. The TIR-1/p38MAPK pathway in epidermal AMP induction after infection is regulated by G-protein signaling and by TPA-1/Protein kinase C δ (Ziegler et al., 2009). Additional epistasis analysis is required to define where DAPK-1 intersects with the signaling cascade upstream of TIR-1. It will also be interesting to see what other

pathways DAPK-1 interacts with to control the expression of the other AMPs that are upregulated after septic or sterile wounding.

Loss of function in the TIR-1/p38 MAPK cascade does not affect the cuticle hypertrophy phenotype of *dapk-1* mutants. Conversely, suppression of *dapk-1* cuticle hypertrophy by loss of function in the pre-mRNA 3' end processing regulatory gene *sydn-1* (Van Epps et al., 2010) did not affect the constitutive induction of epithelial innate immunity genes. Together these results suggest that DAPK-1 acts independently to regulate epidermal morphology and epithelial innate immunity.

2.8 DAPK and innate immunity in vertebrates

Several studies have pointed to roles for mammalian DAPK in regulating innate immune responses, specifically inflammatory responses. Initially, DAPK was found to act as a checkpoint in the macrophage inflammation program (Mukhopadhyay et al., 2008) and as a negative regulator of T-cell receptor-mediated activation of NFκB (Chuang et al., 2008). Interestingly, the negative regulatory role of DAPK1 in NFκB activation may involve PKCθ, a homolog of TPA-1. In addition, DAPK knockout mice suffer from lung inflammation after lipopolysaccharide (LPS) challenge, due to the hypersecretion of cytokines such as IL-6 from macrophages and neutrophils (Nakav et al., 2012). Recent work has elucidated a possible mechanism by which DAPK might regulate innate immunity (Chakilam et al., 2013). DAPK levels were elevated in ulcerative colitis-associated carcinoma (UCC), suggesting a protective role for DAPK in intestinal epithelial cells. DAPK binds and inhibits the transcription factor STAT3;

conversely, STAT3 appears to repress DAPK transcription. This mutual negative regulation of STAT3 and DAPK may provide a finely balanced mechanism for regulating TNF-induced inflammation. Intriguingly, a *C. elegans* STAT-like protein STA-2 has been implicated in epidermal innate immunity. Loss of STA-2 activity by mutation or RNAi prevents up-regulation of *nlp-29* after wounding (Dierking et al., 2011). STA-2 acts downstream of the PMK-1 MAPK cascade, and may regulate transcription in the epidermis, but also localizes to endocytic vesicles in the cytoplasm. It will be interesting to learn if DAPK-1 and STA-2 interact in ways analogous to the DAPK/STAT3 circuit revealed in mammals. In summary, the role of mammalian DAPK as a negative regulator of inflammatory responses has intriguing parallels to its function as a negative regulator of epithelial innate immune responses in *C. elegans*.

2.9 Conclusions and Questions

In contrast to the abundant evidence linking mammalian DAPK to cell death, DAPK family proteins in *C. elegans* and Drosophila appear largely dispensable for developmental apoptosis. *C. elegans* DAPK-1 promotes starvation-induced autophagy, but has not been linked more generally to autophagic cell death. It should be noted that mouse *DAPK1* knockout mutants also display normal developmental apoptosis (Gozuacik et al., 2008). It is possible that these different pictures of the role of the DAPK family in part reflect the differences between loss and gain of function studies.

Instead, *C. elegans* DAPK-1 functions in epithelial integrity, wound healing, and innate immunity; Drosophila DRAK also functions in epithelial development. *C. elegans*

DAPK-1 acts as a coordinated negative regulator of epidermal innate immune defenses. It is not yet understood at a mechanistic level how *C. elegans* DAPK-1 regulates innate immunity, nor whether it is actively regulated during stresses such as epidermal infection or wounding. An important goal is to define where DAPK-1 intersects with the PKC/TIR-1/MAPK pathway in regulation of innate immunity.

Independently of its roles in innate immunity, DAPK-1 regulates the morphology of the epidermis. DAPK-1 is not required for embryonic epidermal morphogenesis, but appears to influence a post-embryonic epidermal maintenance process. It remains to be elucidated whether DAPK-1 primarily affects the epidermal cytoskeleton, polarity, secretion, or a combination of these. In wound repair DAPK-1 likely regulates the actin cytoskeleton via non-muscle myosin, reminiscent of the functions of Drosophila *Drak* and consistent with much evidence that DAPK1 regulates nonmuscle myosin. DAPK1 also interacts with the microtubule cytoskeleton; DAPK1 binds MAP1B (Harrison et al., 2008), and has been shown to inhibit MT assembly via the MARK/PAR-1 kinase family (Wu et al., 2011). It will be interesting to determine whether the aberrant epithelial integrity of *C. elegans dapk-1* mutants involves alterations in the microtubule cytoskeleton. Further studies of DAPK-1 in *C. elegans* may yield additional insights into the functions of this ancient family of kinases.

2.10 Acknowledgments

Chapter 2 is a reformatted reprint in full of Chuang M and Chisholm A. Insights into the functions of the death associated protein kinases from *C. elegans* and other

invertebrates. *Apoptosis*. 2014 Feb;19(2):392-7 with permission of all authors. The dissertation author was the primary author of this paper.

M.C. is supported by the UCSD Cellular and Molecular Genetics Training Grant (NIH T32 GM007240). Work in the laboratory on DAPK is supported by NIH R01 GM054657 to A.D.C.

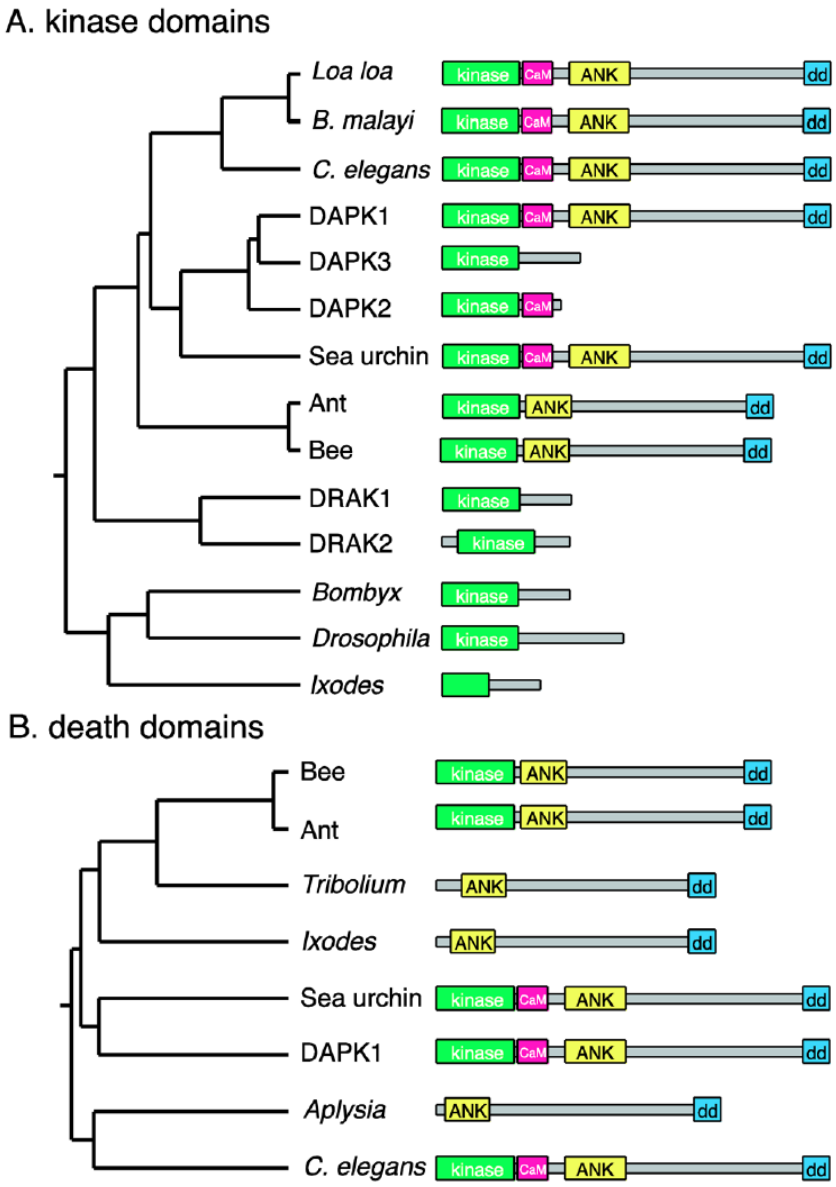

Figure 2.1: Phylogeny of the DAPK family.

A. Tree based on pairwise alignment (ClustalW) analysis of the amino acid sequences of the kinase domains of DAPK family members, along with cartoons of the protein domain architecture, approximately to scale. Human DAPK1 and DAPK family members are compared with related proteins predicted from genome sequences of various invertebrate species. B: Tree based on alignments of the death domains. To simplify the domain structures, the P-loops and ROCO domains are not shown. NCBI sequence accession numbers: *C. elegans* (O44997.2); *Loa loa* (EJD74144.1); *Brugia malayi* (XP_001896664.1), Human DAPK1 (AAI43760.1); Human DAPK3 (NP_001339.1); Human DAPK2 (Q9UIK4.1); sea urchin *Strongylocentrotus purpuratus* (XP_003723347.1); carpenter ant *Camponotus floridanus* (E1ZVV1); honey bee *Apis florea* (XP_003689717.1); Human DRAK1 (BAA34126.1), Human DRAK2 (BAA34127.1); silkworm *Bombyx mori* (E9JEH2); *Drosophila Drak* (E1JJH9); deer tick *Ixodes scapularis* (EEC12134.1). Kinase-less sequences: flour beetle *Tribolium castaneum* (XP_972597.2); *I. scapularis* (EEC05408.1); sea slug *Aplysia californica* (XP_005108326.1).

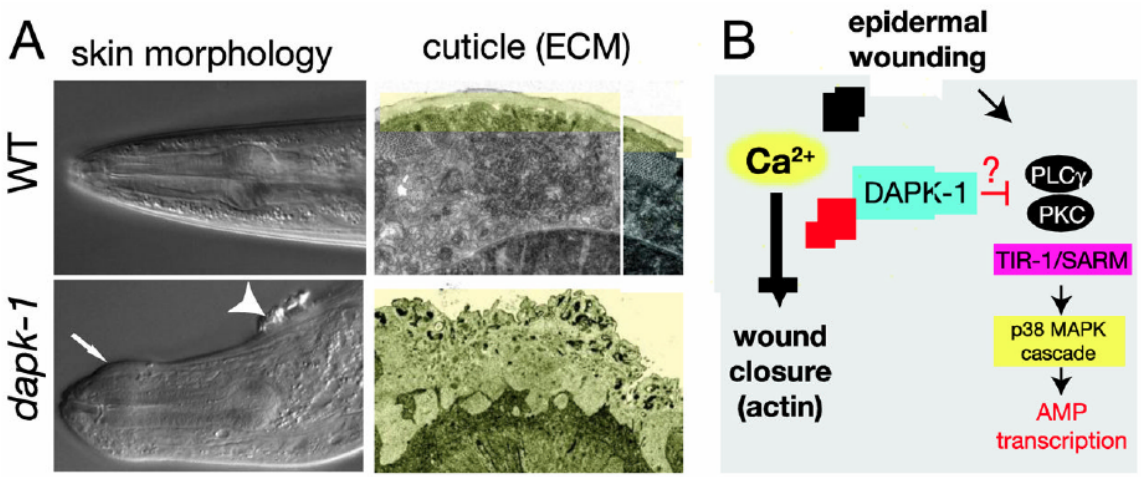

Figure 2.2. *C. elegans* DAPK-1 and epidermal development

A. Images of the *dapk-1* epidermal morphology phenotype, taken from Tong et al., 2009 (10). *dapk-1(ju4)* mutant adults display deformations of the epidermis (arrow and arrowhead, left panels) visible under DIC microscopy. Electron microscopy (right panels) reveals massive expansion of the cuticle (colored yellow) in the head region. B. Model for DAPK-1 function in wound responses as a negative regulator of the actin cytoskeleton and innate immunity (AMP transcription). See also (Xu and Chisholm, 2011).

2.11 References

Bialik S, Bresnick AR, Kimchi A. (2004) DAP-kinase-mediated morphological changes are localization dependent and involve myosin-II phosphorylation. Cell Death Differ 11:631-644.

Bialik S, Kimchi A. (2012) Biochemical and functional characterization of the ROC domain of DAPK establishes a new paradigm of GTP regulation in ROCO proteins. Biochem Soc Trans 40:1052-1057.

Chakilam S, Gandesiri M, Rau TT, Agaimy, A., Vijayalakshmi, M., Ivanovska, J., Wirtz, R. M., Schulze-Luehrmann, J., Benderska, N., Wittkopf, N., Chellappan, A., Ruemmele, P., Vieth, M., Rave-Frank, M., Christiansen, H., Hartmann, A., Neufert, C., Atreya, R., Becker, C., Steinberg, P., Schneider-Stock, R. (2013) Death-associated protein kinase controls STAT3 activity in intestinal epithelial cells. Am J Pathol 182:1005-1020.

Chisholm AD, Xu S. (2012) The epidermis as a model skin. II: differentiation and physiological roles. Wiley Interdiscip Rev Dev Biol 1:879-902.

Chuang YT, Fang LW, Lin-Feng MH, Chen RH, Lai MZ. (2008) The tumor suppressor death-associated protein kinase targets to TCR-stimulated NF-kappa B activation. J Immunol 180:3238-3249.

Cohen O, Feinstein E, Kimchi A. (1997) DAP-kinase is a Ca2+/calmodulin-dependent, cytoskeletal-associated protein kinase, with cell death-inducing functions that depend on its catalytic activity. The EMBO journal 16:998-1008.

Couillault C, Pujol N, Reboul J, Sabatier, L.
Guichou, J. F., Kohara, Y., Ewbank, J. J. (2004) TLR-independent control of innate immunity in *Caenorhabditis elegans* by the TIR domain adaptor protein TIR-1, an ortholog of human SARM. Nature immunology 5:488-494.

Deiss LP, Feinstein E, Berissi H, Cohen O, Kimchi A. (1995) Identification of a novel serine/threonine kinase and a novel 15-kD protein as potential mediators of the gamma interferon-induced cell death. Genes & development 9:15-30.

Dierking K, Polanowska J, Omi S,Engelmann, I., Gut, M., Lembo, F., Ewbank, J. J., Pujol, N. (2011) Unusual regulation of a STAT protein by an SLC6 family transporter in C. elegans epidermal innate immunity. Cell Host Microbe 9:425-435.

Ewbank JJ. (2002) Tackling both sides of the host-pathogen equation with *Caenorhabditis elegans*. Microbes Infect / Institut Pasteur 4:247-256.

Gozuacik D, Bialik S, Raveh T, Mitou, G., Shohat, G., Sabanay, H., Mizushima, N.,

Yoshimori, T., Kimchi, A. (2008) DAP-kinase is a mediator of endoplasmic reticulum stress-induced caspase activation and autophagic cell death. Cell Death Differ 15:1875-1886.

Gozuacik D, Kimchi A. (2006) DAPk protein family and cancer. Autophagy 2:74-79.

Harrison B, Kraus M, Burch L, Stevens, C., Craig, A., Gordon-Weeks, P., Hupp, T. R. (2008) DAPK-1 binding to a linear peptide motif in MAP1B stimulates autophagy and membrane blebbing. The Journal of biological chemistry 283:9999-10014.

Inbal B, Bialik S, Sabanay I, Shani G, Kimchi A. (2002) DAP kinase and DRP-1 mediate membrane blebbing and the formation of autophagic vesicles during programmed cell death. The Journal of cell biology 157:455-468.

Kang C, You YJ, Avery L. (2007) Dual roles of autophagy in the survival of *Caenorhabditis elegans* during starvation. Genes & development 21:2161-2171.

Kuo JC, Wang WJ, Yao CC, Wu PR, Chen RH. (2006) The tumor suppressor DAPK inhibits cell motility by blocking the integrin-mediated polarity pathway. The Journal of cell biology 172:619-631.

Lin Y, Hupp TR, Stevens C. (2010) Death-associated protein kinase (DAPK) and signal transduction: additional roles beyond cell death. Febs J 277:48-57.

Mukhopadhyay R, Ray PS, Arif A, Brady AK, Kinter M, Fox PL. (2008) DAPK-ZIPK-L13a axis constitutes a negative-feedback module regulating inflammatory gene expression. Molecular cell 32:371-382.

Murata-Hori M, Fukuta Y, Ueda K, Iwasaki T, Hosoya H. (2001) HeLa ZIP kinase induces diphosphorylation of myosin II regulatory light chain and reorganization of actin filaments in nonmuscle cells. Oncogene 20:8175-8183.

Nakav S, Cohen S, Feigelson SW, Bialik, S., Shoseyov, D., Kimchi, A., Alon, R. (2012) Tumor suppressor death-associated protein kinase attenuates inflammatory responses in the lung. Am J Respir Cell Mol Biol 46:313-322.

Neubueser D, Hipfner DR. (2010) Overlapping roles of Drosophila Drak and Rok kinases in epithelial tissue morphogenesis. Molecular biology of the cell 21:2869-2879.

Pujol N, Cypowyj S, Ziegler K, Millet, A., Astrain, A., Goncharov, A., Jin, Y., Chisholm, A. D., Ewbank, J. J. (2008) Distinct Innate Immune Responses to Infection and Wounding in the *C. elegans* Epidermis. Curr Biol 18:481-489.

Pujol N, Zugasti O, Wong D,Couillault, C., Kurz, C. L., Schulenburg, H., Ewbank, J. J. (2008) Anti-fungal innate immunity in *C. elegans* is enhanced by evolutionary

diversification of antimicrobial peptides. PLoS Pathogens 4:e1000105.

Robertson F, Pinal N, Fichelson P, Pichaud F. (2012) Atonal and EGFR signalling orchestrate rok- and Drak-dependent adherens junction remodelling during ommatidia morphogenesis. Development (Cambridge, England) 139:3432-3441.

Sanjo H, Kawai T, Akira S. (1998) DRAKs, novel serine/threonine kinases related to death-associated protein kinase that trigger apoptosis. The Journal of biological chemistry 273:29066-29071.

Temmerman K, Simon B, Wilmanns M. (2013) Structural and functional diversity in the activity and regulation of DAPK-related protein kinases. FEBS J in press.

Tong A, Lynn G, Ngo V, Wong, D., Moseley, S. L., Ewbank, J. J., Goncharov, A., Wu, Y. C., Pujol, N., Chisholm, A. D. (2009) Negative regulation of *Caenorhabditis elegans* epidermal damage responses by death-associated protein kinase. Proceedings of the National Academy of Sciences of the United States of America 106:1457-1461.

Van Epps H, Dai Y, Qi Y, Goncharov A, Jin Y. (2010) Nuclear pre-mRNA 3'-end processing regulates synapse and axon development in C. elegans. Development (Cambridge, England) 137:2237-2250.

Wu PR, Tsai PI, Chen GC,Chou, H. J., Huang, Y. P., Chen, Y. H., Lin, M. Y., Kimchi, A., Chien, C. T., Chen, R. H. (2011) DAPK activates MARK1/2 to regulate microtubule assembly, neuronal differentiation, and tau toxicity. Cell Death Differ 18:1507-1520.

Xu S, Chisholm AD. (2011) A Galphaq-Ca(2)(+) signaling pathway promotes actin-mediated epidermal wound closure in C. elegans. Current biology : CB 21:1960-1967.

You YJ, Kim J, Cobb M, Avery L. (2006) Starvation activates MAP kinase through the muscarinic acetylcholine pathway in Caenorhabditis elegans pharynx. Cell Metab 3:237-245.

Ziegler K, Kurz CL, Cypowyj S, Couillault, C., Pophillat, M., Pujol, N., Ewbank, J. J. (2009) Antifungal innate immunity in C. elegans: PKCdelta links G protein signaling and a conserved p38 MAPK cascade. Cell Host Microbe 5:341-352.

Chapter 3

The microtubule minus end binding protein Patronin/PTRN-1 is required for axon regeneration in *C. elegans*

3.1 Abstract

Precise regulation of microtubule dynamics is increasingly recognized as a critical determinant of axon regeneration. In contrast to developing neurons, mature axons exhibit noncentrosomal microtubule nucleation. The factors regulating noncentrosomal MT architecture in axon regeneration remain poorly understood. We report that PTRN-1, the *C. elegans* member of the Patronin/Nezha/CAMSAP family of microtubule minus end binding proteins, is critical for efficient axon regeneration in vivo. *ptrn-1* null mutants display generally normal developmental axon outgrowth but significantly impaired regenerative regrowth after laser axotomy. Unexpectedly, mature axons in *ptrn-1* mutants display elevated numbers of dynamic axonal MTs before and after injury, suggesting PTRN-1 inhibits MT dynamics. The CKK domain of PTRN-1 is necessary and sufficient for its functions in axon regeneration and MT dynamics, and appears to stabilize MTs independent of minus end localization. Whereas in developing neurons PTRN-1 inhibits activity of the DLK-1 MAPK cascade, we find that in regeneration

PTRN-1 and DLK-1 function together to promote axonal regrowth.

3.2 Introduction

The ability of axons to regenerate their structure after injury is now recognized as a fundamental and conserved property of neurons. The ability of axons to regrow in vivo is modulated by a large number of interacting influences, including the extracellular microenvironment and the intrinsic growth state of the neuron. Recent studies have begun to reveal the molecular determinants of the neuronal growth state (Liu et al., 2011). In vertebrate neurons, intrinsic determinants of axon regrowth include PTEN (Park et al., 2008) and the KLF transcription factors (Moore et al., 2009). Studies of axon regrowth in genetic model organisms such as *C. elegans* have also contributed to our understanding of axon regeneration mechanisms (Hammarlund and Jin, 2014). In *C. elegans* the DLK-1 MAPK cascade has been revealed as a key intrinsic regulator of regrowth initiation, and may act to sense axonal damage (Hammarlund et al., 2009; Yan and Jin, 2012; Yan et al., 2009). DLK kinases also play critical roles in axon regrowth in Drosophila and mammals (Tedeschi and Bradke, 2013; Xiong et al., 2010).

Regulation of axonal microtubule (Bounoutas et al.) dynamics has emerged as a key factor in axonal regrowth potential. The MT network of mature axons is largely composed of stable MTs. Axon injury triggers an intricate series of changes in axonal MT organization and dynamics that drive formation of regenerative growth cones and subsequent axon extension (Bradke et al., 2012; Chisholm, 2013). After injury, microtubule dynamics are upregulated by a variety of mechanisms (Sahly et al., 2006; Stone et al., 2010). Interestingly, partial stabilization of axonal MTs by pharmacological

treatment after spinal cord injury promotes axon regrowth (Hellal et al., 2011; Sengottuvel et al., 2011). Loss of function in MT destabilization factors can enhance axon regrowth in *C. elegans* (Chen et al., 2011; Ghosh-Roy et al., 2012). Conversely, failure to regenerate correlates with disorganization of the axonal MT cytoskeleton (Erturk et al., 2007). These studies highlight the importance of MT remodeling as a conserved intrinsic determinant of axon regeneration capacity.

In dividing cells the centrosome is the dominant microtubule organizing center, with minus ends stabilized at the centrosome and plus ends exhibiting growth and dynamic instability. In contrast, the MT cytoskeleton of neurons is predominantly noncentrosomal (Keating and Borisy, 1999). In mature axons, MTs are uniformly oriented with plus ends distal, and their minus ends are not directly associated with the centrosome. A well-established model for axonal MT biogenesis is that axonal MTs are nucleated at the centrosome, then cleaved and translocated into the axon during axonal development and regeneration (Ahmad et al., 1994; Baas et al., 1993; Conde and Caceres, 2009; Yu et al., 1993). However, recent findings suggest that at least some axonal MTs can form independently of the centrosome in mammalian neurons (Stiess et al., 2010). In Drosophila neurons MT organization is unaltered by laser ablation or mutational disruption of the centrosome (Nguyen et al., 2011), and γ-tubulin either at Golgi outposts or at other axonal locations appears to be involved in nucleation of noncentrosomal MT (Nguyen et al., 2014; Ori-McKenney et al., 2012). The control of noncentrosomal MT stabilization in neuronal processes remains poorly understood.

The Patronin/Nezha/CAMSAP family of MT-binding proteins are key regulators of noncentrosomal MT architecture in a variety of cell types. CAMSAPs can bind

specifically (Meng et al., 2008) and directly to MT minus ends (Goodwin and Vale, 2010; Hendershott and Vale, 2014; Jiang et al., 2014). Of the three mammalian CAMSAPs, CAMSAP2 is important for axon specification and dendrite morphology in mouse hippocampal neurons (Yau et al., 2014). *C. elegans* encodes a single Patronin/CAMSAP, PTRN-1. *ptrn-1* null mutants are viable and superficially normal in behavior and morphology, but are hypersensitive to MT destabilizing drugs (Marcette et al., 2014; Richardson et al., 2014). Neurons of *ptrn-1* null mutants display impenetrant synapse morphology and axon overgrowth defects that have been interpreted as the result of activation of a regenerative program involving the DLK-1 cascade. However the role of Patronins in axon regeneration has not been directly evaluated.

Here we report that although *ptrn-1* mutants display near-normal developmental axon outgrowth, they are strongly impaired in axon regeneration. The requirement for PTRN-1 in regeneration is bypassed by loss of function in the MT depolymerase kinesin-13/KLP-7. *ptrn-1* mutants display reduced numbers of axonal MTs, yet have increased numbers of dynamic axonal MTs. The aberrant MT dynamics of *ptrn-1* mutants are suppressed by loss of function in the DLK-1 pathway. Despite this, PTRN-1 can act independently of DLK-1 in regeneration, and PTRN-1 overexpression induces collateral branches in *dlk-1* null mutants. We conclude that PTRN-1 plays a critical role in noncentrosomal MT dynamics in axon regrowth and that the relationship of PTRN-1 and DLK-1 in regeneration is distinct from that in development.

3.3 Results

3.3.1. *C. elegans* Patronin/PTRN-1 is required for axon regeneration

To address the role of PTRN-1 in axon regeneration we examined three *ptrn-1* putative null mutant alleles, collectively *ptrn-1(0)* (see Experimental Procedures). We confirmed previous findings that *ptrn-1(0)* mutants are viable and superficially normal in behavior, with incompletely penetrant defects in touch neuron morphology (Marcette et al., 2014). For example, in *ptrn-1(0)* mutants the cell bodies of ALM neurons extend ectopic posterior neurites of varying lengths (Figure 3.2A). Nonetheless, PTRN-1 is generally dispensable for developmental axon outgrowth.

To investigate roles of PTRN-1 in axon regeneration, we used femtosecond laser surgery to sever the PLM axon in *ptrn-1(0)* mutants and imaged axon regrowth. PLM axon regrowth was significantly impaired in *ptrn-1(0)* mutants, decreasing to 60-75% of wild type regrowth at 24 h post axotomy (24 hpa) (Figure 3.1A,B). The PLM regeneration defects of *ptrn-1(0)* mutants were rescued by pan-neural expression of PTRN-1, consistent with PTRN-1 acting cell autonomously (Figure 3.1A,B). Pan-neural overexpression of PTRN-1 in wild type background did not enhance PLM regrowth (Figure 3.1A), suggesting PTRN-1 levels are not rate limiting in regeneration. In *ptrn-1(lt1)* and *ptrn-1(tm5597)* mutants, and to a lesser extent in *ptrn-1(ju698)*, axotomy of PLM occasionally triggered growth of small neurites ("sprouting") from the soma (Figure 3.1B; Figure 3.2B); this phenotype was fully rescued by PTRN-1::GFP transgenes (Figure 3.2B). Regeneration of the commissures of D type motor neurons was also impaired in *ptrn-1* mutants (Figure 3.2C,D), indicating PTRN-1 is required for efficient regeneration of diverse neuron types.

Reduced axon regrowth at 24 hpa may reflect defects in axon extension or in growth cone formation (Chen et al., 2011). We examined PLM regrowth in *ptrn-1(0)* at 6 and 48 hpa and found that regrowth was significantly reduced at all time points (Figure 3.1C), reflecting a reduced rate of PLM axon extension throughout the period of regrowth (Figure 3.1D). *ptrn-1(0)* mutant axons formed regenerative growth cones at similar frequencies to the wild type at 6 and 24 hpa; by 48 hpa growth cones remained in *ptrn-1(0)* mutants but were mostly absent from wild type axons (Figure 3.1E). Thus, PTRN-1 is not required for formation of regenerative growth cones; the persistence of growth cones at 48 hpa may reflect slower regrowth of *ptrn-1* axons.

To define when in regrowth PTRN-1 was required we induced PTRN-1 expression at different times relative to axotomy and assayed rescue of the *ptrn-1(0)* regrowth phenotypes at 24 hpa (see Experimental Procedures). Induction of PTRN-1 4 h or 1 h before axotomy fully rescued *ptrn-1(0)* regrowth defects (Figure 3.1F). In contrast, induction at 6 hpa failed to rescue *ptrn-1(0)* (Figure 3.1F), suggesting PTRN-1 function is required within the first 6 h after injury and that the decreased regrowth of *ptrn-1(0)* is not caused by earlier developmental defects.

We further probed the temporal requirements for PTRN-1 function by protein inhibition using miniSOG based Chromophore-Assisted Light Inactivation (CALI). miniSOG absorbs blue light and generates singlet oxygen when illuminated with high intensity blue light (Shu et al., 2011), allowing inactivation of tagged proteins via CALI (Lin et al., 2013; Zhou et al., 2013). PTRN-1::miniSOG fully rescued the regrowth defects of *ptrn-1(0)* neurons without blue light illumination (Figure 3.1G). Illumination with blue light a few minutes before axotomy abolished *ptrn-1* rescuing activity (Figure

3.1G), suggesting PTRN-1::miniSOG was efficiently inactivated by CALI. Pan-neuronal expression of a control construct expressing cytosolic miniSOG did not affect regrowth, with or without blue light treatment. We then used blue light illumination at different time points to dissect when PTRN-1 function was required. Blue light illumination 6 h before axotomy, or minutes prior to axotomy ('0 h'), completely abolished PTRN-1::miniSOG rescuing activity, whereas inactivation 6 hpa only partially inhibited PTRN-1 function (Figure 3.1G), consistent with PTRN-1 being required in the first few hours after axon injury.

3.3.2 Axonal MT dynamics are upregulated in *ptrn-1(0)* mutants before and after axon injury

ptrn-1(0) mutants display fewer dynamic MTs in PHC dendrites, and are sensitized to MT depolymerizing drugs, suggesting PTRN-1 stabilizes MTs (Richardson et al., 2014). We therefore tested whether the impaired axon regeneration of *ptrn-1(0)* mutants reflected altered MT dynamics, using GFP-tagged end-binding protein (EBP) to track growing MT plus ends (Ghosh-Roy et al., 2012; Stepanova et al., 2003). In the wild type uninjured PLM axon, few EBP comets are visible, consistent with most MTs being stabilized (Ghosh-Roy et al., 2012). In contrast, *ptrn-1(0)* mutants displayed a two-fold increase in the number of axonal EBP comets in the steady state, as well as increased comet growth velocity and persistence (Figure 3.3A-C, Figure 3.4A). The altered MT dynamics in *ptrn-1(0)*mutants were rescued by pan-neuronally expressed PTRN-1 (Figure 3.3A-C). Over-expression of PTRN-1 in wild type backgrounds did not significantly alter MT dynamics (Figure 3.3A-C), consistent with its lack of effect on

axon regeneration. Axonal MT polarity was normal in *ptrn-1(0)* or in *ptrn-1(++)* backgrounds, before or after injury (Figure 3.5). We conclude that PTRN-1 specifically restrains the number of dynamic MTs in axons.

C. elegans touch neurons contain many 15-protofilament (pf) MTs, as opposed to the 11-pf MTs prevalent in other *C. elegans* neurons or the 13-pf MTs typical of neurons in other species (Topalidou et al., 2012). To assess whether PTRN-1 repressed dynamic MTs in other neurons, we examined D type motor neurons, which contain a small number of 11-pf MTs. As in PLM, *ptrn-1(0)* D neurons displayed increased numbers of dynamic MTs (Figure 3.4B,C). Thus *ptrn-1* mutants display more dynamic MTs in axons with different types of MT.

Axotomy of PLM axons results in an increase in the number of dynamic MTs by 3 h after injury followed by a decrease in catastrophe frequency concurrent with growth cone formation (Ghosh-Roy et al., 2012) (Figure 3.3E-G). In *ptrn-1(0)* mutants the numbers and growth length of dynamic MTs 3 hpa were further elevated compared to wild type (Figure 3.7E). Thus, despite displaying increased numbers of dynamic MTs in the steady state, *ptrn-1(0)* mutants can respond to injury by further increasing dynamic MT numbers.

3.3.3. Axonal MTs in *ptrn-1(0)* mutants are reduced in number and increased in length but display normal minus end morphology

The increased MT growth velocity in uninjured axons of *ptrn-1(0)* might be explained by elevated tubulin concentration due to reduced total MT polymers. Ultrastructural analysis of *ptrn-1(tm5597)* mutants showed that PLM axons contained

fewer MTs than in the wild type (Richardson et al., 2014). Here, we performed serial section electron microscopy on *ptrn-1(lt1)* and *ptrn-1(ju698)* mutants and counted MTs in ALM and PLM axons (Table 3.1). In wild type PLM axons, MT numbers average 46 (4 axons) whereas *ptrn-1(lt1)* animals had an average of 17 (range 12-24, 40 sections from 2 axons), revealing a clear trend of reduced axonal MT numbers. We did not observe small-diameter or morphologically aberrant MTs as reported for *ptrn-1(tm5597)* (Richardson et al., 2014); this may reflect the different axonal regions examined or other differences in genetic background.

As PTRN-1 has been implicated in stabilization or anchoring of MT minus ends in neurons, we reconstructed the MT arrays of an ALM axon segment in wild type and *ptrn-1(0)* animals (Figure 3.6). Counting fully reconstructed MTs, wild type axons contained 8.9 minus ends/μm, whereas in *ptrn-1(ju698)* we saw 1.7 minus ends/μm, a 5-fold reduction in density of minus ends. Interestingly, *ptrn-1(ju698)* mutants also displayed significantly longer individual MTs (7.3 ±0.8 μm vs 3.3 ± 0.2 μm in the wild type), so the number of MT profiles per section is reduced only twofold in *ptrn-1*. We also examined MT end morphology; when an MT end is imaged in a thin section, it appears as *diffuse* (corresponding to the splayed MT lattice at the plus end) or *filled* (minus end) (Chalfie and Thomson, 1979)(Figure 3.6A). MT terminations not imaged close to the section surface resemble the rest of the MT and are scored as *clear*. Most fully reconstructed MTs had diffuse plus distal ends both in the wild type and in *ptrn-1(ju698)* mutants (83% in WT vs. 79% in mutant). A small fraction of MTs have filled/minus ends distal (24% in WT vs. 38% in mutant). This analysis suggests that PTRN-1 does not affect the ultrastructure or orientation of MT ends.

3.3.4. *ptrn-1* defects in MT dynamics and axon regrowth are suppressed by loss of function in the MT depolymerizing kinesin-13/KLP-7

To address mechanistically why PTRN-1 is required for axon regrowth we investigated its potential interactors. In Drosophila embryos and S2 cells, Patronin protects MT minus ends from kinesin-13 mediated depolymerization (Goodwin and Vale, 2010; Wang et al., 2013). In *C. elegans*, KLP-7/kinesin-13 acts to destabilize axonal MTs; in *klp-7(0)* mutants very few growing MTs are seen in the steady state, but become upregulated after injury, and by 24 hpa axon regrowth is essentially normal in *klp-7(0)* animals (Ghosh-Roy et al., 2012). To address whether reduced axon regeneration of *ptrn-1(0)* might reflect excessive KLP-7-dependent depolymerization of MT minus ends we analyzed MT dynamics in *ptrn-1(0) klp-7(0)* double mutants. Few or no EBP comets were visible in *klp-7(0)* axons, and *klp-7(0) ptrn-1(0)* double mutants resembled *klp-7(0)* (Figure 3.7A-C). The track length of individual EBP comets in *ptrn-1(0) klp-7(0)* double mutants was suppressed to wild type levels (Figure 3.7C). *ptrn-1(0) klp-7(0)* double mutants displayed reduced MT dynamics after injury (Figure 3.7A-C). These data indicate that the elevated number of growing MTs in *ptrn-1(0)* requires KLP-7. Remarkably, PLM regrowth was suppressed to wild type levels in the *ptrn-1(0) klp-7(0)* double mutant (Figure 3.7D,E). Thus, the requirement for PTRN-1 can be bypassed by loss of KLP-7, suggesting the inability of *ptrn-1(0)* axons to regrow is due to KLP-7-mediated MT depolymerization.

3.3.5 The CKK domain of PTRN-1 is necessary and sufficient for PTRN-1 function in axon regeneration

To elucidate the roles of PTRN-1 domains in axon regeneration, we expressed fragments and domains of PTRN-1 (Figure 3.8A). PTRN-1, like other CAMSAPs, contains an N-terminal calponin homology (CH) domain, a coiled-coil region, and a C-terminal CKK (CAMSAP/KIAA1078/KIAA1543) domain. The CKK domain is unique to the CAMSAP family, and binds MTs (Baines et al., 2009; Goodwin and Vale, 2010; Jiang et al., 2014). The domain responsible for minus end targeting varies: in human CAMSAPs the CKK domains are sufficient for minus end targeting (Jiang et al., 2014), whereas in Drosophila Patronin the CKK domain binds along the length of MTs and the coiled-coil region is required for minus end targeting (Goodwin and Vale, 2010). We found that transgenic overexpression of the CKK domain, but not the CH or the coiled-coil domains, was both necessary and sufficient to rescue regrowth defects of *ptrn-1(0)* (Figure 3.8B). CKK domain overexpression in a *ptrn-1(0)* background also caused formation of long ALM posterior neurites (not shown), as seen in other conditions where axonal MTs are hyperstabilized (Ghosh-Roy et al., 2012; Kirszenblat et al., 2013). Consistent with the idea that the CKK domain stabilizes MTs, we found that overexpression of the CKK domain in a *ptrn-1(0)* background reduced the number, length, and velocity of EBP tracks (Figure 3.8D-F).

To investigate how the PTRN-1 domains might contribute to axonal regrowth we examined their subcellular localization. PTRN-1 has been shown to localize to puncta along the processes of many neurons (Richardson et al., 2014); we confirmed this with our functional tagged PTRN-1 fusion proteins, expressed either from single-copy insertion transgenes containing the *ptrn-1* promoter or under the control of other neuronal promoters (Figure 3.9). PTRN-1::GFP puncta were dense in touch neurons (e.g. Figure

3.9D,F), while puncta in motor neuron commissures were more sparse (Figure 3.9D,E) correlating with their lower density of axonal MTs. In other neurons PTRN-1::GFP was predominantly punctate (Figure 3.9B), although some filaments were seen in axons (Figure 3.9C). Puncta could also be seen in the regrowing PLM process after injury, including at the tip of the process and the growth cone (Figure 3.9G,H).

The GFP::CC domain fusion protein localized to puncta, similar to full-length PTRN-1::GFP (Figures 3.8C, 3.9), although the puncta were smaller and fewer in number. The GFP::CKK fusion protein was mostly diffuse, yet faint filaments could be seen in some axons close to the soma (Figure 3.8C). This localization differs from full length PTRN-1::GFP, which strongly localizes to MT bundles if overexpressed (Figure 3.9E). The filamentous appearance of GFP::CKK suggests that any requirement for punctate localization of PTRN-1 can be bypassed if the CKK domain is expressed at high levels.

3.3.6 PTRN-1 overexpression can promote axon branching in the absence of DLK-1

DLK kinases are conserved regulators of axon regeneration in multiple organisms (Tedeschi and Bradke, 2013). In *C. elegans,* DLK-1 is essential for PLM and motor neuron axon regeneration (Hammarlund et al., 2009; Yan et al., 2009). DLK-1 acts via multiple targets, including the bZip transcription factor CEBP-1 (Yan et al., 2009) and the MT cytoskeleton (Chen et al., 2011; Ghosh-Roy et al., 2012). The *ptrn-1(0)* developmental defects in touch neurons partially resemble those caused by increased DLK-1 activity, suggesting that PTRN-1 may antagonize the DLK-1 pathway (Marcette et al., 2014; Richardson et al., 2014). We tested whether the DLK-1 pathway interacted

with PTRN-1 in axon regeneration. *dlk-1* null mutants are strongly blocked in PLM regrowth, and lack regenerative growth cones (Figure 3.10A,B). *dlk-1(0) ptrn-1(0)* mutants displayed slightly more severe defects in regrowth compared to *dlk-1(0)* (Figure 3.10A). Similarly, *cebp-1(0) ptrn-1(0)* showed further reduced regrowth compared to single mutants. These data suggest PTRN-1 does not antagonize the DLK-1 pathway in regeneration.

To further address the relationship of PTRN-1 and DLK-1 we overexpressed PTRN-1 in *dlk-1(0) ptrn-1(0)* double mutants. Overexpression of PTRN-1 did not suppress the regeneration defect in *dlk-1(0)*, nor did it enhance regrowth from the severed axon stump. However after injury PTRN-1-overexpressing axons frequently extended one or more short collateral branches (Figure 3.10B,C); these were rarely seen in *dlk-1(0)* or in *dlk-1(0) ptrn-1(0)* animals after axotomy. Overexpression of the PTRN-1 CKK domain was also sufficient to induce formation of collateral branches after axon injury (Figure 3.10A,B). Strikingly, these collateral branches always grew posteriorly towards the PLM soma (Figure 3.10B). This effect of PTRN-1 overexpression was not observed in wild type or in *ptrn-1(0)* single mutant backgrounds (Figure 3.10C), suggesting it is dependent on loss of function in the DLK-1 pathway. Consistently, overexpression of PTRN-1 in the *cebp-1(0) ptrn-1(0)* mutant was also sufficient to trigger posteriorly directed branching after axotomy (Figure 3.10A-C). The ability of PTRN-1 overexpression to induce neurite outgrowth in animals lacking DLK-1 pathway activity suggests that PTRN-1 can act either downstream or in parallel to the DLK-1 pathway.

The posterior orientation of PTRN-1-induced collateral branches suggested that axonal MT organization or polarity might be disrupted in these animals. However the

fraction of retrograde EBP comets in PLM axons was not significantly altered, indicating axonal MT polarity was normal (Figure 3.5). Notably, the increased numbers of dynamic MTs of *ptrn-1(0)* animals were fully suppressed in *ptrn-1(0) dlk-1(0)* double mutants (Figure 3.10F,G). DLK-1 overexpression can upregulate axonal MT dynamics in the absence of injury (Ghosh-Roy et al., 2012), correlating with increased axon regrowth (Hammarlund et al., 2009; Yan et al., 2009). Despite displaying upregulated dynamic MTs, *ptrn-1(0)* axons are unable to regrow efficiently suggesting that PTRN-1 has additional functions important in regeneration.

3.4 Discussion

Here we have shown that PTRN-1 is required for efficient axon regeneration in *C. elegans*. The role of PTRN-1 in regeneration is distinct from its function in development, in that PTRN-1 inhibits axon outgrowth (Marcette et al., 2014) and is required for axon regeneration. The relationship between PTRN-1 and KLP-7 and DLK-1 also differs in regrowth versus development. Our observations of elevated MT dynamics in *ptrn-1* mutant axons provides new insights into PTRN-1 function, and identify Patronin/CAMSAPs as key players in axonal MT organization in regrowth.

3.4.1. PTRN-1 protection from kinesin-13/KLP-7 is required for axonal regrowth

Our results indicate that PTRN-1-dependent MT stabilization is required for successful regeneration. Loss of the MT depolymerase KLP-7 completely suppresses the axon regrowth defects of *ptrn-1(0)*, suggesting that excess destabilizing activity of KLP-7

is detrimental for regrowth, and further that a low level of dynamic MTs is sufficient for regrowth. Expression of the PTRN-1 CKK domain was necessary and sufficient for its function in axon regeneration, and restored MT dynamics to normal levels, indicating that the CKK domain alone can stabilize axonal MTs in vivo. Suppression of *ptrn-1(0)* phenotypes by loss of function in *klp-7* or by CKK overexpression also implies that MT stabilization can be sufficient for normal axon regrowth, and therefore that the primary defect in *ptrn-1(0)* is in stabilization as opposed to minus end anchoring. The CKK domain was sufficient to rescue *ptrn-1* defects but did not show a punctate distribution, and instead weakly localized along filaments, presumably MT bundles. In contrast, the coiled-coil domain displayed punctate localization. These observations suggest that the minus end targeting mechanism of *C. elegans* PTRN-1 resembles that of Drosophila Patronin (Hendershott and Vale, 2014).

3.4.2 *ptrn-1* mutants display elevated levels of dynamic axonal MTs

ptrn-1 mutants display consistently increased numbers of dynamic MTs in axons. This was unexpected, both in view of recent studies of CAMSAPs (see below), and because an increase in dynamic MT number correlates with enhanced regrowth in mutants such as *efa-6* (Chen et al., 2011). These observations suggest that the absolute level of dynamic MTs may not be the critical determinant of regrowth capacity, and that instead, the change in the number of dynamic MTs after injury may be more critical. Alternatively, the ratio of dynamic to stable MTs may be important. Ultrastructural analysis confirms that *ptrn-1* mutants display fewer axonal MTs in the steady state (Richardson et al., 2014; and this study). In either case, the increased number of dynamic

MTs in *ptrn-1* appears to reflect MT destabilization, just as the reduced number of dynamic MTs in *klp-7* is due to hyperstabilization.

Our observations of increased numbers of dynamic MTs in *ptrn-1(0)* axons may be compared to a previous report that *ptrn-1(0)* mutants displayed fewer dynamic MTs in the dendrites of PHC sensory neurons (Richardson et al., 2014). This difference might reflect the opposing polarities of axonal MTs (oriented plus end out) versus dendritic MTs (in PHC, oriented with minus ends out) or differences in levels of free tubulin as the result of MT disruption in these different compartments. Dendritic MTs may be particularly dependent on PTRN-1. Indeed, knockdown of CAMSAP2 in mouse embryonic hippocampal neurons reduces the numbers of EBP comets most strongly in dendrites (Yau et al., 2014). Conversely, the upregulation of dynamic axonal MTs in *ptrn-1(0)* mutants could be a chronic response to the destabilization of the MT array in mature axons.

3.4.3 Relationship of PTRN-1 and DLK-1 in MT dynamics and regeneration

Consistent with the idea that increased dynamic MTs are a regulated response to MT destabilization, loss of function in *dlk-1* suppressed the upregulated MT dynamics of *ptrn-1*. However *ptrn-1 dlk-1* double mutants display essentially normal numbers of dynamic axonal MTs. Thus, DLK-1-dependent MT upregulation does not mask an underlying loss of dynamic MTs. It is striking that although the *ptrn-1(0)* phenotypes in dendritic and axonal MT dynamics are opposite (fewer EBP-GFP comets in mutant dendrites, more in mutant axons) (Richardson et al., 2014; and this study), in both cases loss of DLK-1 restores the number of dynamic MTs to normal levels. DLK-1 can sense

MT depolymerization (Bounoutas et al., 2011b), and may act homeostatically to upregulate or downregulate MT dynamics.

Our analysis of MT dynamics is consistent with the model that DLK-1 activity is upregulated in uninjured axons of *ptrn-1* mutants. However PTRN-1 does not appear to inhibit DLK-1 in regeneration. *ptrn-1(0)* and *dlk-1(0)* mutants both displayed reduced regrowth, and double mutants were further impaired, consistent with PTRN-1 and DLK-1 acting in concert. Overexpression of PTRN-1 was not sufficient to enhance axon regrowth in wild type or in *dlk-1(0)*. However in the absence of DLK-1 pathway activity, the combination of axon injury and PTRN-1 overexpression induced collateral branching, suggesting PTRN-1 has a neurite outgrowth promoting activity that is normally repressed by the dominant DLK-1 pathway.

In conclusion, we have shown that PTRN-1 is critical for axon regrowth, and that this role differs significantly from its function in development. Numerous questions remain to be addressed regarding PTRN-1's role in axon regeneration, and it will be of interest to examine the roles of CAMSAPs in other models of axon regeneration.

3.5 Methods

C. elegans genetics

C. elegans strains were maintained on NGM agar plates between 15 and 25°C using standard methods. We used the following published alleles and transgenes: *dlk-1(tm4024)*, *klp-7(tm2143)*, *cebp-1(tm2807),* P*mec-7*-GFP(*muIs32*) for touch neurons, and P*unc-25*-GFP(*juIs76*) for GABAergic motor neurons. *ptrn-1(ju698)* was isolated in a

screen for suppressors of an epidermal morphology mutant (Amy Tong, M.C., and A.D.C., unpublished results) and creates a premature stop in PTRN-1A. *ptrn-1(tm5597)* was obtained from the Mitani lab. *ptrn-1(lt1)* was generated by MosDEL (Frokjaer-Jensen et al., 2010) and deletes most of *ptrn-1* (S.W. and K.O., unpublished). Plasmids were constructed by standard methods; new strains, plasmids, and transgenes are listed in Table 3.2.

Laser Axotomy, Confocal Imaging, and Image Analysis

Single axons were severed in L4 stage animals using femtosecond laser irradiation and imaged using a Zeiss LSM510 essentially as described (Wu et al., 2007). For other imaging we used a Zeiss LSM710 confocal; to image EBP-2::GFP dynamics we used spinning disk confocal microscopy essentially as described (Ghosh-Roy et al., 2012), using beads or 4 mM levamisole to immobilize animals. Movies were taken for 100-200 frames. Extrachromosomal (*juEx2843*) or integrated (*juIs338*) versions gave indistinguishable results. We cut the PLM axon 80 μm from the cell body. Kymographs were generated in Metamorph (Molecular Devices) by drawing a line scan along 40 μm of the axon proximal to the cut site. We manually traced EBP::GFP tracks on the kymographs and calculated comet number, growth distance, and growth velocity using Metamorph. For analysis of EBP::GFP dynamics in the ventral processes of GABAergic motor neurons we analyzed an ROI extending 30 μm anteriorly from the VD11 cell body (Figure S2B).

Statistics

Statistical analysis used GraphPad Prism. Categorical data were analyzed using the Chi squared or Fisher exact test. Continuous variables were tested for normality using

the D'Agostino Pearson test; pairwise comparisons used Student's t test or the Mann-Whitney test; multiple comparisons used one-way ANOVA or a Kruskal-Wallis test followed by a post test.

3.6 Acknowledgements

Chapter 3 is a reformatted reprint in full of Chuang M, Goncharov A, Wang S, Oegema K, Jin Y, Chisholm AD. The microtubule minus-end-binding protein Patronin/PTRN-1 is required for axon regeneration in *C. elegans*. Cell Reports. Volume 9, Issue 3, p874–883, 6 November 2014. The dissertation author was the primary researcher and author of this paper.

ptrn-1(ju698) was isolated by Amy Tong and mapped by Tiffany Hsiao. We thank Zilu Wu for assistance with the femtosecond laser and Naina Kurup for P*unc-25*-EBP-2::GFP. We thank our lab members for advice and discussion, the Japanese National Bioresource Project for *ptrn-1(tm5597)* and the Caenorhabditis Genetics Center (CGC) for strains. M.C. was supported by the UCSD Cellular and Molecular Genetics Training Grant (NIH T32 GM007240). K.O. receives salary and additional support from the Ludwig Institute for Cancer Research. Y.J. is an Investigator and A.G. an Associate of the Howard Hughes Medical Institute. Supported by NIH R01 NS057317 to A.D.C. and Y.J. and R01 GM074207 to K.O.

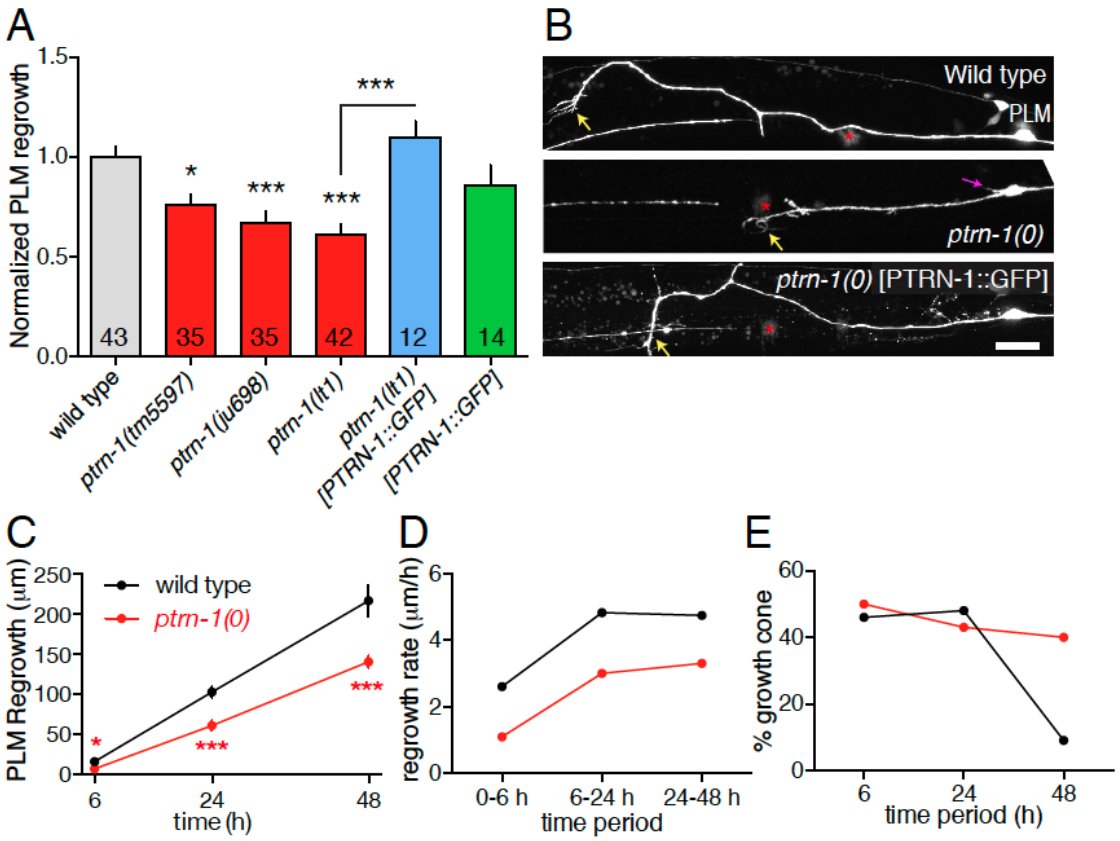

Figure 3.1. PTRN-1 is required for axon regeneration

(A) PLM axon regrowth is significantly reduced in *ptrn-1(0)*mutants and fully rescued by pan-neural expression of PTRN-1 (P*rgef-1*-PTRN-1::GFP,*juEx5676*). Statistics: Kruskal-Wallis test and Dunn's post test; *, P < 0.05; ***, P <0.001. (B) PLM axons (*muIs32[Pmec-7-GFP])* at 24 hpa in wild type, *ptrn-1(lt1)*, and in *ptrn-1(lt1)* rescued by P*rgef-1*-PTRN-1::GFP(*juEx5676*). Anterior is to the left and dorsal up; red asterisks, site of axotomy. Regenerative growth cones (yellow arrows) appear normal in *ptrn-1(0)* mutants. Axon injury in *ptrn-1(lt1)* triggers sprouting of extra neurites from the PLM soma in ~20% of animals (magenta arrow; see also Figure 3.2B). (C) *ptrn-1(lt1)*mutants display reduced regrowth throughout PLM regeneration. (D) *ptrn-1(lt1)* mutants display reduced axon extension rates. (E) In *ptrn-1(lt1)* mutants regrowing axons retain growth cones at 48 hpa. (F) The *ptrn-1(lt1)* regrowth defect is rescued by heat-shock induced expression of PTRN-1 either 4 h or 1 h before axotomy, but not by heat shock at 6 hpa. Animals were heat shocked at 34°C for 1 h. Statistics: Student's t test; ***, P < 0.001, **, P < 0.01. (G) PTRN-1::miniSOG-induced CALI at 6 h or 0 h prior to axotomy abolishes PTRN-1 rescue activity, whereas CALI at +6 h does not significantly reduce rescue. (H) PLM regrowth is normalized to WT of corresponding time point in the absence of blue light. Genotypes: wild type (*muIs32*), pan-neural cytosolic miniSOG (*juEx3701*), and *ptrn-1(lt1);* P*rgef-1*-PTRN-1::miniSOG (*juEx6307*). Kruskal-Wallis test, Dunn post test; ***, P < 0.001 compared to WT + blue light at same time point.

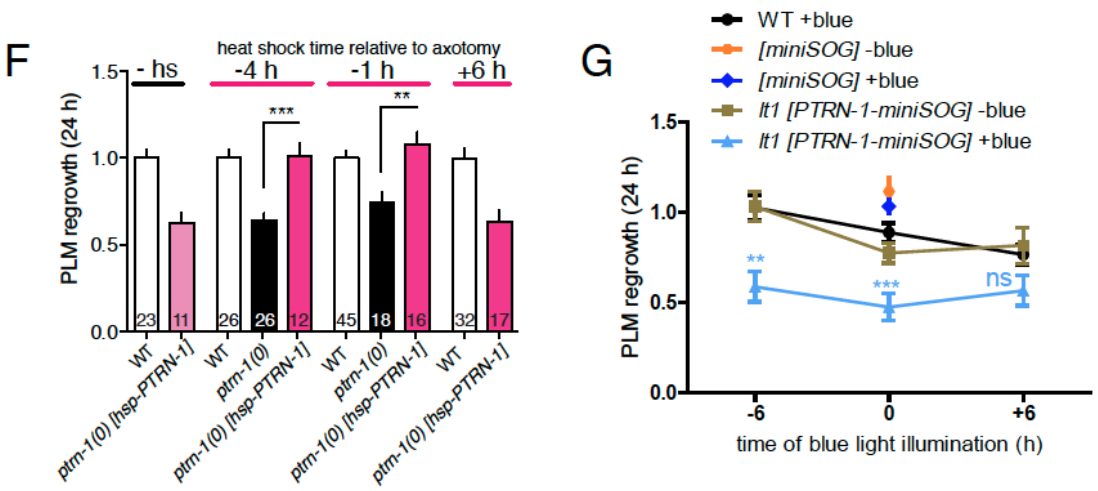

Figure 3.1, PTRN-1 is required for axon regeneration, continued

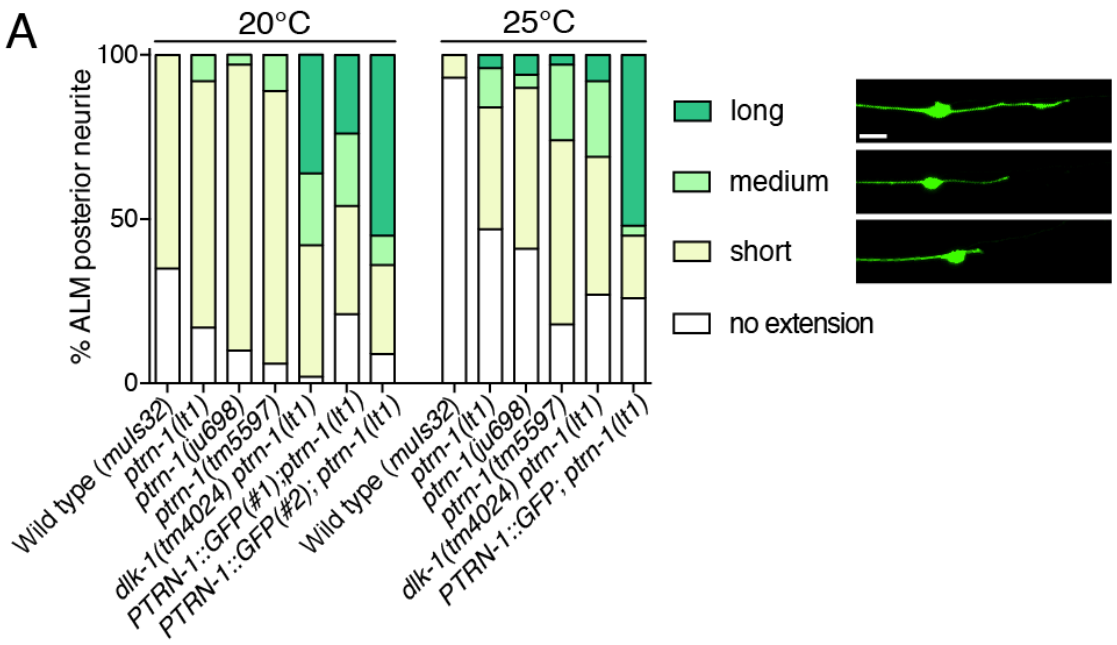

Figure 3.2. *ptrn-1* mutants extend ectopic neurites from the ALM cell body prior to axotomy and from PLM after axotomy

(A)ALM neurons display ectopic posterior neurites in *ptrn-1(0)* mutants. This phenotype is more severe at 25°C compared to 20°C. The posterior neurite defect is enhanced by over-expressing PTRN-1 in neurons, or by introducing *dlk-1(lf)* into the background. n > 30 animals per genotype. Extension length was categorized as follows: short 0-10 μm; medium 10 – 20 μm; Long: > 20 μm (representative images on right; scale, 10 μm). (B) Axotomy of PLM can induce sprouting of neurites from the cell body in *ptrn-1(lt1)* and *ptrn-1(tm6697)*, and to a lesser extent in *ptrn-1(ju698)*. Neurites are defined as outgrowths from the PLM cell body > 10 μm, scored 24 h post axotomy; such neurites are not counted in scoring PLM axonal regrowth, and are rarely observed in intact neurons. The *ptrn-1(lt1)* neurite phenotype is fully rescued by PTRN-1::GFP transgenes (*juEx5676, juEx5677*). *dlk-1(0)* significantly enhances *ptrn-1(lt1)* neurite formation from the PLM soma; this is distinct from the collateral axon branches induced by axotomy (Figure 3.10). Transgenic expression of the CKK domain (*juEx6301*) alone does not rescue the *ptrn-1(lt1)* neurite phenotype, and significantly enhances the *ptrn-1(0) dlk-1(0)* neurite phenotype. n > 10 animals per genotype. (C) D motor neuron regrowth is impaired in *ptrn-1(lt1)* mutants. D neuron commissures were severed laterally in the L4 stage; in the wild type, ~60% of commissures regrow fully to the dorsal nerve cord by 24 h after axotomy (see D) and ~30% display partial regrowth. In *ptrn-1(lt1)* mutants fewercommissures fully regrow to the dorsal nerve cord, and most commissures display partial regrowth. Statistics: Fisher exact test. ***, P <0.001 compared to WT, n> 60 commissures. (D) Confocal images of VD3, DD2, and VD4 commissure regrowth 24 h after axotomy in wild type (*juIs76*) and in *ptrn-1(lt1)*. Anterior is to the left and dorsal up. Scale (B, G): 10 μm.

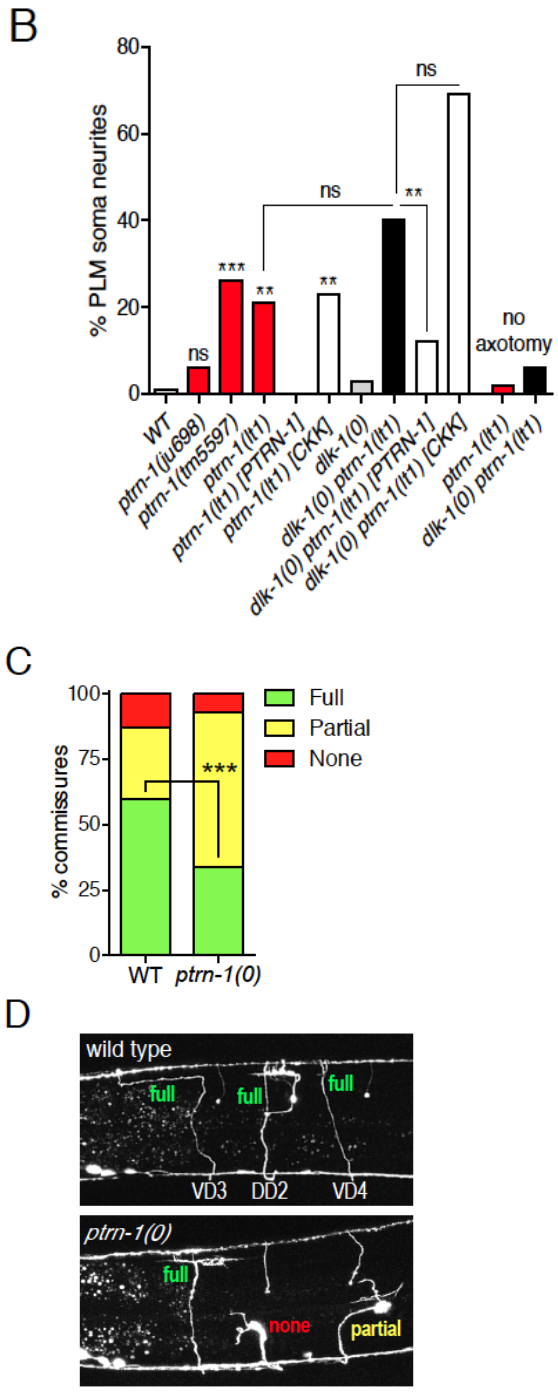

Figure 3.2. *ptrn-1* mutants extend ectopic neurites from the ALM cell body prior to axotomy and from PLM after axotomy, continued

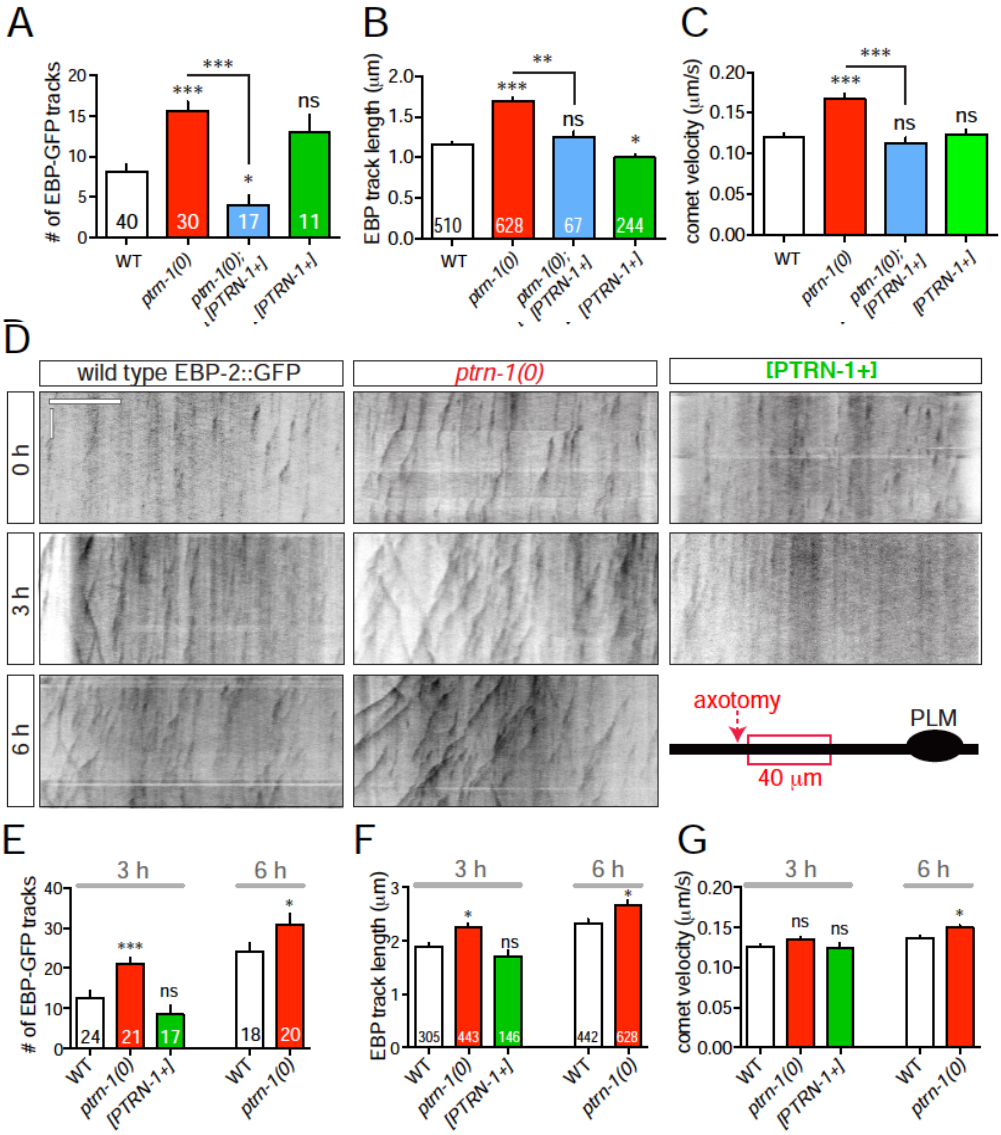

Figure 3.3. *ptrn-1* mutants display elevated numbers of dynamic axonal microtubules before and after axon injury

(A-C) Quantitation of MT plus end dynamics in the uninjured PLM axon using P*mec-4*-EBP-2::GFP(*juIs338*). Bars show mean ± SEM; Statistics, ANOVA and Sidak post test. (A) *ptrn-1(lt1)* mutants display more EBP-2::GFP comets in the PLM axon prior to axotomy; this phenotype is rescued by pan-neural expression of PTRN-1(*juEx5580*); overexpression of PTRN-1 in wild type background does not significantly affect MT dynamics. In (A) and (E) numbers on bars indicate number of axons. (B) EBP-2::GFP track length is significantly increased in *ptrn-1(lt1)* mutants. Statistics (B, C), Kruskal-Wallis test and Dunn's post test. In (B) and (F) numbers on bars indicate number of tracks; same tracks analyzed in (C) and (G). (C) EBP-2::GFP comets grow faster in *ptrn-1(lt1)* PLM axons. (D) Representative kymographs (inverted grayscale) of EBP-2::GFP (*juIs338*) tracks in WT and *ptrn-1(lt1)*, and PTRN[+] (*juEx6178*) PLM axons, before and 3 and 6 h after axotomy. In all kymographs of PLM, the length (x axis) and time (y axis) scales are 10μm and 10 s respectively. (E-G) *ptrn-1(lt1)* mutants have increased numbers of dynamic MTs, EBP track length, and velocity at 3 and 6 h post injury compared to wild type; n>10 axons per genotype. Statistics, Kruskal-Wallis test (3 h), Mann-Whitney test (6 h).

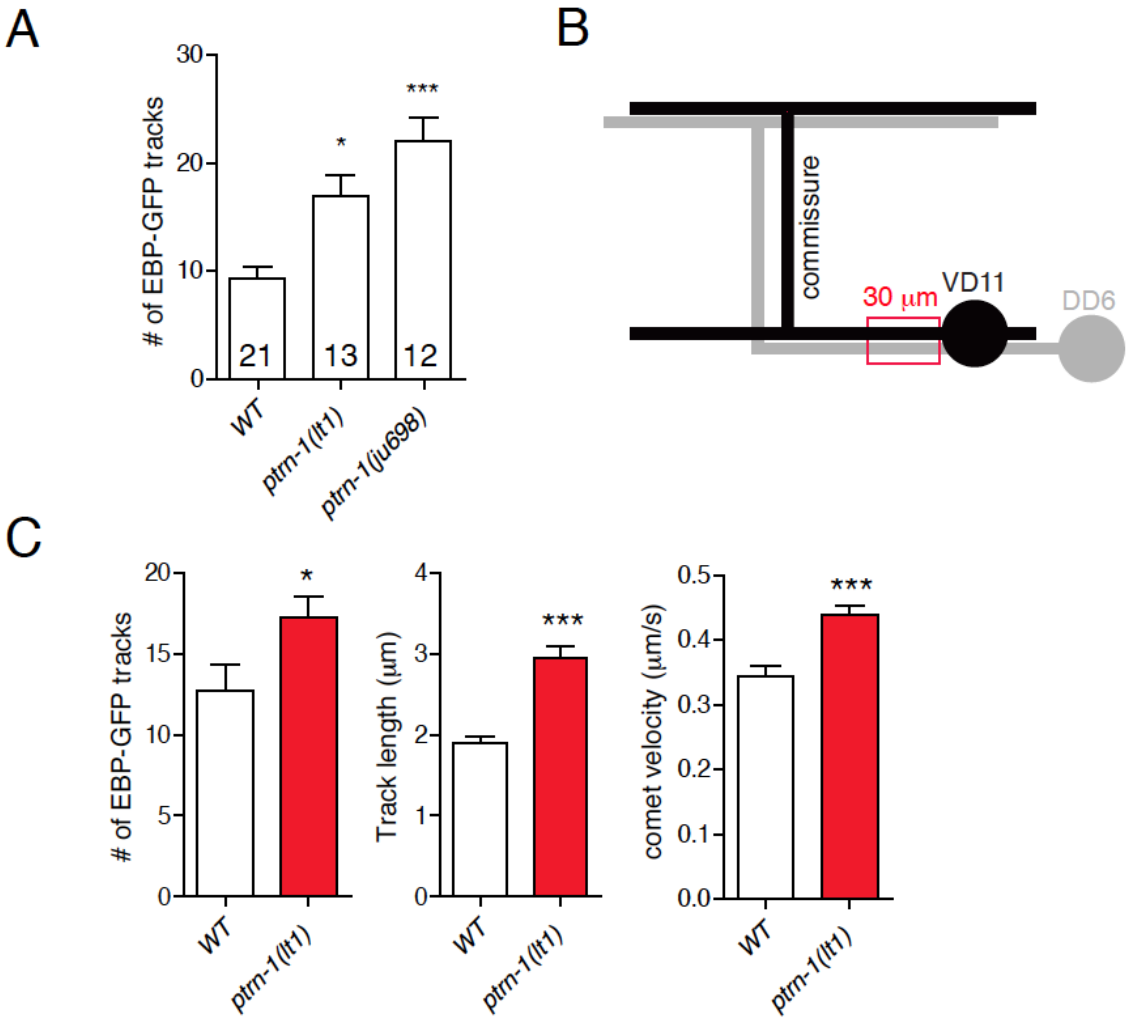

Figure 3.4. *ptrn-1(0)* mutants display increased numbers of dynamic MTs in touch neuron axons and in motor neuron axons

(A) *ptrn-1(ju698)* displays increased numbers of growing MTs in the PLM axon in the steady state; marker, P*mec-4*-EBP-2::GFP(*juEx2843*). *ptrn-1(lt1)* data are included for comparison. Statistics: One-way ANOVA and Dunn's post test. (B) Diagram illustrating position of ROI used to image MT dynamics in D type motor neurons. The ROI extends 30 μm anterior to the VD11 cell body in L4 stage animals. (C-E) *ptrn-1(lt1)* mutants display increased EBP::GFP dynamics in the ventral cord process of VD11 in the steady state. Bars show mean ±SEM. Statistics: Mann-Whitney test. ***, $P < 0.001$.

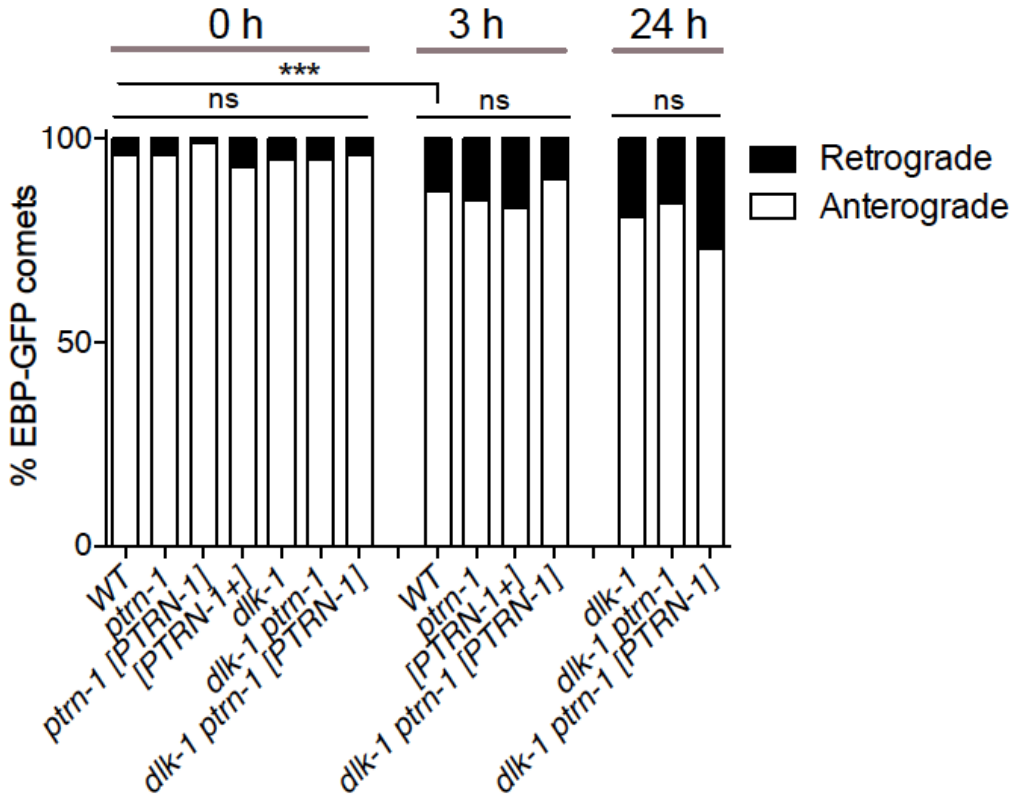

Figure 3.5. Axonal MT polarity is unaffected in *ptrn-1* mutants

ptrn-1 mutants display normal axonal MT polarity in PLM. In the steady state, approximately 5% of comets are retrograde in the wild type, compared to 3% in *ptrn-1(lt1)*. By 3 h after injury, 13% of comets are retrograde in the wild type, compared to 15% in *ptrn-1(lt1)* or 17% in PTRN-1-overexpressing animals. PLM axonal MT polarity is also normal in *dlk-1(0)*, *dlk-1(0) ptrn-1(0)*, and in *dlk-1(0) ptrn-1(0) [PTRN-1]*, prior to and at 3 h and 24 h after injury. n > 100 comets per condition.

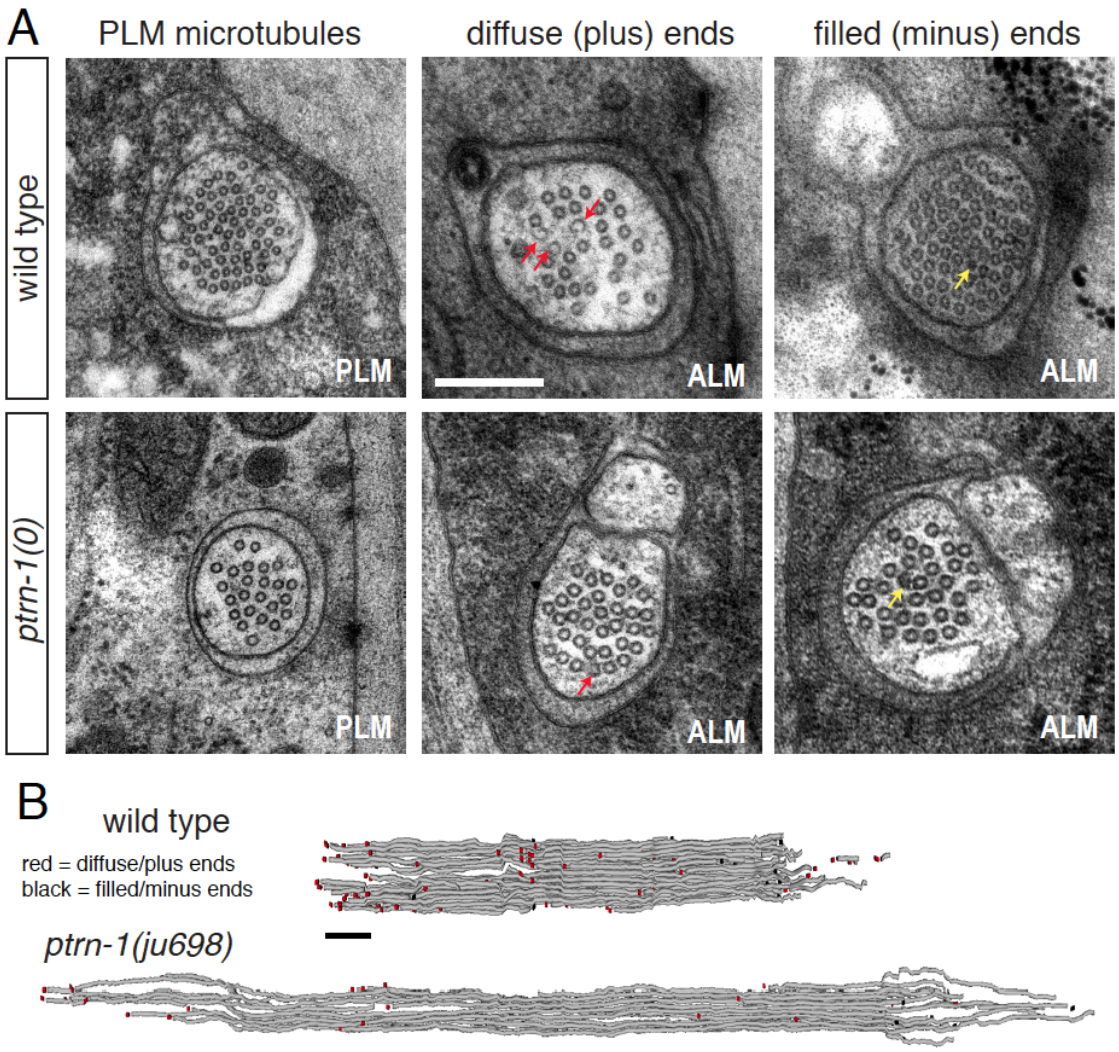

Figure 3.6. *ptrn-1* mutants display reduced axonal MT numbers but otherwise normal MT ultrastructure

(A) Representative electron micrographs of cross sections of distal regions of PLM and ALM axons in wild type (N2) and in *ptrn-1(0)* mutants. *ptrn-1(0)* mutants display a marked reduction in PLM axonal MT number. However the morphology of individual MT terminations is essentially normal; micrographs from ALM show the characteristic diffuse (plus-end, yellow arrows) and filled (minus-end, red arrows) MT terminations. Scale, 500 nm. (B) 3D views of completely reconstructed MTs from ALM in the wild type and in *ptrn-1(ju698)* showing locations of plus (red) and minus (black) ends. Scale, 1 µm.

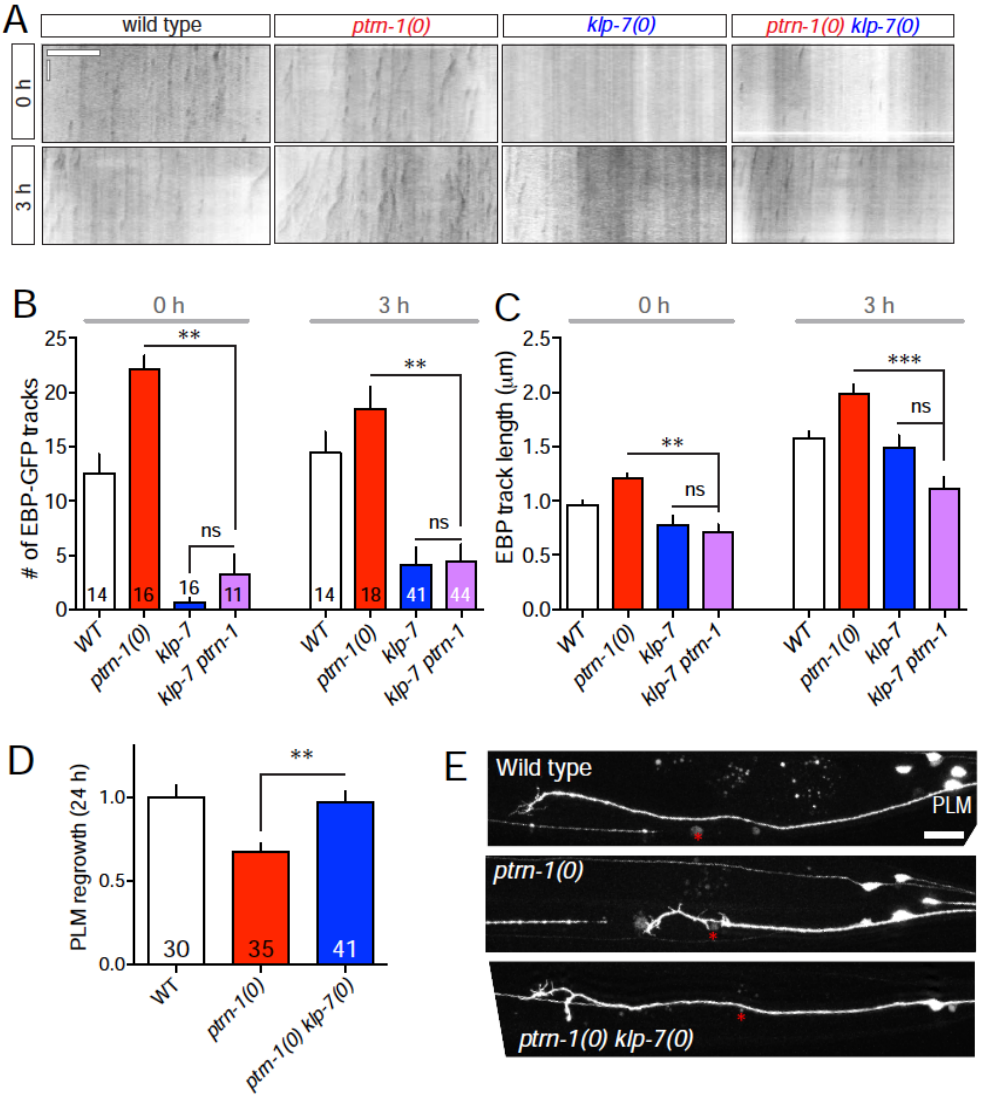

Figure 3.7. *ptrn-1(0)* defects in MT dynamics and axon regeneration are suppressed by loss of kinesin-13/KLP-7

(A) Representative kymographs of P*mec-4*-EBP-2::GFP(*juIs338*) dynamics in PLM axons, before and after injury. *klp-7(tm2143)* mutants display few dynamic MTs before injury, and upregulate MT dynamics at 3 h post injury. (B) Quantitation of EBP::GFP track numbers before and 3 h after injury; n > 10 axons per condition. (C) *klp-7(tm2143)* suppresses the increased EBP::GFP track length of *ptrn-1(lt1)*; n> 70 tracks per condition. Bars indicate mean ± SEM. Statistics, Kruskal-Wallis test. ***, P <0.001, **, P < 0.01. (D,E) The *ptrn-1(ju698)* defect in PLM axonal regrowth is suppressed by the *klp-7(tm2143)* null mutation; *klp-7* single mutants display normal regrowth (Ghosh-Roy et al., 2012); scale, 10 µm. Statistics, t test.

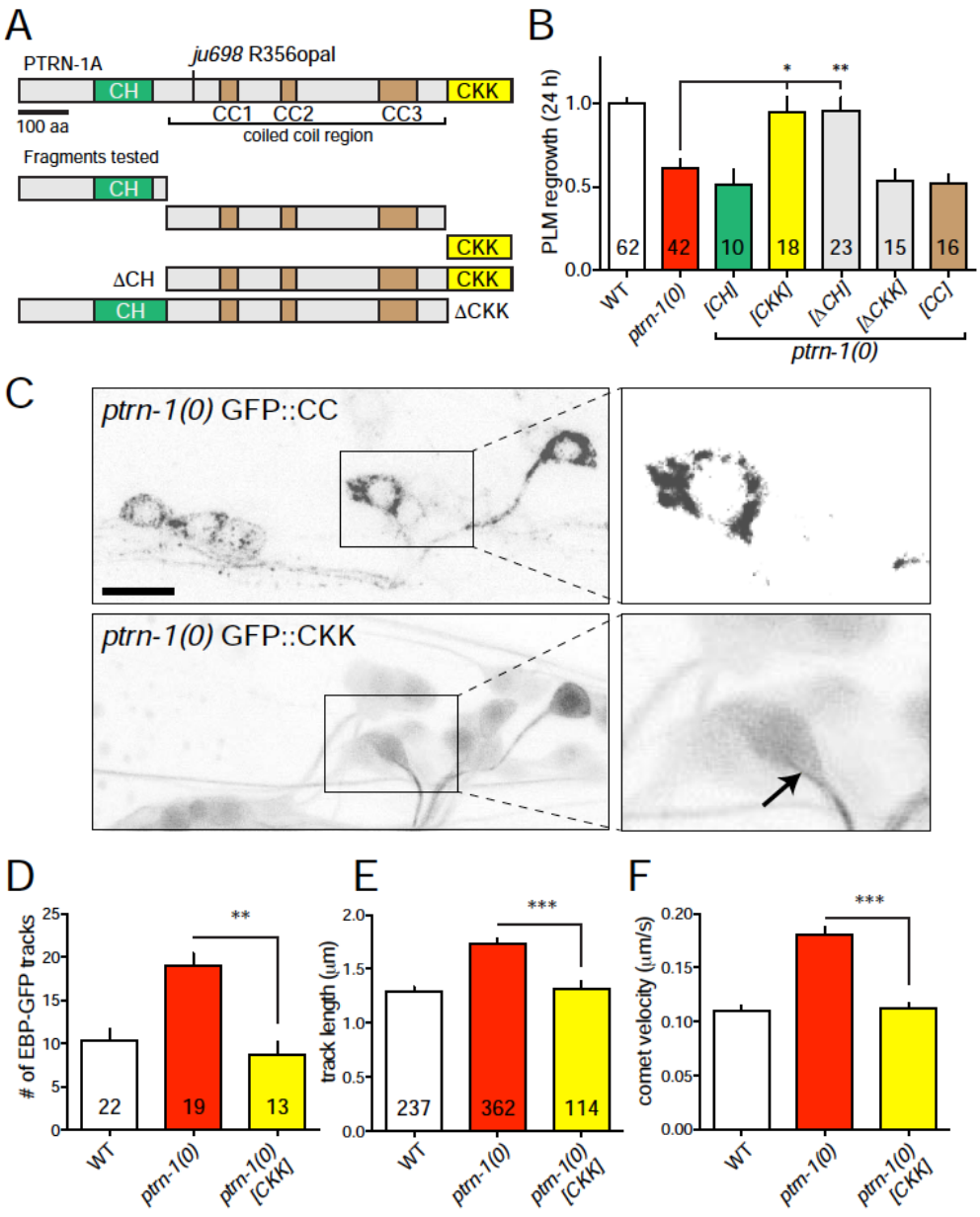

Figure 3.8 The CKK domain of PTRN-1 is necessary and sufficient for its function in axon regeneration and in inhibition of dynamic MTs

(A) Domain architecture of PTRN-1 full-length and fragments and *ju698* mutation. PTRN-1A contains a calponin homology (CH) domain (aa 153-270), three coiled-coil (CC) regions, and a CKK domain (aa 969-1098). (B) The CKK domain is sufficient to rescue *ptrn-1(lt1)* axon regrowth defects to wild type levels. Statistics: Kruskal-Wallis test, Dunn post test; ***, $P < 0.001$, **, $P < 0.01$ compared to *ptrn-1(lt1)*. (C) The coiled coil domain (GFP::CC, *juEx6308*) displays similar localization to full length PTRN-1 (see Figure 3.9) in a *ptrn-1(lt1)* mutant background. In contrast, the GFP::CKK fusion protein (*juEx6311*) is largely diffuse but displays faint filamentous localization in proximal axons (arrow). (D-F) Expression of the CKK domain alone is sufficient to rescue the increased EBP::GFP (*juIs338*) dynamics of *ptrn-1(lt1)* in the uninjured PLM. Statistics: Kruskal-Wallis test, Dunn's post test.

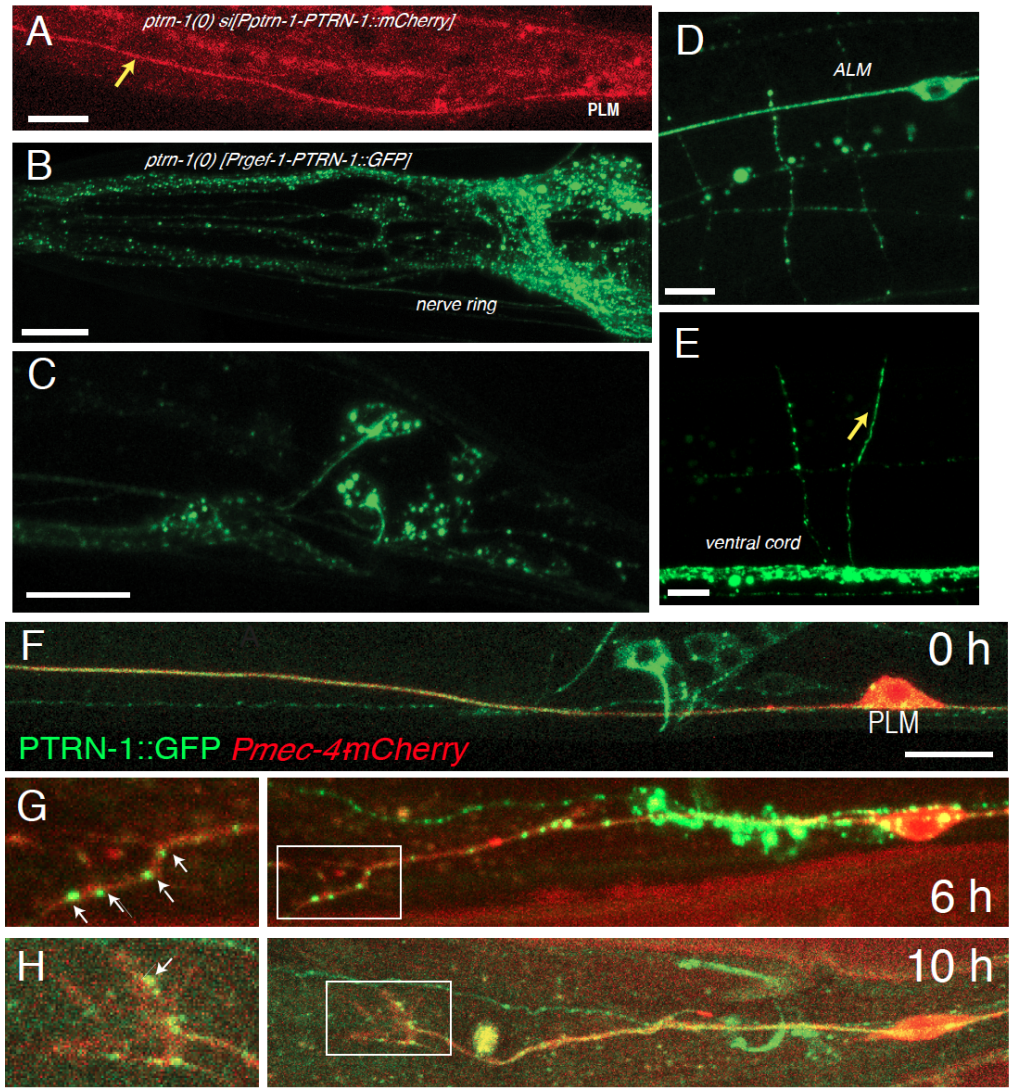

Figure 3.9. PTRN-1 localizes to puncta and filaments in neuronal processes before and after injury.

(A) PTRN-1::mCherry, expressed under control of the *ptrn-1* promoter as a single copy insertion (*ltSi183*), is expressed in PLM (cell body indicated by arrowhead) and localizes along the axon (arrow). Strain OD893, genotype *ltSi183 II; unc-119(ed3) III; ptrn-1(lt1) X*. (B-D) PTRN-1::GFP, expressed under control of the pan-neural *rgef-1* promoter (*juEx5676*), localizes to puncta in the processes of head neurons (B), tail neurons (C), and motor neuron commissures (D). In some neurons PTRN-1::GFP localizes to filaments in the process close to the cell soma (arrow, C). In touch neurons such as ALM, PTRN-1::GFP expression is very high and separate puncta cannot always be defined (D). (E) At higher injection concentrationsof 50 ng/µl, P*rgef-1*-PTRN-1::GFP (*juEx6483)* localization becomes less punctate (arrow) in motor neuron commissures. (F) Functional PTRN-1::GFP localizes to puncta along the length of the PLM axon in the steady state. Transgene: P*rgef-1*-PTRN-1::GFP(*juEx5676*) in *ptrn-1(lt1)* background; axon marked in red by P*mec-4*-mCherry (*juIs252*). (G) At 6 h post axotomy, sparsely distributed PTRN-1::GFP puncta appear in the regrowing axon. (H) At 10 h post axotomy,large PTRN-1::GFPpuncta can be observed in the regrowing growth cone (arrows). Scales, 10 µm.

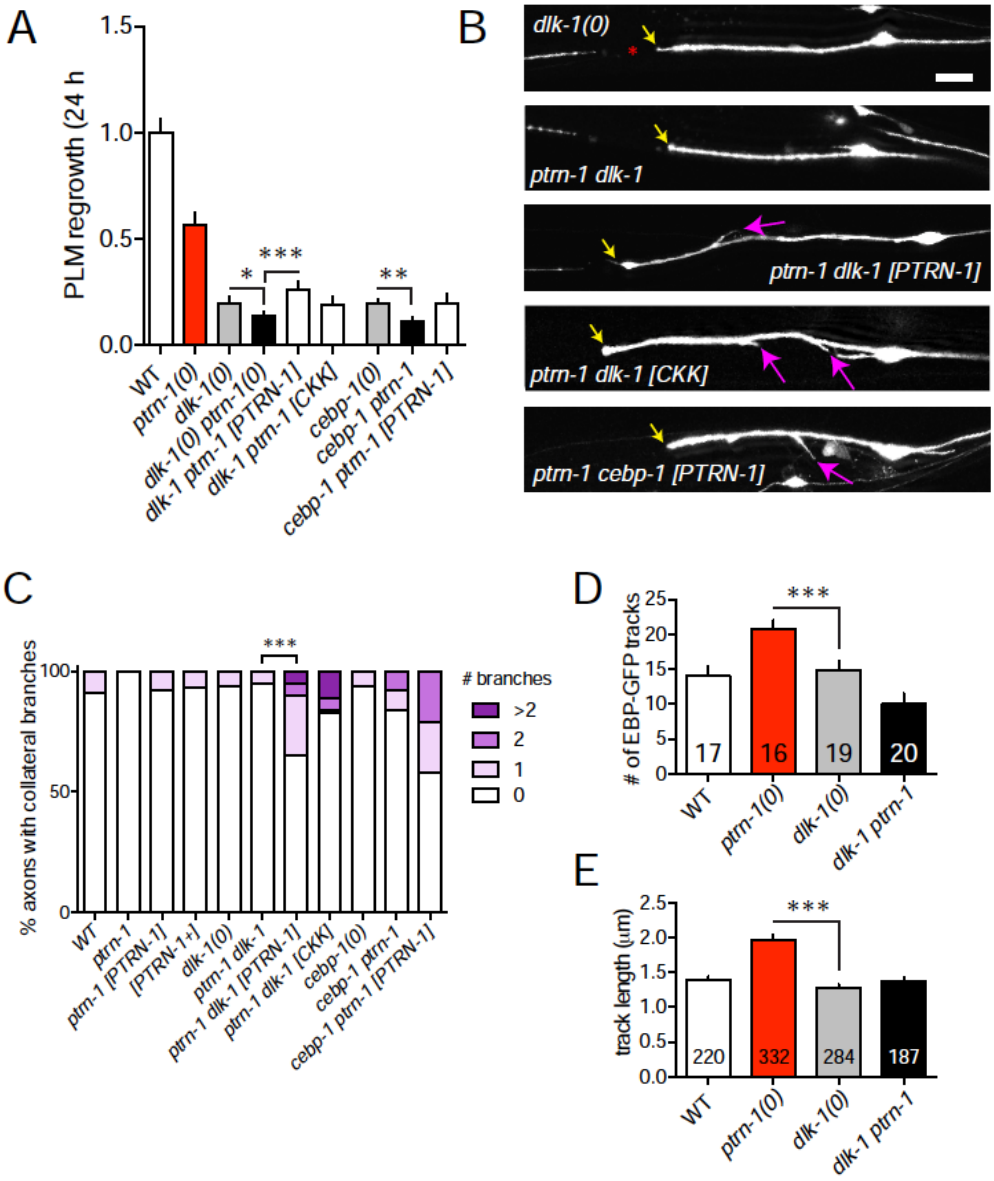

Figure 3.10. PTRN-1 can function independently of DLK-1 in regrowth and collateral branching after injury

(A) PLM axon regeneration is severely impaired in *dlk-1(tm4024)* or *cebp-1(tm2807)* mutants; these defects are slightly enhanced in double mutants with *ptrn-1(0)*. PTRN-1 over-expression causes increased growth in the *dlk-1(0) ptrn-1(0)* background due to increased collateral branching. Statistics, Mann-Whitney or t test.*, P <0.05. (B) Collateral branches formed in PTRN-1 or CKK-overexpressing animals in *dlk-1* or *cebp-1* backgrounds (magenta arrowheads) are oriented towards the posterior. Representative confocal images of PLM 24 hpa; yellow arrows, axon stumps; scale, 10 µm. (C) Overexpression of PTRN-1 in *dlk-1* pathway background leads to collateral branch formation after axotomy. Chi squared test; n>10 animals per genotype. (D,E) The elevated EBP::GFP comet number and track length of *ptrn-1(lt1)* mutants in the steady state is suppressed to wild type levels in *dlk-1(0)* double mutants. Statistics: ANOVA; ***, P < 0.01.

Table 3.1. Quantitation of axonal MT numbers in *ptrn-1* touch neurons

Genotype	Animal, Neuron	Region of sections	Average MT number ± SEM (n)
Wild type N2	1.1, ALML	Proximal	35.4 ± 0.7 (15)
	1.1, ALMR		27.4 ± 0.5 (15)
	1.3, ALML	Distal	58.8 ± 0.5 (22)
	1.3, ALMR		54.9 ± 4.3 (22)*
	2.1, ALML	Distal	34.5 ± 0.3 (23)
	2.2, ALMR		30.2 ± 1.1 (26)
			40.8 ± 1.4 (123)
ptrn-1(ju698)	1.1, ALML	Distal	26.2 ± 0.6 (19)
	1.1, ALMR		30.4 ± 0.4 (18)
	1.2, ALML	Distal	31.5 ± 0.7 (26)*
	1.2, ALMR		29.8 ± 0.5 (19)
			29.7 ± 0.4 (82)
ptrn-1(lt1)	1.3, ALML	Distal	47.9 ± 0.4 (20)
	1.3, ALMR		43.5 ± 0.7 (20)
			45.7 ± 0.5 (40)
Wild type N2	1.2, PLML	Distal	78.1 ± 1.2 (16)
	1.2, PLMR		52.7 ± 2.2 (16)
	4.2, PLML	Distal	27.0 ± 0.5 (22)
	4.2, PLMR		22.8 ± 0.5 (22)
			46.3 ± 2.3 (61)
ptrn-1(lt1)	1.2, PLML	Distal	13.2 ± 0.3 (20)
	1.2, PLMR		20.0 ± 0.5 (20)
			16.6 ± 0.6 (40)

'Proximal' ALM = close to cell body, no AVM process in ventral cord. 'Distal' ALM = AVM and PVM processes in ventral cord, or close to nerve ring. All PLM sections are from the distal axon, close to the PLM ventral branch or PVM. n, number of sections. See also Ghosh-Roy et al. (2012) Figure 3.2 for additional MT count data.

*Axons in which MTs were fully reconstructed from serial sections.

Table 3.2. New strains, transgenes and constructs

Strain	New DNA construct	New Transgene	Genetic background
OD854			*ptrn-1(lt1)*
OD893	P*ptrn-1*-PTRN-1::mCherry(*ltSi183*)		*ptrn-1(lt1); unc-119(ed3)*
CZ17510			*muIs32; ptrn-1(lt1)*
CZ17949			*muIs32; ptrn-1(tm5597)*
CZ17887			*muIs32; ptrn-1(ju698)*
CZ17998			*muIs32; klp-7(tm2143); ptrn-1(ju698)*
CZ18102			*ptrn-1(ju698)*
CZ18442			*juIs76; ptrn-1(lt1)*
CZ18379			*ptrn-1(lt1); juEx2843*
CZ18626	pCZGY2432 [P*rgef-1*-PTRN-1]	*juEx5580*	*juIs338; ptrn-1(lt1)*
CZ18904	pCZGY2423 [P*rgef-1*-PTRN-1::GFP]	*juEx5676*	*ptrn-1(lt1)*
CZ18912	pCZGY2432 [P*rgef-1*-PTRN-1]	*juEx5684*	*dlk-1(tm4024); juIs338; ptrn-1(lt1)*
CZ18917	pCZGY2423 [P*rgef-1*-PTRN-1::GFP]	*juEx5676*	*muIs32; cebp-1(tm2807); ptrn-1(lt1)*
CZ18918			*muIs32; cebp-1(tm2807) ptrn-1(lt1)*
CZ19399			*ptrn-1(ju698); juEx2843*
CZ19881			*klp-7(tm2143); ptrn-1(lt1); juIs338*
CZ19883			*ptrn-1(lt1); juIs338*
CZ19884			*klp-7(tm2143); juIs338*
CZ19318			*dlk-1(tm4024); muIs32; ptrn-1(lt1)*
CZ19471	pCZGY2423 [P*rgef-1*-PTRN-1::GFP]	*juEx5677*	*muIs32; ptrn-1(lt1)*
CZ19470	pCZGY2423 [P*rgef-1*-PTRN-1::GFP]	*juEx5676*	*muIs32; ptrn-1(lt1)*
CZ19745		*juEx5676*	*dlk-1(tm4024); ptrn-1(lt1)*
CZ19751		*juEx5676*	N2
CZ19811			*dlk-1(tm4024); juIs338*
CZ19814			*dlk-1(tm4024); juIs338; ptrn-1(lt1)*
CZ19887		*juEx5676*	*juIs252; ptrn-1(lt1)*

Table 3.2. New strains, transgenes and constructs, continued

CZ20133		*juEx5676*	*muIs32*
CZ20136	pCZGY2427 [P*rgef-1*-PTRN-1(CH)]	*juEx6102*	*muIs32; ptrn-1(lt1)*
CZ20139	pCZGY2430 [P*rgef-1*-PTRN-1(ΔCH)]	*juEx6105*	*muIs32; ptrn-1(lt1)*
CZ20147	pCZGY2431 [P*rgef-1*-PTRN-1(ΔCKK)]	*juEx6112*	*muIs32; ptrn-1(lt1)*
CZ20149	pCZGY2433 [P*rgef*-1-PTRN-1::miniSOG] @ 50 ng/µl	*juEx6037*	*muIs32; ptrn-1(lt1)*
CZ20161	pCZGY2429 [P*rgef-1*-PTRN-1(CKK)]	*juEx6125*	*muIs32; ptrn-1(lt1)*
CZ20270	P*rgef-1*-miniSOG; P*myo-2*-mCherry	*juEx3701*	*muIs32*
CZ20271	pCZGY2433 [P*rgef-1*-PTRN-1::miniSOG] @ 20 ng/µl	*juEx6115*	*muIs32; ptrn-1(lt1)*
CZ20274	pCZGY2435 [P*hsp-16.2*-PTRN-1::GFP]	*juEx6177*	*muIs32; ptrn-1(lt1)*
CZ20275	pCZGY2432 [Prgef-1-PTRN-1]	*juEx6178*	*juIs338*
CZ20452	pCZGY2428 [P*rgef-1*-PTRN-1(CC)]	*juEx6214*	*muIs32; ptrn-1(lt1)*
CZ20806	pCZGY2429 [P*rgef-1*-PTRN-1(CKK)]	*juEx6294*	*juIs338; ptrn-1(lt1)*
CZ20807	pCZGY2429 [P*rgef-1*-PTRN-1(CKK)]	*juEx6295*	*juIs338; ptrn-1(lt1)*
CZ20813	pCZGY2429 [P*rgef-1*-PTRN-1(CKK)]	*juEx6301*	*dlk-1(tm4024); muIs32; ptrn-1(lt1)*
CZ20816	[P*rgef-1*-crimson] @ 50 ng/µl + pCZGY2423 [P*rgef*-1-PTRN-1::GFP] @ 20 ng/µl	*juEx6304*	*ptrn-1(lt1)*
CZ20825	pCZGY2424 [P*rgef-1*-GFP::PTRN-1(CC)]	*juEx6308*	*ptrn-1(lt1)*
CZ20828	pCZGY2425 [P*rgef-1*-GFP::PTRN-1(CKK)]	*juEx6311*	*ptrn-1(lt1)*
CZ21227	pCZGY2429 [P*rgef-1*-PTRN-1(CKK)]	*juEx5676*	*dlk-1(tm4024); muIs32; ptrn-1(lt1)*
CZ21410	pCZGY2423 [P*rgef-1*-PTRN-1::GFP] @ 50 ng/µl	*juEx6483*	*ptrn-1(lt1)*
CZ17825	pCZGY2332 [P*unc-25*-EBP-2::GFP]	*juEx5317*	N2

A full-length *ptrn-1A* cDNA was generated by RT-PCR from wild type total RNA. Full length and deletion constructs, generated using Phusion PCR, were made as Gateway entry clones in pCR8 and recombined with destination vectors containing the *rgef-1* promoter. For most other cloning we used Gibson isothermal assembly. Extrachromosomal array transgenes were created by microinjection, following standard procedures.) Constructs were injected at 10 ng/µl unless indicated, together with either the P*ttx-3*-RFP or P*gcy-8*-GFP coinjection marker.

3.7 References

Ahmad, F.J., Joshi, H.C., Centonze, V.E., and Baas, P.W. (1994). Inhibition of microtubule nucleation at the neuronal centrosome compromises axon growth. Neuron *12*, 271-280.

Baas, P.W., Ahmad, F.J., Pienkowski, T.P., Brown, A., and Black, M.M. (1993). Sites of microtubule stabilization for the axon. J Neurosci *13*, 2177-2185.

Baines, A.J., Bignone, P.A., King, M.D., Maggs, A.M., Bennett, P.M., Pinder, J.C., and Phillips, G.W. (2009). The CKK domain (DUF1781) binds microtubules and defines the CAMSAP/ssp4 family of animal proteins. Mol Biol Evol *26*, 2005-2014.

Bounoutas, A., Kratz, J., Emtage, L., Ma, C., Nguyen, K.C., and Chalfie, M. (2011). Microtubule depolymerization in *Caenorhabditis elegans* touch receptor neurons reduces gene expression through a p38 MAPK pathway. Proc Natl Acad Sci U S A *108*, 3982-3987.

Bradke, F., Fawcett, J.W., and Spira, M.E. (2012). Assembly of a new growth cone after axotomy: the precursor to axon regeneration. Nat Rev Neurosci *13*, 183-193.

Chalfie, M., and Thomson, J.N. (1979). Organization of neuronal microtubules in the nematode *Caenorhabditis elegans*. J Cell Biol *82*, 278-289.

Chen, L., Wang, Z., Ghosh-Roy, A., Hubert, T., Yan, D., O'Rourke, S., Bowerman, B., Wu, Z., Jin, Y., and Chisholm, A.D. (2011). Axon regeneration pathways identified by systematic genetic screening in *C. elegans*. Neuron *71*, 1043-1057.

Chisholm, A.D. (2013). Cytoskeletal dynamics in *Caenorhabditis elegans* axon regeneration. Annu Rev Cell Dev Biol *29*, 271-297.

Conde, C., and Caceres, A. (2009). Microtubule assembly, organization and dynamics in axons and dendrites. Nat Rev Neurosci *10*, 319-332.

Erturk, A., Hellal, F., Enes, J., and Bradke, F. (2007). Disorganized microtubules underlie the formation of retraction bulbs and the failure of axonal regeneration. J Neurosci *27*, 9169-9180.

Frokjaer-Jensen, C., Davis, M.W., Hollopeter, G., Taylor, J., Harris, T.W., Nix, P., Lofgren, R., Prestgard-Duke, M., Bastiani, M., Moerman, D.G., Jorgensen, E. M.. (2010). Targeted gene deletions in *C. elegans* using transposon excision. Nature methods *7*, 451-453.

Ghosh-Roy, A., Goncharov, A., Jin, Y., and Chisholm, A.D. (2012). Kinesin-13 and tubulin posttranslational modifications regulate microtubule growth in axon regeneration. Dev Cell *23*, 716-728.

Goodwin, S.S., and Vale, R.D. (2010). Patronin regulates the microtubule network by protecting microtubule minus ends. Cell *143*, 263-274.

Hammarlund, M., and Jin, Y. (2014). Axon regeneration in *C. elegans*. Curr Opin Neurobiol *27C*, 199-207.

Hammarlund, M., Nix, P., Hauth, L., Jorgensen, E.M., and Bastiani, M. (2009). Axon regeneration requires a conserved MAP kinase pathway. Science *323*, 802-806.

Hellal, F., Hurtado, A., Ruschel, J., Flynn, K.C., Laskowski, C.J., Umlauf, M., Kapitein, L.C., Strikis, D., Lemmon, V., Bixby, J., Hoogenraad, C. C., Bradke, F. (2011). Microtubule stabilization reduces scarring and causes axon regeneration after spinal cord injury. Science *331*, 928-931.

Hendershott, M.C., and Vale, R.D. (2014). Regulation of microtubule minus-end dynamics by CAMSAPs and Patronin. Proc Natl Acad Sci U S A *111*, 5860-5865.

Jiang, K., Hua, S., Mohan, R., Grigoriev, I., Yau, K.W., Liu, Q., Katrukha, E.A., Altelaar, A.F., Heck, A.J., Hoogenraad, C.C., Akhamanova, A. (2014). Microtubule minus-end stabilization by polymerization-driven CAMSAP deposition. Dev Cell *28*, 295-309.

Keating, T.J., and Borisy, G.G. (1999). Centrosomal and non-centrosomal microtubules. Biol Cell *91*, 321-329.

Kirszenblat, L., Neumann, B., Coakley, S., and Hilliard, M.A. (2013). A dominant mutation in *mec-7*/beta-tubulin affects axon development and regeneration in *Caenorhabditis elegans* neurons. Mol Biol Cell *24*, 285-296.

Lin, J.Y., Sann, S.B., Zhou, K., Nabavi, S., Proulx, C.D., Malinow, R., Jin, Y., and Tsien, R.Y. (2013). Optogenetic inhibition of synaptic release with chromophore-assisted light inactivation (CALI). Neuron *79*, 241-253.

Liu, K., Tedeschi, A., Park, K.K., and He, Z. (2011). Neuronal intrinsic mechanisms of axon regeneration. Annu Rev Neurosci *34*, 131-152.

Marcette, J.D., Chen, J.J., and Nonet, M.L. (2014). The *Caenorhabditis elegans* microtubule minus-end binding homolog PTRN-1 stabilizes synapses and neurites. Elife *3*, e01637.

Meng, W., Mushika, Y., Ichii, T., and Takeichi, M. (2008). Anchorage of microtubule minus ends to adherens junctions regulates epithelial cell-cell contacts. Cell *135*, 948-959.

Moore, D.L., Blackmore, M.G., Hu, Y., Kaestner, K.H., Bixby, J.L., Lemmon, V.P., and Goldberg, J.L. (2009). KLF family members regulate intrinsic axon regeneration ability. Science *326*, 298-301.

Nguyen, M.M., McCracken, C.J., Milner, E.S., Goetschius, D.J., Weiner, A.T., Long, M.K., Michael, N.L., Munro, S., and Rolls, M.M. (2014). Gamma-tubulin controls neuronal microtubule polarity independently of Golgi outposts. Mol Biol Cell 25, 2039-2050.

Nguyen, M.M., Stone, M.C., and Rolls, M.M. (2011). Microtubules are organized independently of the centrosome in *Drosophila* neurons. Neural Dev *6*, 38.

Ori-McKenney, K.M., Jan, L.Y., and Jan, Y.N. (2012). Golgi outposts shape dendrite morphology by functioning as sites of acentrosomal microtubule nucleation in neurons. Neuron *76*, 921-930.

Park, K.K., Liu, K., Hu, Y., Smith, P.D., Wang, C., Cai, B., Xu, B., Connolly, L., Kramvis, I., Sahin, M., He, Z. (2008). Promoting axon regeneration in the adult CNS by modulation of the PTEN/mTOR pathway. Science *322*, 963-966.

Richardson, C.E., Spilker, K.A., Cueva, J.G., Perrino, J., Goodman, M.B., and Shen, K. (2014). PTRN-1, a microtubule minus end-binding CAMSAP homolog, promotes microtubule function in *Caenorhabditis elegans* neurons. Elife *3*, e01498.

Sahly, I., Khoutorsky, A., Erez, H., Prager-Khoutorsky, M., and Spira, M.E. (2006). On-line confocal imaging of the events leading to structural dedifferentiation of an axonal segment into a growth cone after axotomy. J Comp Neurol *494*, 705-720.

Sengottuvel, V., Leibinger, M., Pfreimer, M., Andreadaki, A., and Fischer, D. (2011). Taxol facilitates axon regeneration in the mature CNS. J Neurosci *31*, 2688-2699.

Shu, X., Lev-Ram, V., Deerinck, T.J., Qi, Y., Ramko, E.B., Davidson, M.W., Jin, Y., Ellisman, M.H., and Tsien, R.Y. (2011). A genetically encoded tag for correlated light and electron microscopy of intact cells, tissues, and organisms. PLoS Biol *9*, e1001041.

Stepanova, T., Slemmer, J., Hoogenraad, C.C., Lansbergen, G., Dortland, B., De Zeeuw, C.I., Grosveld, F., van Cappellen, G., Akhmanova, A., and Galjart, N. (2003). Visualization of microtubule growth in cultured neurons via the use of EB3-GFP (end-binding protein 3-green fluorescent protein). J Neurosci *23*, 2655-2664.

Stiess, M., Maghelli, N., Kapitein, L.C., Gomis-Ruth, S., Wilsch-Brauninger, M., Hoogenraad, C.C., Tolic-Norrelykke, I.M., and Bradke, F. (2010). Axon extension occurs independently of centrosomal microtubule nucleation. Science *327*, 704-707.

Stone, M.C., Nguyen, M.M., Tao, J., Allender, D.L., and Rolls, M.M. (2010). Global up-regulation of microtubule dynamics and polarity reversal during regeneration of an axon from a dendrite. Mol Biol Cell *21*, 767-777.

Tedeschi, A., and Bradke, F. (2013). The DLK signalling pathway--a double-edged sword in neural development and regeneration. EMBO Rep *14*, 605-614.

Topalidou, I., Keller, C., Kalebic, N., Nguyen, K.C., Somhegyi, H., Politi, K.A., Heppenstall, P., Hall, D.H., and Chalfie, M. (2012). Genetically separable functions of the MEC-17 tubulin acetyltransferase affect microtubule organization. Curr Biol *22*, 1057-1065.

Wang, H., Brust-Mascher, I., Civelekoglu-Scholey, G., and Scholey, J.M. (2013). Patronin mediates a switch from kinesin-13-dependent poleward flux to anaphase B spindle elongation. J Cell Biol *203*, 35-46.

Wu, Z., Ghosh-Roy, A., Yanik, M.F., Zhang, J.Z., Jin, Y., and Chisholm, A.D. (2007). *Caenorhabditis elegans* neuronal regeneration is influenced by life stage, ephrin signaling, and synaptic branching. Proc Natl Acad Sci USA *104*, 15132-15137.

Xiong, X., Wang, X., Ewanek, R., Bhat, P., Diantonio, A., and Collins, C.A. (2010). Protein turnover of the Wallenda/DLK kinase regulates a retrograde response to axonal injury. J Cell Biol *191*, 211-223.

Yan, D., and Jin, Y. (2012). Regulation of DLK-1 kinase activity by calcium-mediated dissociation from an inhibitory isoform. Neuron *76*, 534-548.

Yan, D., Wu, Z., Chisholm, A.D., and Jin, Y. (2009). The DLK-1 kinase promotes mRNA stability and local translation in *C. elegans* synapses and axon regeneration. Cell *138*, 1005-1018.

Yau, K.W., van Beuningen, S.F., Cunha-Ferreira, I., Cloin, B.M., van Battum, E.Y., Will, L., Schatzle, P., Tas, R.P., van Krugten, J., Katrukha, E.A., Jiang, K., Wulf, P.S., Mikhaylova, M., Harterink, M., Pasterkamp, R.J., Akhmanova, A., Kapitein, L.C., Hoogenraad, C.C. (2014). Microtubule Minus-End Binding Protein CAMSAP2 Controls Axon Specification and Dendrite Development. Neuron *82*, 1058-1073.

Yu, W., Centonze, V.E., Ahmad, F.J., and Baas, P.W. (1993). Microtubule nucleation and release from the neuronal centrosome. J Cell Biol *122*, 349-359.

Zhou, K., Stawicki, T.M., Goncharov, A., and Jin, Y. (2013). Position of UNC-13 in the active zone regulates synaptic vesicle release probability and release kinetics. Elife *2*, e01180.

Chapter 4

DAPK interacts with Patronin and the microtubule cytoskeleton in epidermal development and wound repair

4.1 Abstract

Epidermal barrier epithelia form a first line of defense against the environment, protecting animals against infection and repairing physical damage. In *C. elegans*, death-associated protein kinase (DAPK-1) regulates epidermal morphogenesis, innate immunity and wound repair. Combining genetic suppressor screens and pharmacological tests, we find that DAPK-1 maintains epidermal tissue integrity through regulation of the microtubule (MT) cytoskeleton. *dapk-1* epidermal phenotypes are suppressed by treatment with microtubule-destabilizing drugs and mimicked or enhanced by microtubule-stabilizing drugs. Loss of function in *ptrn-1*, the *C. elegans* member of the Patronin/Nezha/CAMSAP family of MT minus-end binding proteins, suppresses *dapk-1* epidermal and innate immunity phenotypes. Over-expression of the MT-binding CKK domain of PTRN-1 triggers epidermal and immunity defects resembling those of *dapk-1*

mutants, and PTRN-1 localization is regulated by DAPK-1. Moreover, DAPK-1 itself undergoes MT-dependent transport. Our results uncover an unexpected interdependence of DAPK-1 and the microtubule cytoskeleton in maintenance of epidermal integrity.

4.2 Introduction

Death Associated Protein Kinase 1 (DAPK1) and its related calcium-regulated serine/threonine kinases play a wide variety of roles in cell death and tumor suppression (Bialik and Kimchi, 2006). Mammalian DAPK1 has been implicated in stress responses (Tu et al., 2010), antiviral immunity (Zhang et al., 2014), and in IL-1ß-associated inflammatory diseases (Chakilam et al., 2013; Chuang et al., 2010). In addition, DAPK1 can act as a checkpoint in the macrophage inflammation program (Mukhopadhyay et al., 2008) and as a negative regulator of T-cell receptor-mediated activation of NFκB (Chuang et al., 2008).

In the nematode *C. elegans* the sole DAPK family member, DAPK-1, plays roles in autophagy and in excitotoxic neuronal death (Del Rosario et al., 2015; Kang and Avery, 2009). DAPK-1 also regulates epidermal development and wound repair, independently of known cell death programs. The nematode epidermis is a barrier epithelium that forms the first line of defense against environmental stresses, such as pathogens and physical damage (Engelmann and Pujol, 2010). Mutations in *dapk-1* result in progressive degeneration of the epidermis, cuticle hypertrophy, and constitutive activation of epidermal innate immune responses via a p38 MAPK cascade (Tong et al., 2009). Such *dapk-1* mutants behave as if they are constitutively wounded even without

injury, and when wounded exhibit faster wound repair (Xu and Chisholm, 2011). How DAPK-1 regulates these multiple aspects of epidermal maintenance and wound repair is not yet understood.

Here we took a genetic approach to understanding DAPK-1's functions in the epidermis. We identified genetic suppressors and enhancers of *dapk-1* morphological defects, revealing novel roles for microtubule (MT) regulators in the mature epidermis. Genetic and pharmacological manipulations suggest aberrant *dapk-1* function causes excessive MT stabilization, resulting in morphological defects. *dapk-1* epidermal defects can be suppressed by loss of function in the MT minus end binding protein PTRN-1 and by pharmacological destabilization of MTs. Moreover, expression of the MT-binding domain of PTRN-1 is sufficient to induce *dapk-1*-like epidermal defects. Our data suggest DAPK-1 destabilizes epidermal MTs by inhibiting the function of PTRN-1. We further show for the first time that DAPK-1 itself undergoes MT-dependent transport. Our findings reveal an unexpected interplay between DAPK-1, the epithelial MT cytoskeleton, and epidermal morphology and wound repair.

4.3 Results

4.3.1 *dapk-1* epidermal morphological defects can be suppressed or enhanced by loss of function in microtubule regulators

To identify new *dapk-1* genetic interactors, we screened for genetic suppressors of *dapk-1* epidermal phenotypes. All *dapk-1* mutants display epidermal morphological (Mor) defects, with penetrance varying depending on the allele (Figure 4.1A, 4.2A)

(Tong et al., 2009). The Mor phenotype reflects a progressive accumulation of cuticle and degeneration of the underlying epidermis at the extreme anterior, posterior, and dorsal midline of the epidermis. *dapk-1(ju4)*, which causes a missense alteration S179L in the DAPK-1 kinase domain, causes 100% of the animals to display this aberrant morphology. We mutagenized *dapk-1(ju4)* animals and screened for suppression of the Mor phenotype (see Methods). We identified multiple extragenic suppressors of *dapk-1(ju4)*, two of which are described here. One suppressor, *ju698,* causes a nonsense mutation in *ptrn-1*, which encodes the *C. elegans* member of the Patronin/CAMSAP/Nezha family of MT minus end binding proteins. A null allele *ptrn-1(lt1)* suppressed *dapk-1(ju4)* phenotypes to the same extent as *ptrn-1(ju698)* (Figure 4.1B; 4.2C). Suppression of *dapk-1(ju4)* by *ptrn-1(0)* was rescued by a single-copy insertion (Mos-SCI) *ptrn-1(+)* transgene and by transgenes expressing PTRN-1 under the control of the *dpy-7* promoter, specific to the larval epidermis, indicating that loss of PTRN-1 function in the larval epidermis is required for suppression of the *dapk-1(ju4)* phenotype.

Our screen also identified a mutation in dynein heavy chain, *dhc-1(ju697),* which results in a missense change G2537S in the fifth P-loop of DHC-1. Complete loss of function in *dhc-1* causes lethality (Gonczy et al., 1999); an independent loss-of-function allele *dhc-1(or195*ts*)* fully suppressed *dapk-1(ju4)* morphological defects at 20°C (Figure 4.1B, 4.2C). This suppression was rescued by a DHC-1::GFP single-copy insertion transgene (Figure 4.1B). PTRN-1 and other CAMSAP proteins interact with MT minus ends (Goodwin and Vale, 2010; Jiang et al., 2014), and dynein is critical for MT minus-end dependent transport and MT organization. We found that *dhc-1(or195)* or *dhc-1(or195); ptrn-1(0)* caused more complete suppression of *dapk-1(ju4)* phenotypes than

did *ptrn-1(0)*, suggesting DHC-1 might affect additional pathways required for *dapk-1* function.

We also isolated two intragenic suppressors, *ju1143* and *ju1145,* which result in nonsense mutations (Q608stop and R48stop) in *dapk-1(ju4)* (Figure 4.2B). These mutations reduce the penetrance of *dapk-1(ju4)* Mor phenotypes from 100% to 40% and 30% respectively, and resemble the *dapk-1(gk219)* deletion allele and other CRISPR-generated *dapk-1* knockout alleles (Figure 4.2B, D). Although *dapk-1(ju4)* phenotypes are recessive, the identification of such intragenic suppressors suggests *ju4* causes a gain of function (see Discussion). Both *ptrn-1(lt1)* and *dhc-1(or195)* completely suppressed *dapk-1(gk219)* morphological phenotypes (Figure 4.1B), suggesting loss of function in PTRN-1 or DHC-1 bypasses the requirement for DAPK-1.

Based on our identification of two MT-interacting proteins in our suppressor screen we tested additional MT-associated factors, as well as orthologs of genes known to interact with DAPK1 or CAMSAPs (Table 1). Partial loss of function in *unc-116,* which encodes a kinesin-1 plus-end directed motor, suppressed *dapk-1(ju4)* morphological defects. DAPK family members have previously been implicated in MT stability, promoting function of the MT-associated protein tau via the Pin1 prolyl isomerase or the MARK kinase (Kim et al., 2014; Wu et al., 2011). However, loss of function in orthologs of these genes (*ptl-1, pinn-1, par-1*) did not modify *dapk-1(ju4)* phenotypes (Table 1), suggesting DAPK-1 regulates epidermal MTs via a novel mechanism.

CAMSAPs are thought to promote MT stability in part by protecting minus ends from the MT depolymerizing enzyme kinesin-13 (Goodwin and Vale, 2010). Consistent with this model, loss of function in *klp-7*/kinesin-13 strongly enhanced morphological

defects of *dapk-1(gk219)*, both in *ptrn-1(+)* and in *ptrn-1(0)* backgrounds (Figure 4.1B). Partial loss of function of the MT severing enzymes MEI-1/p60 katanin or SPAS-1/Spastin also enhanced *dapk-1(gk219)* Mor phenotypes. None of these mutants conferred morphological defects in a *dapk-1(+)* background (Figure 4.2D). These analyses suggest that aberrant *dapk-1* function causes epidermal integrity to be sensitized to MT stability. *dapk-1(ju4)* defects were not suppressed by loss of function in several other genes implicated in MT dynamics (Table 1), suggesting a specific subset of MT regulators can affect epidermal morphogenesis.

4.3.2 PTRN-1/Patronin is required for the upregulated epidermal innate immune responses and accelerated wound repair in *dapk-1(ju4)* mutants

In *C. elegans* sterile wounding or fungal infection induces expression of antimicrobial peptides (AMPs) in the epidermis (Couillault et al., 2004; Pujol et al., 2008). *dapk-1(ju4)* animals constitutively express high levels of AMPs such as *nlp-29* and *nlp-30*, and this hyperactive epidermal immune response is genetically separable from *dapk-1(ju4)* epidermal morphological defects (Tong et al., 2009). To address whether the extragenic suppressors or enhancers of *dapk-1* morphological defects also interacted with the innate immune response, we examined *nlp29* expression in *dhc-1(or195)* and *unc-116(e2310)*. Neither mutant suppressed the elevated innate immune response in *dapk-1(ju4)* (Figure 4.3A; Figure 4.4B), as measured using a P*nlp-29*-GFP transcriptional reporter. In contrast, *ptrn-1(0)* fully suppressed the elevated immune response of *dapk-1(ju4)* (Figure 4.3A,B). Among all suppressors tested, only PTRN-1 interacted with DAPK-1 in epidermal morphology and in innate immunity. Given the

unique and specific genetic interactions of *ptrn-1* and *dapk-1*, we focused our analysis on PTRN-1.

DAPK-1 acts in the epidermis to maintain epidermal morphology (Tong et al., 2009). Although epidermal development is overtly normal in *ptrn-1(0)* mutants, PTRN-1 acts redundantly with γ-tubulin and the ninein-like protein NOCA-1 to assemble noncentrosomal MT arrays essential for epidermal development (Wang et al., 2015). However, loss of function in γ-tubulin/TBG-1 did not suppress *dapk-1(ju4)* epidermal defects (Table 1), suggesting DAPK-1 specifically interacts with the PTRN-1 pathway.

dapk-1(ju4) mutants also display accelerated epidermal wound closure, manifested by the rate of closure of actin rings that form around puncture wounds (Figure 4.3C,D) (Xu and Chisholm, 2011). We found that *ptrn-1* mutations suppressed this accelerated wound closure to wild type rates. Moreover, *ptrn-1(0)* single mutants displayed significantly delayed wound closure compared to the wild type. Thus, DAPK-1 and PTRN-1 play antagonistic roles in epidermal development and in wound repair.

4.3.3 Pharmacological modulation of MT stability can suppress or enhance *dapk-1* morphological defects

Because the *dapk-1* epidermal phenotypes are suppressed by loss of function in a MT stabilizing factor (Patronin/*ptrn-1*) and enhanced by loss of function in MT destabilizing factors (Kinesin-13/*klp-7*, Katanin/*mei-1*, Spastin/*spas-1*) we hypothesized that epidermal defects in *dapk-1* mutants might result from excessive stabilization of epidermal MTs. We therefore tested whether drugs that depolymerize MTs (colchicine,

nocodazole) or stabilize MTs (paclitaxel) could modify epidermal Mor defects; some experiments used the *cat-4* cuticle mutant background, which enhances drug sensitivity (Loer et al., 2015).

Colchicine treatment significantly suppressed the epidermal morphology defects of *dapk-1(gk219)* animals (Figure 4.5A). *cat-4* itself strongly enhanced *dapk-1(gk219)*, suggesting that *dapk-1* is also sensitized to defects in cuticle integrity (Figure 4.6A). The morphological defects of *dapk-1(gk219) cat-4* animals were suppressed by colchicine in a dose-dependent manner, and high concentrations of colchicine (5 mM) significantly suppressed *dapk-1(ju4)* phenotypes (Figure 4.6A). Conversely, treatment with the MT stabilizing drug paclitaxel enhanced *dapk-1(gk219)* morphological defects, consistent with Mor phenotypes in *dapk-1(ju4)* mutants being caused by hyper-stabilized MTs (Figure 4.5A). Indeed, paclitaxel treatment of wild type animals could induce *dapk-1*-like epidermal defects, albeit at very low penetrance (Figure 4.5A,B).

ptrn-1(0) mutants display overtly normal epidermal morphology, but were six times more sensitive to the effects of paclitaxel compared to WT animals (Figure 4.5A,B). Paclitaxel also induced morphological defects in *dapk-1(gk219) ptrn-1(0)* double mutants (Figure 4.6A), although not to the same extent as in *dapk-1(gk219)* single mutants (Figure 4.5A). *dhc-1(or195)* single mutants were also hypersensitive to paclitaxel, compared to wild type (Figure 4.6A), possibly reflecting increased free tubulin concentration in these mutants. Taken together, these data are consistent with the model that *dapk-1* mutants display excessively stabilized MTs that cause aberrant epidermal morphology.

We also asked whether pharmacological manipulation of MTs affected the epidermal innate immune response. At high concentrations of colchicine we noted significant suppression of *dapk-1(ju4)* innate immune responses. Conversely, 5 μM paclitaxel induced P*nlp-29*-GFP expression in 40% of *ptrn-1(0)* mutants, including in animals not displaying strong Mor phenotype (Figure 4.6B), while higher concentrations of paclitaxel (15 μM) could induce P*nlp-29*-GFP in a subset of WT animals. Thus, destabilization of epidermal MTs can reverse the upregulation of epidermal innate immune responses in *dapk-1* mutants, while hyper-stabilization of MTs is sufficient to induce the innate immune response, possibly by compromising epidermal integrity.

4.3.4 *dapk-1* mutants display aberrant MTs resembling those of paclitaxel-stabilized animals

The above analyses suggest *dapk-1* mutants might display excessively stabilized MTs. We therefore analyzed epidermal MT architecture using the tubulin marker TBB-2::GFP (see Methods; Figure 4.8A). In the lateral hyp7 epidermal syncytium MTs form a dense meshwork mostly oriented along the anteroposterior axis. In contrast, the dorsoventral compartment of hyp7, overlying body wall muscles, contains parallel circumferential MT bundles spaced 1-1.5 μm apart (Figure 4.5C; Figure 4.8BC; Figure 4.7E). These arrays extend from the lateral epidermis to the dorsal or ventral midlines.

Chronic treatment with colchicine caused breakage and loss of circumferential MT bundles in the dorsoventral epidermis (Figure 4.5D); in the lateral compartment, MTs became sparse and less bundled than in the WT. Conversely, paclitaxel treatment caused circumferential MT bundles to be straighter and thicker (Figure 4.5D, E). At high

paclitaxel concentrations (15 μM), circumferential MT bundles became disorganized and lateral MT bundles were thicker (Figure 4.5D,E). Thus, MT stabilization by paclitaxel results in MTs becoming straighter and more bundled.

We then examined MTs in *dapk-1(ju4)* mutants, focusing on the anterior epidermis, where *dapk-1* morphological defects begin. In early (L2) larvae the MT architecture of *dapk-1(ju4)* animals appeared normal (Figure 4.5C; Figure 4.8B,C). By the late larval (L4) stage a region devoid of MTs appeared in the anterior lateral epidermis of *dapk-1(ju4)* animals (Figure 4.5C, asterisk), apparently due to local degeneration of the epidermis and cuticle overgrowth (Tong et al., 2009). Nearby circumferential MT bundles were disorganized (Figure 4.5C, white arrowheads), however most circumferential MT bundles appeared normal (Figure 4.8B, C), suggesting the local MT defects might be a secondary consequence of the epidermal degeneration. In *dapk-1(ju4)* adults MT bundles were spaced normally (Figure 4.7E,F) but were thinner (Figure 4.8C). In the lateral epidermis of *dapk-1(ju4)* animals MT bundles were straighter and more bundled than in wild type (Figure 4.7A, yellow arrowheads), resembling those of paclitaxel-treated animals. We used FibrilTool to measure anisotropy (directional dependence) of lateral MT bundles (see Methods) and found that *dapk-1(ju4)* mutants displayed increased MT bundle anisotropy compared to wild type (Figure 4.7C). *dapk-1(gk219)* mutants displayed similar MT phenotypes as *dapk-1(ju4)* (Figure 4.8D-H). The similarities between *dapk-1* mutants and paclitaxel-treated animals suggest DAPK-1 destabilizes epidermal MTs.

We next asked whether loss of function in PTRN-1 affected the disorganization of MT architecture in *dapk-1(ju4)*. *ptrn-1(0)* mutant larvae have slightly fewer

circumferential MT bundles (Wang et al., 2015). We found that *ptrn-1(0)* adults displayed a significant loss of circumferential MT bundles (~50% of WT; Figure 4.7A,E,F); remaining bundles were shorter than in the wild type (Figure 4.7D). Lateral MT bundles in *ptrn-1(0)* adults displayed normal anisotropy (Figure 4.7C). In *dapk-1(ju4) ptrn-1(0)* double mutants the number and length of circumferential MT bundles resembled that of *ptrn-1(0)* mutants (Figure 4.7D,E,F). However *ptrn-1(0)* suppressed the increased anisotropy of lateral MTs in *dapk-1(ju4)* to wild type levels (Figure 4.7C). These results indicate that antagonistic interactions between PTRN-1 and DAPK-1 balances MT architecture in epidermis.

We next assessed the effects of *dapk-1* mutants on epidermal MT dynamics using the MT plus end marker EBP-2::GFP (EBP-GFP for brevity). We found that MT plus ends in the wild type adult epidermis were highly dynamic, with 0.09 ± 0.015 comets/μm^2 in the lateral epidermis, and slightly more (0.12 ± 0.015 comets/μm^2) in the dorsoventral epidermis (Video 1,2). The overall density of comets in *ptrn-1(0)* animals was similar to that in wild type (Figure 4.7H), as previously reported for larvae (Wang et al., 2015). By contrast, *dapk-1(ju4)* mutants, as well as *dapk-1(ju4) ptrn-1(0)* double mutants, had significantly more comets in the lateral epidermis than in WT or *ptrn-1(0)* (Video 3,4). In wild type adults, EBP-GFP comets grew at 0.35 ± 0.006 μm/s in the lateral epidermis, and 0.26 ± 0.01 μm/s in the dorsoventral epidermis, comparable growth rates in larval epidermis (Wang et al., 2015). MT growth rates in the lateral epidermis were significantly reduced in *dapk-1(ju4)* mutants, and increased in *ptrn-1(0)* single and in *dapk-1(ju4) ptrn-1(0)* mutants (Figure 4.7G). *dapk-1(ju4)* mutants thus display more

slower-growing MT plus ends in the lateral epidermis, consistent with a partial stabilization of MT dynamics.

Finally we analyzed the directionality of plus-end growth. In the lateral epidermis most EBP-GFP comets grew anteriorly or posteriorly, without a strong bias in directionality. Similarly, in the dorsoventral epidermis equal numbers of EBP-GFP comets grew towards or away from lateral epidermal ridges (Figure 4.7I). EBP-GFP comet directionality was normal in *ptrn-1(0)* mutant and *dapk-1(ju4) ptrn-1(0)* backgrounds. However, *dapk-1(ju4)* mutants displayed a significant bias in comet directionality in the dorsoventral epidermis, such that fewer comets grew away from the lateral epidermis. Thus in *dapk-1* mutants growing MTs are more confined to the lateral epidermis and less likely to extend into the dorsoventral epidermis.

4.3.5 Over-expression of the PTRN-1 CKK domain induces *dapk-1*-like morphology defects

To understand how PTRN-1 might regulate epidermal MTs in the *dapk-1* mutant we tested individual PTRN-1 domains. Like other CAMSAP proteins, PTRN-1 has three conserved regions: an N-terminal calponin homology (CH) domain, of unknown function; a central coiled-coil (CC) domain, known to interact with cytoskeleton associated proteins, and a C-terminal MT-binding CKK domain specific to CAMSAPs (Figure 4.9A). We expressed GFP-tagged fragments of PTRN-1 in the larval epidermis of *dapk-1(ju4) ptrn-1(0)* mutants as multicopy transgenes using the *dpy-7* promoter. As shown above, expression of full-length PTRN-1 rescued the *ptrn-1(0)* suppression phenotypes (Figure 4.1B). Expression of the CKK domain alone also restored the *dapk-1*

epidermal morphology phenotype in *dapk-1(ju4) ptrn-1(0)* double mutants, whereas constructs lacking the CKK domain could not rescue, suggesting the CKK domain is required for PTRN-1 function (Figure 5B). However, constructs containing the CKK domain and either the CC or CH domains (i.e. ΔCH or ΔCC respectively) had significantly weaker rescuing activity compared to the CKK domain alone (Figure 5B). These observations suggest that the CKK domain is critical for PTRN-1 function in the epidermis and is inhibited by the CH or CC domains.

Strikingly, expression of the CKK domain alone in *ptrn-1(0)* mutants caused highly penetrant Mor phenotypes, resembling those of *dapk-1(ju4)* (Figure 4.9B,C). This is in contrast to transgenic animals expressing full-length PTRN-1, which do not induce such phenotypes. The CKK domain acts cell autonomously in the epidermis, as pan-neuronal expression of the CKK domain in *ptrn-1(0)* mutants did not induce Mor phenotypes (not shown). Paralleling our rescue analysis, transgenes expressing the CKK domain and the CH or CC domains did not cause epidermal defects in *ptrn-1(0)* animals. Moreover, expression of the CKK domain only caused aberrant development in a *ptrn-1(0)* background and not in a wild type background (Figure 4.9B), suggesting that the CKK domain activity is inhibited by endogenous PTRN-1. In addition, expression of the CKK domain in *ptrn-1(0)* mutants induced P*nlp-29-GFP* expression, similar to that seen in *dapk-1(ju4)* mutants (Figure 4.9D), and accelerated wound closure (Figure 4.9E). These data are consistent with DAPK-1 and PTRN-1 acting antagonistically in epidermal development, and suggest that DAPK-1 might specifically inhibit the activity of the PTRN-1 CKK domain.

4.3.6 Localization of PTRN-1 along MTs, mediated by its CKK domain, correlates with defective epidermal morphogenesis

In other CAMSAP proteins the CKK domain binds MTs (Baines et al., 2009), whereas the CC domain confers minus-end targeting (Goodwin and Vale, 2010). We therefore investigated whether PTRN-1 localization correlated with its effects on epidermal morphology. Full-length GFP::PTRN-1 localized to puncta and to short filaments ranging that were either thin (0.22 ± 0.01 μm wide) or thick (0.38 ± 0.01 μm) (Figure 4.9F); the latter co-localized with MTs (Figure 4.10E). In contrast, the CKK domain localized to longer thin filaments (Figure 4.9G; Figure 4.10C) and co-localized with MTs (Figure 4.9H). GFP::PTRN-1(ΔCKK) was almost completely punctate (Figure 4.9G). Taken together, the CKK domain is critical for localization along MTs, and MT localization is necessary but insufficient to trigger aberrant epidermal morphology (Table 2).

The PTRN-1 CH domain did not confer subcellular localization, whereas fragments lacking the CH domain localized to filaments and puncta, resembling full length PTRN-1 (Figure 4.9G, Table 4.2). The PTRN-1 CC domain localized primarily to puncta, whereas constructs lacking this domain (ΔCC) did not form puncta or thick filaments (Figure 4.9G). Further dissections suggest the coiled-coil subregions of the CC domain have distinct roles such that CC1 and CC2 promote localization to puncta and thick filaments (Figure 4.9A; Figure 4.10A) and inhibit the CKK domain's ability to induce epidermal morphology defects (Figure 4.10B).

We hypothesized that expression of the CKK domain in the absence of other PTRN-1 domains causes excessive MT stabilization and aberrant epidermal development.

Both full-length PTRN-1 and CKK domain transgenes restored circumferential MTs to *ptrn-1(0)* mutants (Figure 4.10D). However, expression of the CKK domain in a *ptrn-1(0)* background caused circumferential MT bundles to be straighter than in wild type, resembling the effects of paclitaxel treatment (Figure 4.8D). *ptrn-1(0)* mutants expressing full-length PTRN-1 did not display straighter MT bundles or Mor phenotypes (Figure 4.10D). Thus the MT-stabilizing effects of the CKK domain can induce aberrant epidermal development, and are normally inhibited by other PTRN-1 domains.

4.3.7 *dapk-1* mutants display increased PTRN-1 in the epidermis

The above observations suggest that in *dapk-1(ju4)* mutants, PTRN-1's MT stabilization activity, mediated by its CKK domain, might be aberrantly active. We therefore assessed whether PTRN-1 localization or expression was altered in *dapk-1(ju4)* mutants. In the wild type, PTRN-1::GFP formed thick filaments or puncta in the anterior lateral epidermis, and sparse filaments in the body epidermis (Figure 4.11A). By contrast, in *dapk-1(ju4)* adults, PTRN-1::GFP formed twice as many thick filaments in the head (Figure 4.11B,C,D,E). The increased number of PTRN-1 filaments could reflect increased PTRN-1 expression in *dapk-1(ju4)*, as multicopy GFP::PTRN-1 transgenes (Figure 4.11F) also displayed more filaments compared to those seen from a single-copy transgene. However, immunoblotting suggested overall PTRN-1 protein levels were lower in *dapk-1(ju4)* mutants compared to WT (Figure 4.12A).

Increased PTRN-1 filaments in *dapk-1* mutants might be secondary to an increase in MT number or stability. Consistent with this, paclitaxel treatment in *ptrn-1(0)* and *dapk-1(ju4) ptrn-1(0)* double mutants caused increased GFP::PTRN-1 filament formation

(Figure 4.12B,C). The increased association of PTRN-1 with MTs in *dapk-1(ju4)* could reflect a positive feedback loop whereby stabilized MTs recruit more PTRN-1, resulting in further MT stabilization.

We also examined whether DAPK-1 can associate with PTRN-1. Results from co-immunoprecipitation in transfected HEK293T cells show that PTRN-1 can be successfully pulled down with DAPK-1 (Figure 4.12D), suggesting DAPK-1 indeed can physically interact with PTRN-1.

4.3.8 DAPK-1 undergoes directional MT-dependent transport in the epidermis

To further address whether DAPK-1 might affect PTRN-1 or MTs directly, we examined the localization of functional GFP::DAPK-1. Unexpectedly, GFP::DAPK-1 formed discrete puncta that underwent rapid, directed movement within the larval or adult epidermis (*dpy-7* promoter, Figure 4.13A,B,C,D, Video 5; *col-19* promoter, Video 6, 7). In the lateral epidermis GFP::DAPK-1 puncta moved along the anteroposterior body axis, occasionally reversing direction (Figure 4.13C). In contrast, puncta in the dorsoventral epidermis were strongly biased towards moving away from the lateral epidermis (Figure 4.13B,D). GFP::DAPK-1 puncta also aggregated at the edges of the epidermal ridges along the body (Figure 4.13A), as well as in the anterior epidermis, where morphological defects were prominent (Figure 4.14A).

As the pattern of GFP::DAPK-1 dynamics was reminiscent of the arrangement of the MT cytoskeleton, we assessed whether GFP::DAPK-1 dynamics were MT-dependent. In the lateral epidermis GFP::DAPK-1 puncta moved at 1.33 ± 0.028 μm/s; GFP::DAPK-1 movement in the dorsoventral epidermis was slightly slower (Table 4.4). Colchicine

treatment severely reduced the number of moving GFP::DAPK-1 puncta (Figure 4.13E); movement of the remaining puncta was slightly slowed (Figure 4.14B). GFP::DAPK-1 puncta moved ~5 times faster than EBP-2::GFP comets (Figure 4.13F; Table 4.4). Moreover, in contrast to the unidirectional movement of GFP::DAPK-1 away from epidermal ridges plus-end growth occurred in both directions in the dorsoventral epidermis (Figure 4.13G). We infer that GFP::DAPK-1 dynamics reflect MT-based transport.

MT-dependent transport within the mature *C. elegans* epidermis has not been previously characterized. To understand whether other cellular components are transported within the epidermis we examined an early endosome marker, GFP::RAB-5, as endocytosis has been implicated in innate immune responses (Dierking et al., 2011). GFP::RAB-5 formed motile puncta that were smaller and slower-moving than those of GFP::DAPK-1, and moved in both directions in the dorsoventral epidermis (Video 8; Figure 4.13F,G), suggesting GFP::DAPK-1 dynamics are distinct from endosomal transport.

We asked whether DAPK-1's transport correlated with its functions in epidermal morphology. DAPK-1, like mammalian DAPK, contains an N-terminal kinase domain, a Calcium/Calmodulin binding domain, a set of ankyrin repeats, a P-loop, a cytoskeleton-interacting domain and a C-terminal death domain (Shiloh et al., 2013) (Figure 4.2). Constructs lacking any one of these domains, or containing a K57A point mutation predicted to abolish kinase activity (Deiss et al., 1995), were unable to rescue *dapk-1(ju4)* nor did they induce *dapk-1*-like phenotypes (Figure 4.14C, Table 4.3). Uniquely, constructs lacking the kinase domain (ΔKinase) strongly enhanced the Mor phenotype of

a partial loss of function allele *dapk-1(ju469)* (Figure 4.14C), and caused lethality in a *ju4* mutant background (Table 4.3). The enhancement of *dapk-1* phenotypes suggests DAPK-1(ΔKinase) inhibits DAPK-1 in a dominant-negative manner and may also inhibit parallel pathways.

We examined the localization and dynamics of these truncated proteins. Both GFP::DAPK-1(ΔKinase) and GFP::DAPK-1(S179L) formed dynamic puncta that moved at normal or slightly slower velocities (Table 4.3; Figure 4.14B). Conversely GFP::DAPK lacking either the cytoskeletal binding domain or the death domain did not form puncta (Figure 4.14A). No single domain was sufficient for the formation of motile puncta (Table 4.3). However, the kinase domain, ankyrin domain, and cytoskeleton-binding domain by themselves occasionally formed stationary puncta (Figure 4.14A). In summary, multiple non-kinase domains are required for formation of motile DAPK-1 puncta; formation of motile puncta could be necessary but not sufficient for DAPK-1 function.

We next asked whether DAPK-1 transport required motor proteins identified as *dapk-1* suppressors. The velocity of DAPK-1 puncta did not change in *unc-116*/kinesin-1 mutants, but decreased two-fold in *dhc-1(or195)* mutants (Figure 4.13H). *ptrn-1(0)* mutants had fewer moving DAPK-1 puncta in the dorsoventral epidermis, consistent with their reduced numbers of circumferential MTs (Figure 4.13I); the velocity of the remaining GFP::DAPK-1 puncta was normal. Neither *ptrn-1(0)* nor *dhc-1* mutants affected the directional bias of GFP::DAPK-1 transport (Figure 4.13J).

4.4 Discussion

C. elegans DAPK-1 acts as a negative regulator of epidermal maintenance and wound responses, through previously unknown mechanisms (Tong et al., 2009). Here we identify a role for DAPK-1 in regulating the stability or dynamics of the MT cytoskeleton. The minus end factor PTRN-1 is closely linked to DAPK-1 function. DAPK-1 itself is transported along MTs, indicating a complex relationship between DAPK-1 and MT dynamics in epidermal growth and repair.

4.4.1 Normal and mutant functions of DAPK-1

We screened for suppression of morphological defects of the *dapk-1(ju4)* allele, which results in a missense S179L alteration in the peptide-binding ledge of the DAPK-1 kinase domain. This allele, unlike dapk-1(gk219) and CRISPR knockouts of the entire gene locus, displays fully penetrant morphological phenotypes. Our identification of stop codon mutations as intragenic revertants, as well as the fact that transgenic expression of S179L DAPK-1 induced Mor phenotypes, suggests *dapk-1(ju4)* is a gain of function mutation.

How the S179L change causes a gain of function remains to be determined. One hypothesis on why dapk-1(ju4) has a more negative effect than the null is that the mutation disrupts its phosphorylation targets. DAPK-1 has many phosphorylation targets (), and though some may promote the Mor phenotype, such as possibly PTRN-1, others may inhibit it. Loss of function of many factors, either MT associated (klp-7, spas-1, mei-1) or others (cat-4, Tong et al, 2009) can enhance, but not induce, the Mor phenotype. One of these factors may have aberrant function in a dapk-1(ju4) background, and combined with the loss of WT DAPK-1, will enhance the null penetrance to 100%.

This may explain why dapk-1(ju4) is recessive; only when WT DAPK-1 is absent can the Mor phenotype form and be enhanced.

One clue on S179L function lies in our structure function study. Several kinds of truncated versions of mammalian DAPK1 can have dominant-negative behavior (Cohen et al., 1997; Cohen et al., 1999; Lin et al., 2007). In our assays, DAPK-1(Δkinase) strongly enhanced, but did not induce, *dapk-1* phenotypes, while DAPK-1(kinase dead) did neither. DAPK-1(S179L) mayl retain kinase activity, but mis-phosphorylate certain targets to cause the Mor phenotype, while its other domains together can somehow act like DAPK-1(deltakinase) to enhance the Mor phenotype.

Our pharmacological data suggest DAPK-1's normal function is to restrain epidermal MT stabilization. Our suppressor screen and tests of candidate genes suggests a specific interaction between *ptrn-1* and *dapk-1*; thus, DAPK-1 may be regulating epidermal MT stability at least partially through PTRN-1. In addition, we identified *dhc-1* and other cytoskeletal associated proteins that specifically modify *dapk-1* morphological phenotypes; such genes may act downstream of DAPK-1.

Upregulation of the epidermal innate immune response observed in *dapk-1(ju4)* is genetically separable from epidermal morphology defects (Tong et al., 2009) (Fig4.4A,B). Our analysis using MT drugs shows that the concentrations of drugs sufficient to suppress or induce morphological defects are insufficient to suppress or induce innate immune responses, consistent with previous observations (Zhang et al., 2015). Thus, epidermal morphology is more sensitive to MT disruption than is the innate immune response, and MT stabilization may affect innate immune responses indirectly via effects on epidermal integrity.

4.4.2 PTRN-1's function in epidermal development and the MT cytoskeleton

The Patronin/CAMSAP family of MT minus end-binding proteins has become the focus of intense investigation in several organisms (Akhmanova and Hoogenraad, 2015). The sole *C. elegans* member of this family, PTRN-1, is dispensable for epidermal development in part due to a parallel pathway involving γ-tubulin and the Ninein-related protein NOCA-1 (Wang et al., 2015). *ptrn-1(0)* single mutant larvae show grossly wild-type epidermal MT plus-end dynamics and have slightly fewer circumferential MT bundles in the epidermis (Wang et al., 2015), a phenotype that worsens in adults (this work). Thus during development the epidermis becomes more dependent on PTRN-1 and on noncentrosomal MT arrays. Although *ptrn-1* is largely dispensable for epidermal morphology, its requirement becomes evident in wound repair in adults, paralleling the requirement for PTRN-1 in adult axon regeneration in *C. elegans* (Chuang et al., 2014). The requirement for PTRN-1 in repair but not in development may reflect the prominent role of noncentrosomal MT arrays in mature neurons and epithelia.

The MT-binding PTRN-1 CKK domain is not only sufficient to rescue *ptrn-1(0)* suppression phenotypes, but can induce epidermal defects when overexpressed. Depending on the particular CAMSAP family member, the CKK domain can target MT minus ends, or can bind along the lattice (Goodwin and Vale, 2010; Jiang et al., 2014). In *C. elegans* PTRN-1 requires the CKK domain to localize to MTs in neurons and muscles (Richardson et al., 2014), and the CKK domain can stabilize neuronal MTs (Chuang et al., 2014), consistent with MT stability being a determinant of epidermal morphology.

Little is known about how CKK domain activity is regulated, but our data suggest DAPK-1 might directly or indirectly inhibit CKK activity; moreover, the CH or CC domains of PTRN-1 appear to inhibit CKK activity. As the CC domain of PTRN-1 appears to target to minus ends, a possible mechanism is that in the absence of the CC domain, ectopic association of the CKK domain along the MT lattice (long thin filaments) results in aberrant MT stabilization. DAPK-1 might inhibit activity of the CKK domain indirectly via the CC or CH domains (Figure 4.17).

4.4.3 DAPK-1 and MT-dependent transport in the epidermis

To our knowledge, DAPK family members have not been previously shown to undergo MT-dependent transport. Many questions remain concerning the mechanism of DAPK-1 transport; here we speculate on the possible function of DAPK-1 motility in the *C. elegans* epidermis, and why aberrant DAPK-1 function should trigger altered epidermal morphology.

In the *C. elegans* epidermis the MT cytoskeleton is required for cell shape changes (Priess and Hirsh, 1986; Quintin et al., 2016) and for nuclear migrations (Starr, 2011). Epidermal MTs are critical for larval development: noncentrosomal arrays of the larval epidermis require PTRN-1 and the NOCA-1/γ-tubulin pathway (Wang et al., 2015). In contrast, PTRN-1 is required non-redundantly for *dapk-1* epidermal defects, suggesting that in this context PTRN-1 and NOCA-1 pathways are not equivalent.

A key question is why MT stabilization should cause progressive cuticle hypertrophy in specific regions of the epidermis. We speculate that architecture of the epidermis may make it increasingly dependent on intracellular transport as it grows

during larval development and adult life. Epidermal nuclei are confined to lateral and ventral ridges. The squamified dorsoventral epidermis is a barrier to diffusion. Thus, as in neuronal axons, extensive intracellular transport may be required to supply distant regions of the cell with cellular constituents. DAPK-1 may maintain MT dynamics required for active transport of materials to the remoter areas of the epidermis.

In conclusion, we have revealed an unexpected regulatory interaction between DAPK-1 kinase and the MT cytoskeleton in epidermal development and wound responses. Many questions remain to be explored, especially whether PTRN-1 or other MT-associated proteins are direct substrates of DAPK-1. More broadly, the mechanisms and roles of intracellular transport within the epidermis could be a model for intracellular transport in other syncytial tissues.

4.5 Methods

C. elegans genetics

Strains were maintained at 20-22.5°C on NGM agar plates with *E. coli* OP50, unless otherwise indicated. Epidermal morphology defects (Mor phenotypes) were scored in animals grown at 20°C unless stated otherwise. Strains were constructed using standard procedures, and were genotyped by PCR or sequencing. Previously described mutations include: *dapk-1(ju4, gk219, ju469*), *ptrn-1(tm5597, lt1)*. New *dapk-1* suppressor mutations and additional candidate genes tested are listed in Table 1. New transgenic strains are listed in Supplemental File 1A. Representative extrachromosomal arrays are listed; at least three arrays were tested for each experiment.

Molecular biology

New plasmids were made by Gateway cloning or by Gibson isothermal assembly. Site directed mutagenesis of the *dapk-1* cDNA used Gibson assembly. Mutant versions of *ptrn-1* cDNAs have been described (Chuang et al., 2014). New plasmids are listed in Supplemental File 1B.

***dapk-1* suppressor screens, mapping, and whole genome sequencing**

We mutagenized *dapk-1(ju4)* animals with 47 mM EMS using standard protocols and screened the F_2 progeny (~5,000 haploid genomes) for suppression of Mor phenotypes. *dapk-1(ju4)* suppressors were outcrossed once prior to extraction of genomic DNA and whole genome sequencing (BGI Americas). Sequence data were processed and analyzed using MAQgene (*ju697, ju698*) or a Galaxy workflow, comparing datasets to each other and to the wild type reference sequence WS220. We used SNP mapping to locate suppressor *ju698* to a 2.2 Mb interval within which we identified a stop codon mutation in *ptrn-1*. We mapped *ju697* to chromosome I, where we identified a missense alteration in *dhc-1*.

Microtubule drug treatment

Solutions of drugs in M9 were pipetted onto small NGM agar plates (final concentrations 1-5 mM colchicine, 5-15 μM paclitaxel, all from Sigma-Aldrich). Plates were dried for 24 h, then seeded with *E. coli* OP50. Two days later, embryos were plated and allowed to develop at 20°C. Three days later, young adult animals were scored for epidermal defects or assayed for antimicrobial reporter gene expression. To visualize MTs after drug treatment, L4 animals were anesthetized in 0.5 mM levamisole and 2 μM paclitaxel or 2 mM colchicine solution for 2 h before imaging.

Wounding assay

Needle wounding assays were performed as described (Xu and Chisholm, 2011).

Imaging and analysis of epidermal protein dynamics

We found that GFP::TBB-2, EBP-2::GFP, and GFP::DAPK-1 dynamics were inhibited by several anesthetics used to immobilize *C. elegans* for imaging, including muscimol, 1-phenoxy-2-propanol, and levamisole. GFP::DAPK-1 dynamics were also highly sensitive to physical stress; for example, immobilization in 10% agarose and 0.05 μm beads (Kim et al., 2013) immediately blocked dynamics. For the analyses reported here we immobilized animals in 0.5 mM levamisole solution for 50 min, then imaged dynamics in the next 30 min.

We imaged subcellular dynamics using a custom-built microscope (Solamere Technologies) with a Yokogawa CSU-X spinning disk confocal head, a Photometrics Cascade II EM-CCD camera, and a Zeiss NA 1.46 objective. Images were acquired at 4.2 Hz, with exposure time 114 ms at 1000 x magnification, for 100 or 200 frames. We generated kymographs using Metamorph software and determined particle velocity by manual measurement of track angles. We manually counted moving puncta or comets in a 10 frame window, using a 200 μm^2 region of interest (ROI) in the lateral epidermis or a 300 μm^2 ROI in the dorsoventral epidermis.

Western blotting and Co-IP

Worm protein samples were prepared by boiling 10 μl pellets of mixed-stage worms in SDS-mercaptoethanol solution. We detected PTRN-1 using antibody OD208A (Wang et al., 2015); we used the anti-actin antibody ACTN05 (Abcam, C4) as a loading control. We used HRP-linked anti-rabbit IgG NA934V and anti-mouse NXA931 as

secondary antibodies (GE Healthcare Lifesciences) at 1:1000 dilution in TBS, and added SuperSignal West Pico Chemiluminescent substrate (Thermo Scientific). The blot result was replicated once.

DAPK-1 and PTRN-1 were co-transfected into HEK293 cells at a 1:1 ratio. M2-FLAG conjugated magnetic beads were used for IP, and mouse anti FLAG (F1807, Sigma, 1:1000) and anti HA (HA-7, Sigma, 1:5000) antibodies used for western blotting.

Analysis of antimicrobial peptide reporter expression

For visual comparisons of P*nlp-29*-GFP/P*col-12*-dsRed (*frIs7*) expression we took images on a Zeiss compound microscope using a GFP long-pass filter set. To quantify P*nlp-29*-GFP (*frIs7*) expression levels we used the COPAS *C. elegans* BIOSORTer (Troemel lab, UCSD). We calculated the ratio of green fluorescence to the internal control P*col-12*-dsRed.

Imaging and quantitation of epidermal MT and PTRN-1 distribution

Quantitation of MT bundles (P*col-19*-GFP::TBB-2, *juSi239*): (1) We calculated the anisotropy index using the ImageJ plugin FibrilTool (Boudaoud et al., 2014) analyzing a rectangular ROI of 300 μm^2 in the anterior lateral epidermis. (2) We measured MT bundle length by drawing a line scan along a circumferential MT, from the edge of the lateral epidermis or the dorsal or ventral midline, to the end of the bundle. MT bundles detached from the epidermal ridges were not measured. (3) We counted MT bundles in a 40 μm ROI along the lateral epidermis along the anteroposterior axis. (4) We counted MT bundles crossing a 40 μm line in the dorsoventral region, including bundles not attached to the lateral or dorsoventral networks. For parameters 2-4 the ROI begins

40 μm behind the nose tip and extends 40 μm posteriorly. Schematics of ROIs are in Figure 4.7B.

Quantitation of GFP::PTRN-1 filaments (P*dpy-7*-GFP::PTRN-1, *ltSi541*): (1) Number of filaments in the dorsoventral regions of the head were counted in an ROI extending 40 μm from the nose tip (Figure 4.11B). (2) Filaments in the lateral head epidermis were counted in a 200 μm^2 ROI, beginning 40 μm behind the nose. (3) Filaments were counted in the anterior lateral epidermis in a 200 μm^2 ROI. A line of GFP > 1 μm was considered a filament. We did not examine the defective region to avoid quantifying changes in localization secondary to the aberrant epidermal morphology.

Statistics

All statistical analyses were performed with GraphPad Prism.

4.6 Acknowledgements

Chapter 4, in part, has been submitted for publication in eLife, 2016, Chuang M, Hsiao, TI, Tong A, Xu S, Chisholm AD. DAPK interacts with Patronin and the microtubule cytoskeleton in epidermal development and wound repair. The dissertation author was the primary researcher and author of this paper.

We thank our lab members for advice and discussion, Yishi Jin and Nathalie Pujol for comments on the manuscript, and the *Caenorhabditi*s Genetics Center (CGC) and the Mitani lab for strains. We thank Shaohe Wang and Karen Oegema for discussions and reagents, and Kirthi Reddy and Emily Troemel for use of their COPAS worm sorter. We thank Salvatore Cherra for developing the Galaxy workflow. M.C. was supported by the

UCSD Cellular and Molecular Genetics Training Grant (NIH T32 GM007240) and by the UCSD Frontiers of Innovation Scholars Program. This work was supported by NIH R01 GM054657 to A.D.C.

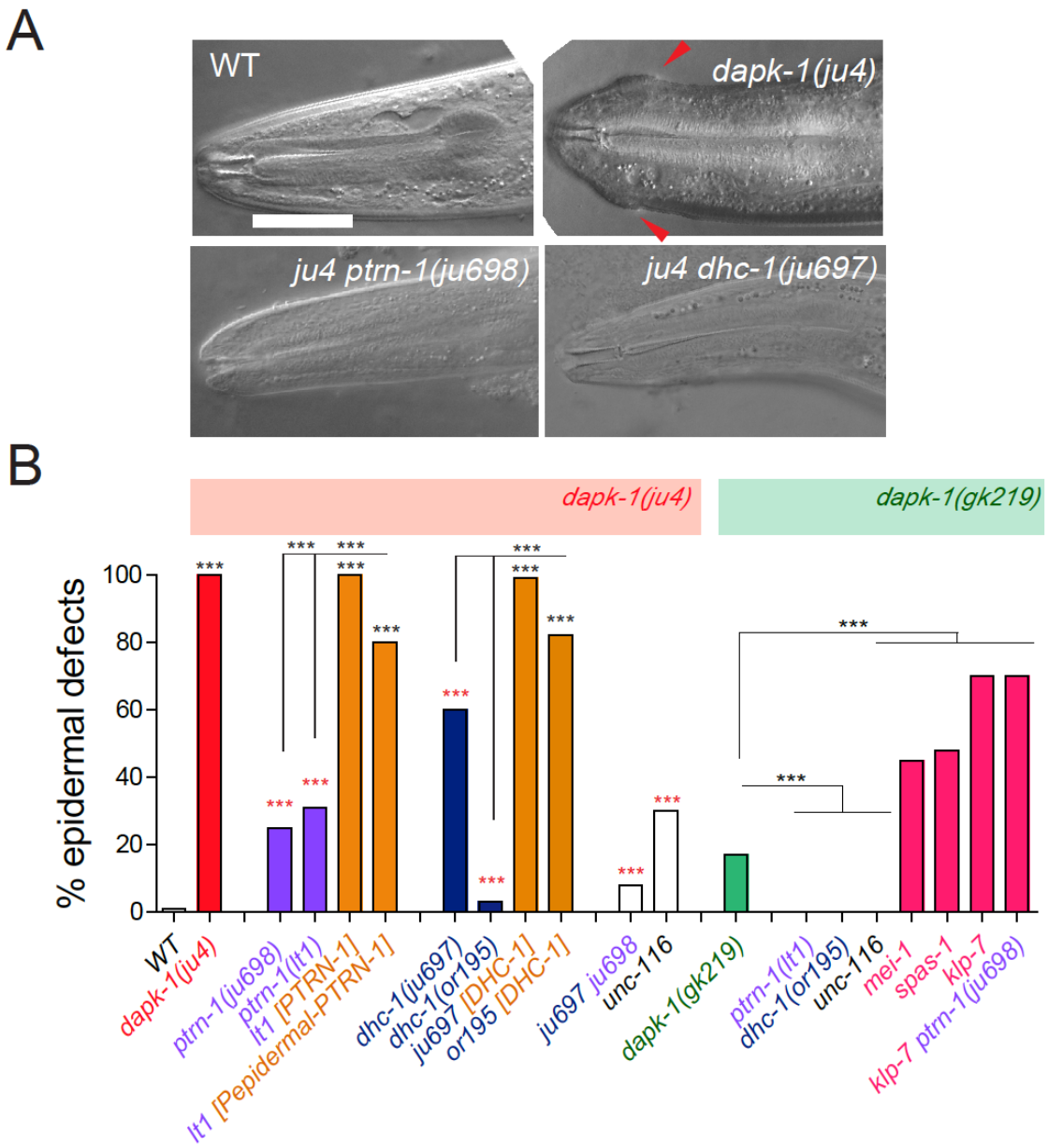

Figure 4.1. *dapk-1* epidermal phenotypes are modified by mutations in cytoskeletal regulating genes

A. Anterior epidermal morphology of wild type adult and aberrant morphology (Mor phenotype, red arrowhead) of *dapk-1(ju4)* animals; suppression by *ptrn-1(ju698)* and *dhc-1(ju697)*. DIC images; scale bar, 10 µm. Anterior is to the left and dorsal up. B. Loss of function in *ptrn-1* and *dhc-1* suppresses the anterior epidermal morphology defects of *dapk-1(ju4)* and *dapk-1(gk219)*. Mor penetrance at 20°C; N>100 per genotype. Fisher's exact test; ***p<0.001. Black stars in B are comparisons to WT; red stars are comparisons to *dapk-1(ju4)*

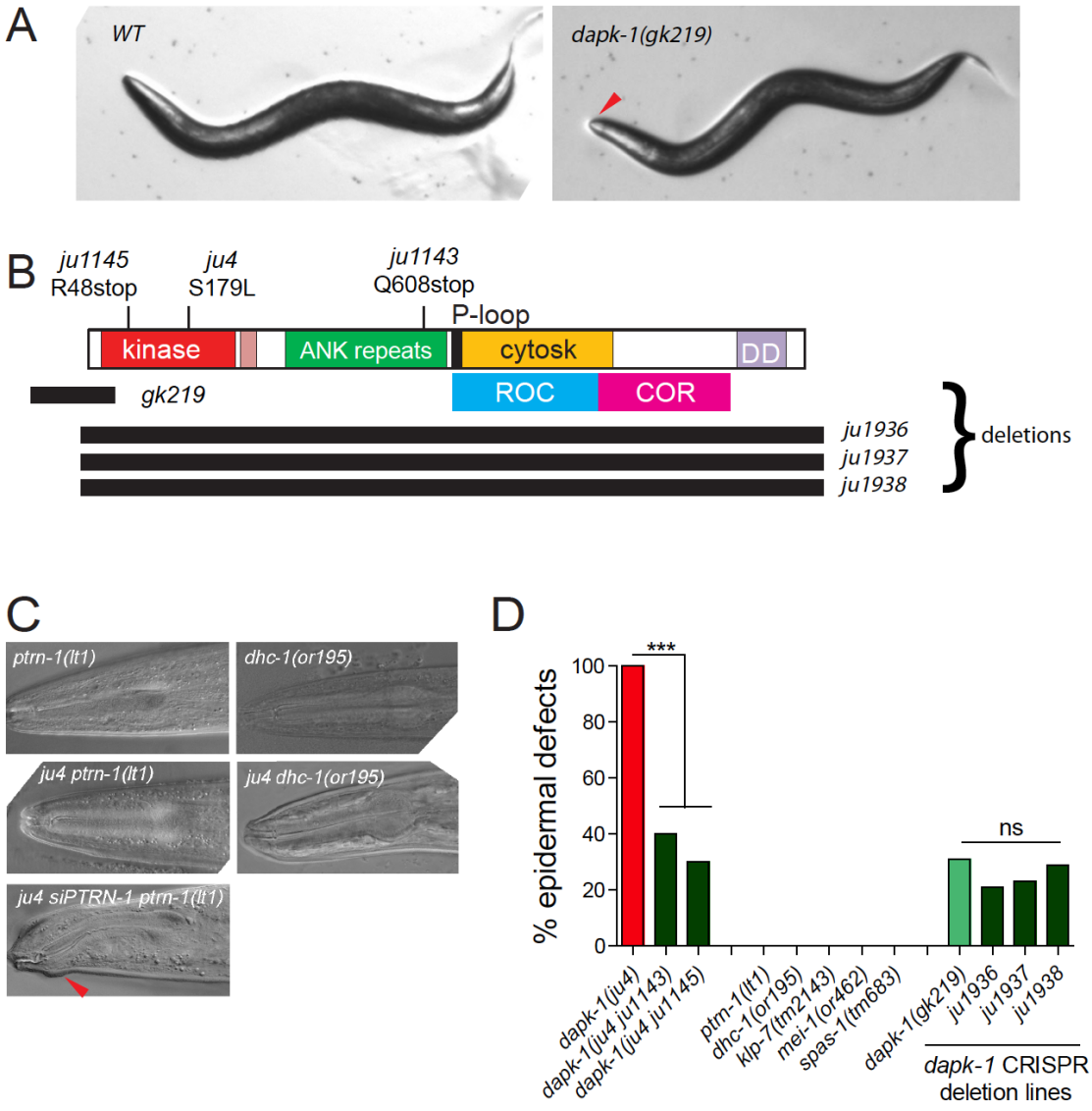

Figure 4.2. Partial suppression of *dapk-1* phenotypes by loss of function in cytoskeletal regulators

A. Dissection scope images of WT and Mor animals. B. Schematic of DAPK-1 protein showing domains and locations of previous and newly identified or generated alleles. C. Suppression of *dapk-1(ju4)* Mor phenotypes by additional alleles of *ptrn-1* and *dhc-1*, and rescue by PTRN-1(+) single copy insertion. *ptrn-1* and *dhc-1* single mutants display normal head morphology. D. Partial suppression of *dapk-1(ju4)* by intragenic stop codon mutations. Mutants that modify *dapk-1(ju4)* do not induce epidermal defects in a *dapk-1(+)* background. *dapk-1(gk219)* mutants have similar penentrance of Mor phenotype as mutants with the entire *dapk-1* gene deleted. N>100. Fisher's exact test; ***p<0.001.

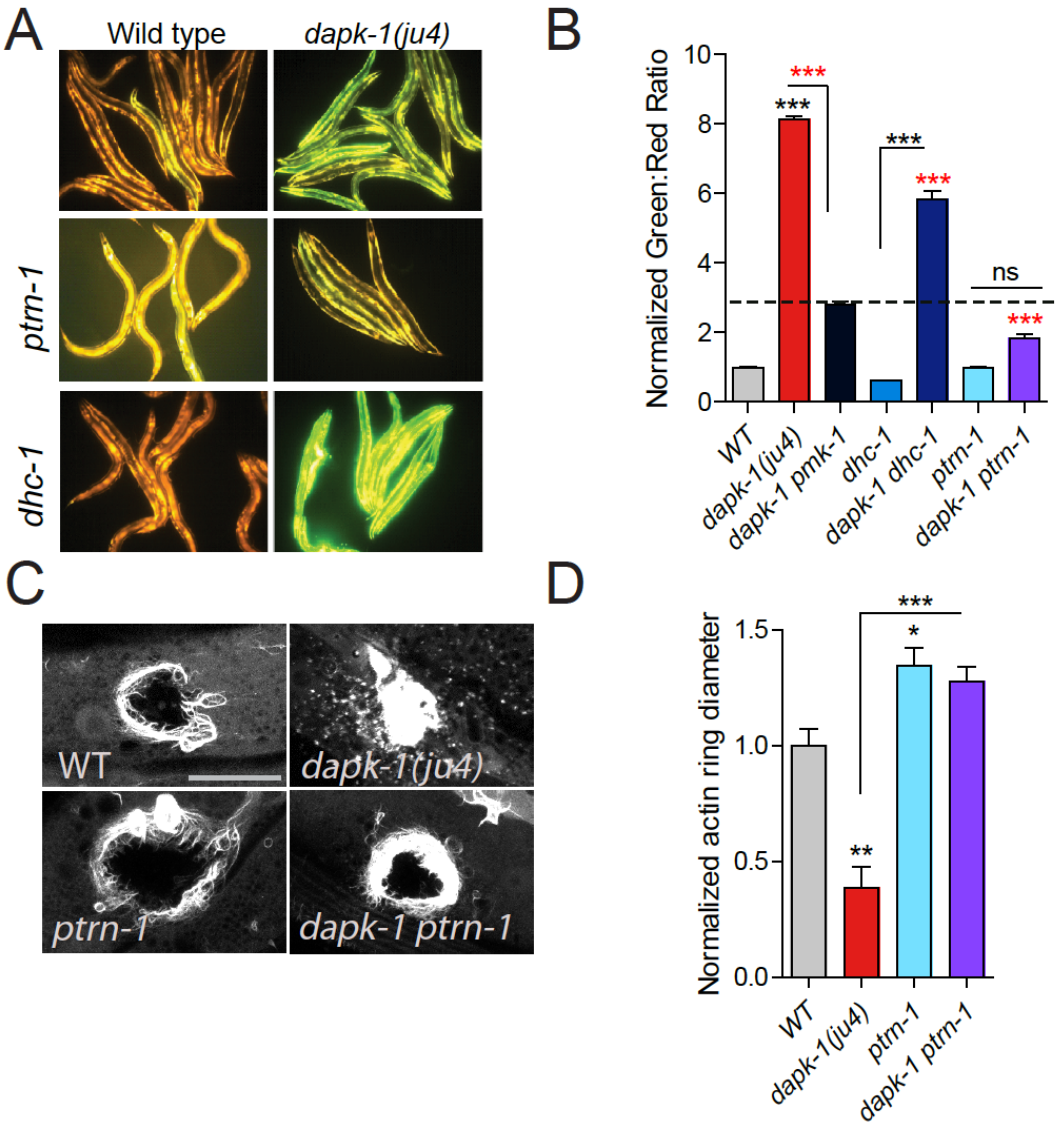

Figure 4.3. *ptrn-1* suppresses *dapk-1(ju4)* innate immune and wound repair phenotypes

A. *dapk-1(ju4)* animals display elevated expression of the antimicrobial peptide *nlp-29* (P*nlp-29*-GFP, *frIs7*); this is suppressed by *ptrn-1(0)*, whereas mutations in *dhc-1(or195)* and other genes do not suppress (see also Figure 4.4A). Day 1 adults. B. Quantitation of fluorescence intensity ratio (Green:Red, normalized to WT = 1) of animals in A, using the COPAS Biosort. N>100. Fisher's exact test; ***p<0.001. *pmk-1* is a MAPK required for activation of *nlp-29* transcription; mutant serves as negative control. C. *ptrn-1(0)* suppresses the accelerated actin ring closure in *dapk-1(ju4)* mutants after needle wounding. The wound-triggered actin ring is visualized using P*col-19*-GFP::moesin (*juIs352*); scale, 10 µm. D. Quantitation of actin ring diameter, mean ± SEM. One-way ANOVA and Dunn's post test; *p<0.05; **p<0.01; ***p<0.001.

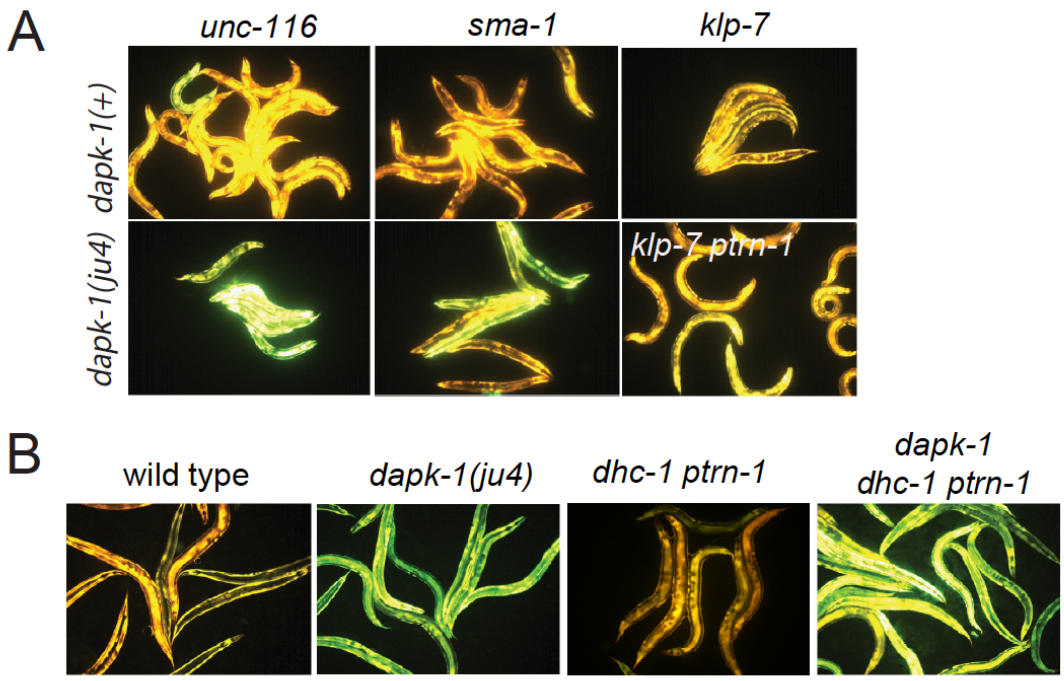

Figure 4.4. Most *dapk-1* modifiers do not affect the *dapk-1(ju4)* constitutitve active innate immune response.

A. *unc-116*, *sma-1*, and *klp-7* do not drastically modify the elevated expression of the *Pnlp-29*-GFP transcriptional reporter in *dapk-1(ju4)* mutants. B. *dhc-1(or195)* is epistatic to *ptrn-1* for the innate immune response phenotype in *dapk-1(+)* background.

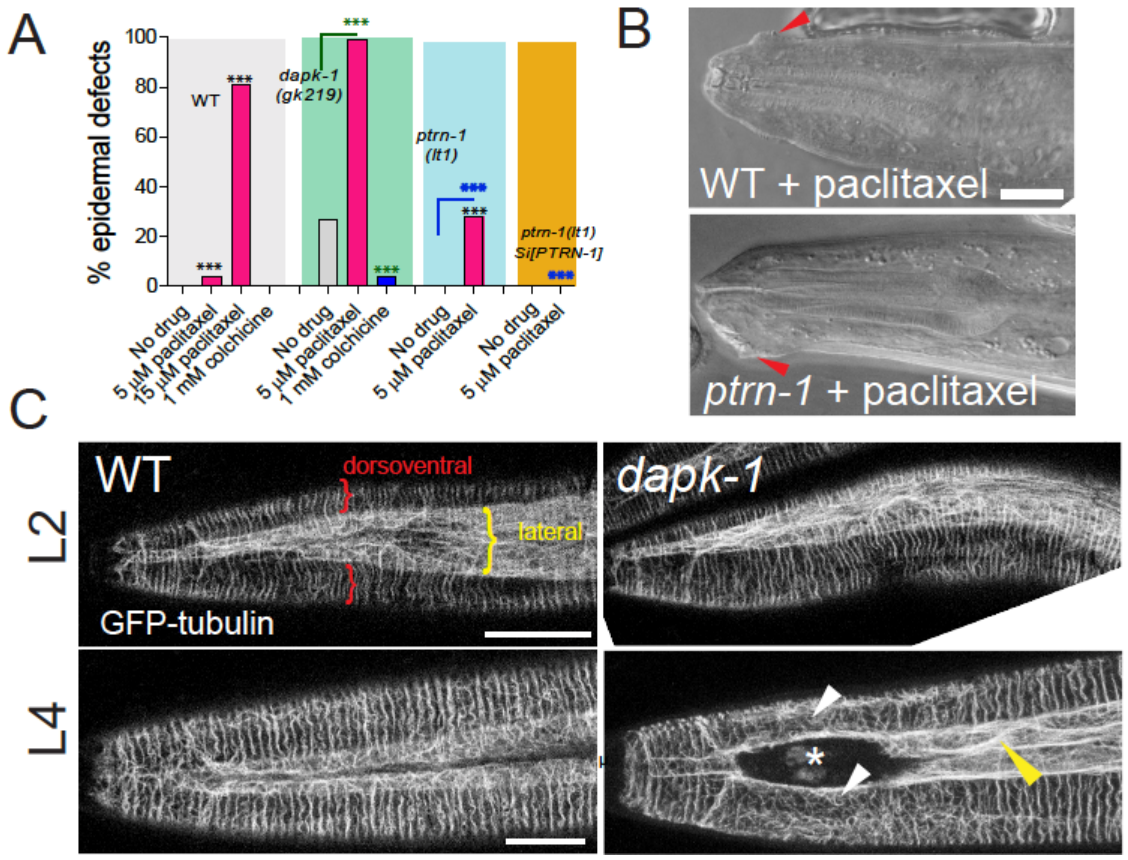

Figure 4.5. *dapk-1* epidermal morphology defects are mimicked or enhanced by MT stabilization and suppressed by MT depolymerization

A, MT stabilization by paclitaxel treatment induces *dapk-1*-like morphological defects in the wild type and in *ptrn-1(0)* mutants, and enhances the morphological defects of *dapk-1(gk219)*. Colchicine treatment suppresses *dapk-1(gk219)* morphological defects. Statistics: Fisher's exact test; ***p<0.001; n > 100 animals per condition. B, DIC images of epidermal defects in representative wild type and *ptrn-1(0)* animals after paclitaxel treatment. C, Confocal images of epidermal MT architecture in the heads of WT and *dapk-1(ju4)* L2 and L4 larvae (P*dpy-7*-GFP::TBB-2, *ltSi570*). Yellow bracket indicates lateral epidermal ridge, red brackets mark dorsoventral epidermis overlying muscles. *dapk-1(ju4)* L4 animals display bundling of MTs in the lateral epidermis (yellow arrowhead) and disorganized circumferential MTs (white arrowhead). D, Effects of MT drugs on epidermal MT organization (*ltSi570*) in heads of L4 animals. Treatment with colchicine causes loss of circumferential MT bundles (yellow asterisks). Treatment with low concentrations of paclitaxel (5 µM) causes circumferential bundles to be brighter and straighter than in wild type (blue arrow); higher concentrations of paclitaxel (15 µM) induce overt MT bundling (yellow arrow), crossing of circumferential MTs (green arrow), and *dapk-1*-like morphological defects (red arrowhead). All scale bars, 10 µm. E, Treatment with 15 µM paclitaxel significantly increases the anisotropy of MT bundles in the lateral epidermis. Statistics, Kruskal-Wallis and Dunn's post test; *p<0.05, ***p<0.001; N>8 animals.

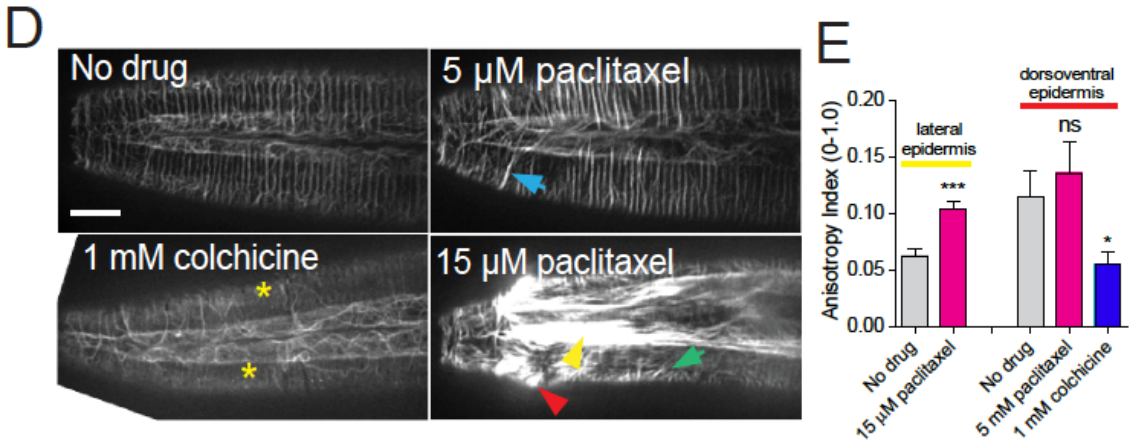

Figure 4.5. ***dapk-1*** **epidermal morphology defects are mimicked or enhanced by MT stabilization and suppressed by MT depolymerization, continued**

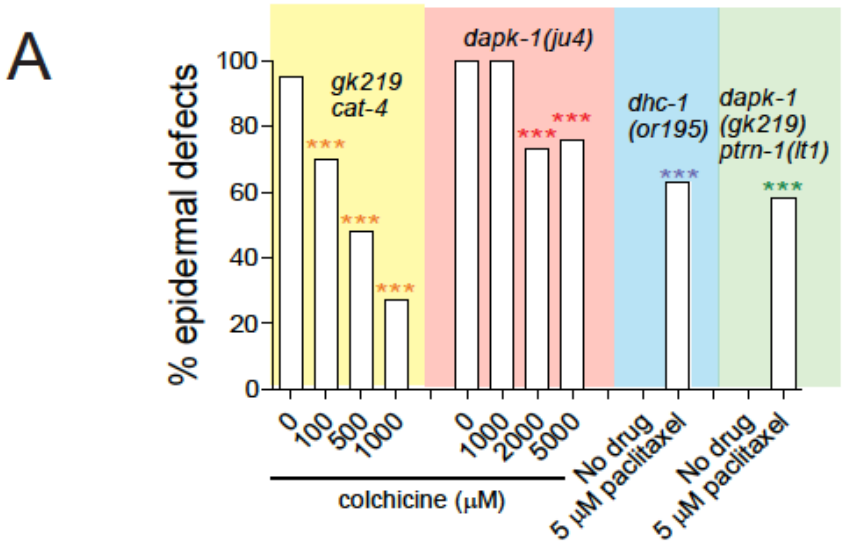

Figure 4.6. Effects of MT-altering drugs on epidermal morphology and innate immune responses in mutant backgrounds

A., MT modulation of epidermal morphology in *dapk-1* mutants. Colchicine suppresses the epidermal morphology defects of *dapk-1(gk219) cat-4* in a dose-dependent manner. *dhc-1(or195)* and *dapk-1(gk219) ptrn-1(0)* backgrounds are hypersensitive to effects of paclitaxel. N>100. Fisher's exact test; ***p<0.001. B. Adult animals with extreme Mor defects after paclitaxel treatment (*Pcol-19*-GFP::TBB-2, *juSi239*). Scale, 10 µm. C. Treatment with colchicine does not induce *nlp-29* expression, while only high concentration colchicine can suppress the constitutively active *nlp-29* expression of *dapk-1(ju4)* mutants; marker: P*nlp-29*-GFP, *frIs7*. D. Treatment with paclitaxel induces *nlp-29* expression in *ptrn-1(0)* mutants, and to a lower extent, in WT animals.

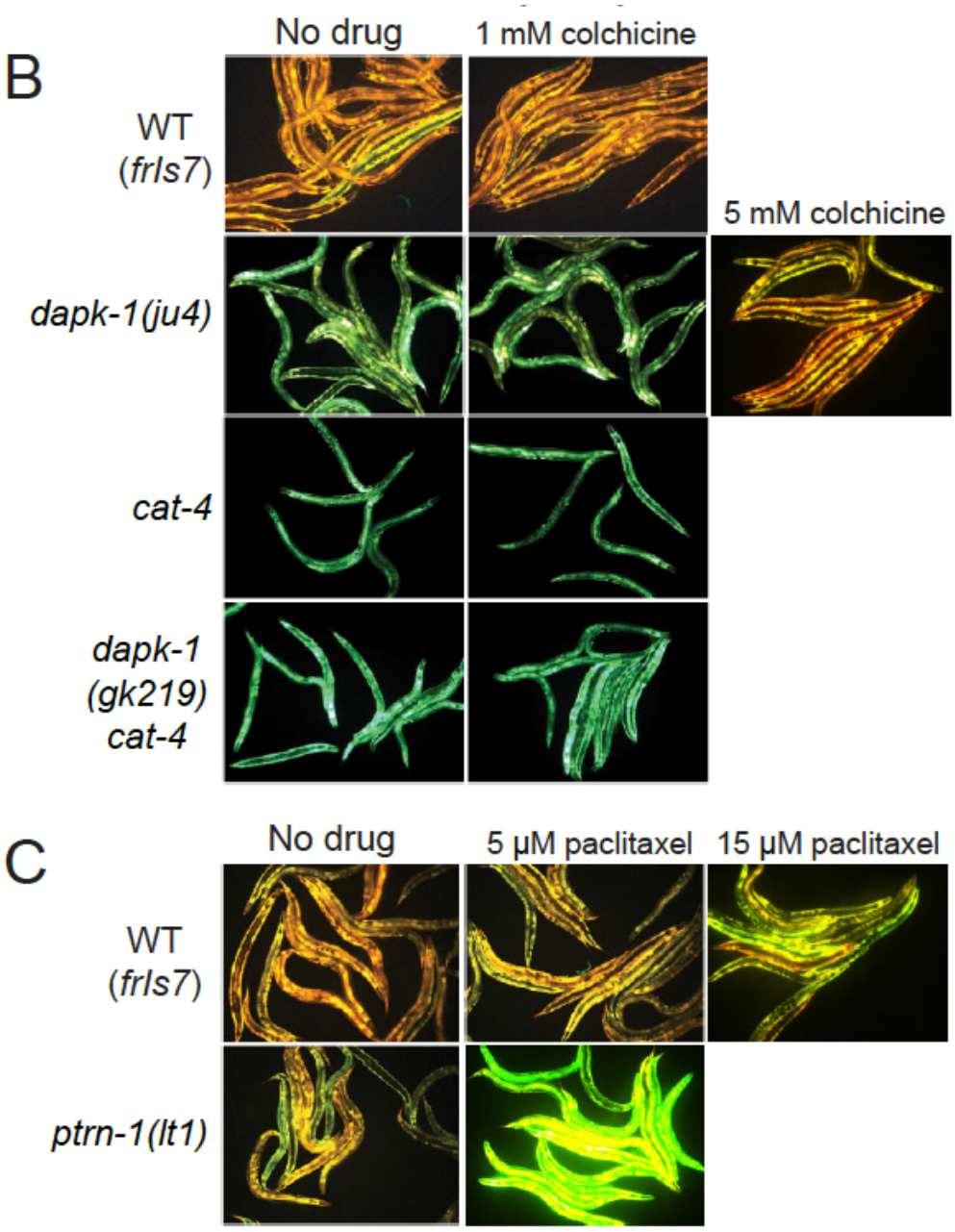

Figure 4.6. Effects of MT-altering drugs on epidermal morphology and innate immune responses in mutant backgrounds, continued

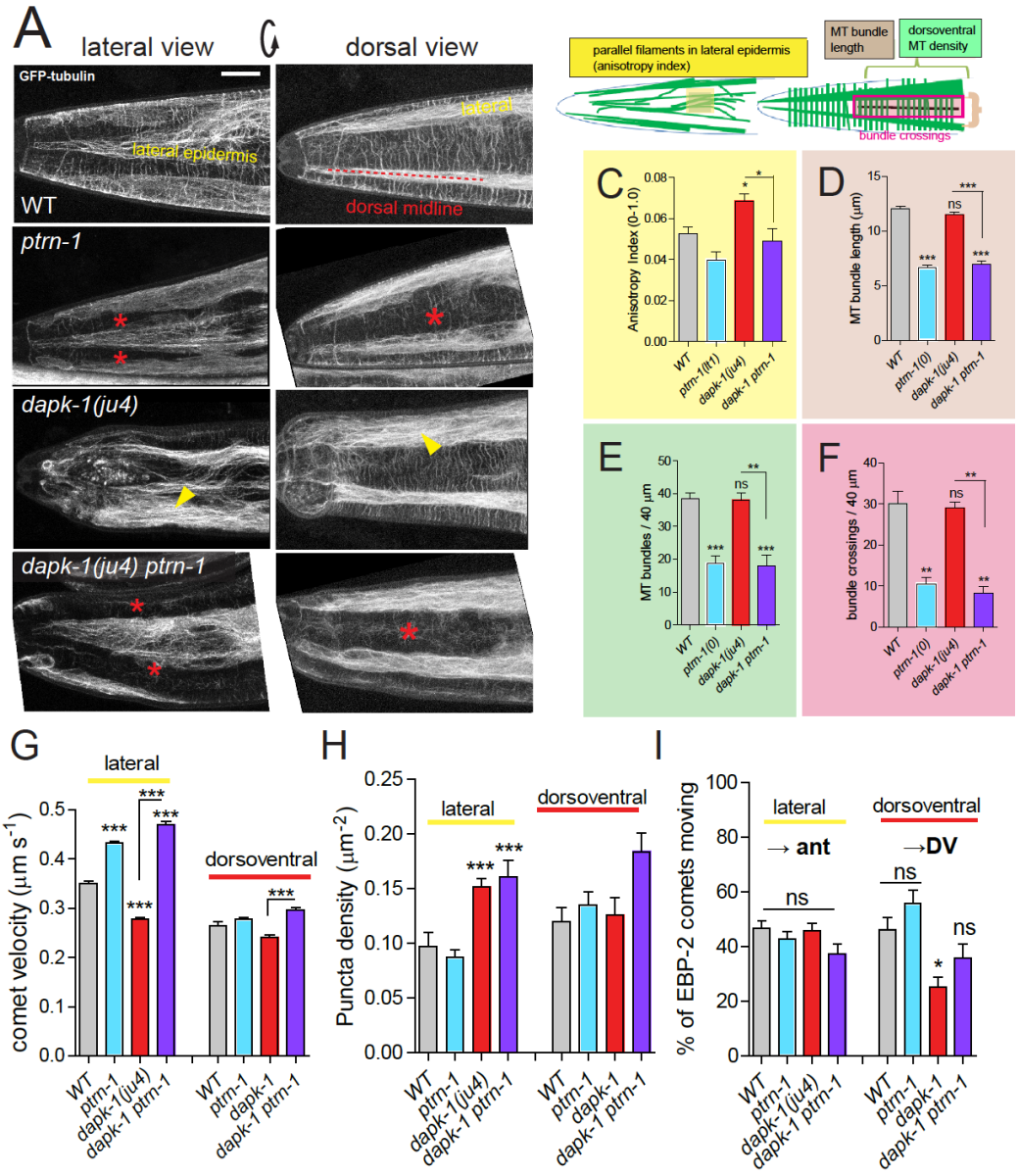

Figure 4.7 *dapk-1* defects in epidermal MT architecture are suppressed by *ptrn-1*

A, *ptrn-1(0)* and *dapk-1(ju4)* display distinct effects on epidermal MT organization; MTs visualized in young adults (P*col-19*-GFP::TBB-2, *juSi239*). Left column, lateral views of the head; right column, dorsal view. *ptrn-1(0)* mutant adults display fewer circumferential MT bundles in the dorsoventral epidermis (red asterisks). *dapk-1(ju4)* mutants display increased bundling in lateral epidermis (yellow arrowhead), quantified by anisotropy index in panel C. *dapk-1(ju4) ptrn-1(0)* double mutants display normal MT bundling in the lateral epidermis and reduced dorsoventral MTs (red asterisks). Scale, 10 µm. B, Cartoon of MT organization in the *C. elegans* lateral and dorsoventral epidermis; colored boxes indicate ROIs used for quantitation of MT parameters in panels C-F. C, *dapk-1(ju4)* animals display elevated MT bundle anisotropy in the lateral epidermis, which is suppressed by *ptrn-1(0)*. D-F, MT bundle length, density and crossing frequency in the dorsoventral epidermis is reduced in *ptrn-1(0)* and in *dapk-1(ju4) ptrn-1(0)* double mutants. N>8 animals per genotype. Bars show mean ± SEM. Kruskal-Wallis and Dunn's post test; *p<0.05; **p<0.01; ***p<0.001. G-I. Quantitation of epidermal EBP-2::GFP comet dynamics in the lateral and dorsoventral epidermis. N>10 animals per genotype.

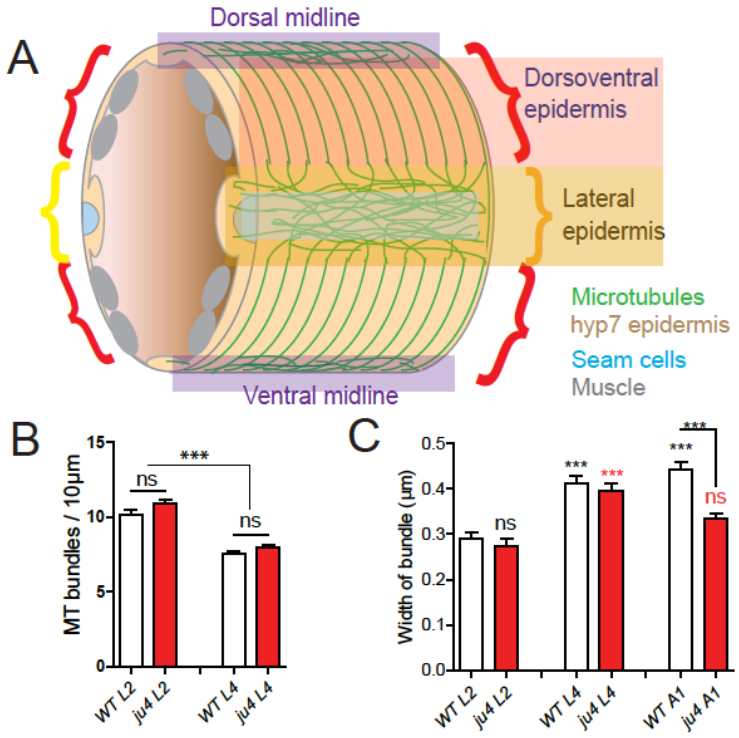

Figure 4.8. Epidermal MTs in wild type and *dapk-1* mutants

A. Cartoon of *C. elegans* post-embryonic epidermis (hyp7 syncytium and lateral seam cells) showing organization of MTs in the lateral and dorsoventral (muscle-adjacent) compartments. A large syncytium (hyp7) encloses most of the adult animal and forms two compartments: thin layers adjacent to the body wall muscle quadrants, and thickened ridges laterally and at the dorsal and ventral midlines (Figure 4.8). The dorsoventral epidermis is extremely thin (~50 nm) along its apicobasal axis and is packed with arrays of hemidesmosome-like attachment structures that link muscles to the external cuticle. In contrast, the lateral epidermis is several µm thick and contains most nuclei. The two sets of MTs, in the lateral and in the dorsoventral epidermis, are seen throughout the hyp7 syncytium and in the smaller epidermal cells of the head and tail. B. MT bundle density in WT and *dapk-1(ju4)* L2 and L4 animals. C. *dapk-1(ju4)* adults display thinner MT bundles. D-G. Quantitation of the different aspects of *dapk-1(gk219)* MT architecture. Graph color scheme matches colored ROIs in Figure 4.7B. All graphs: Kruskal-Wallis test and Dunn's post test; *p<0.05, ***p<0.001, N>8. H. Confocal images of lateral epidermis (P*col-19*-GFP-tbb-2, *juSi239*). Scale, 10 µm.

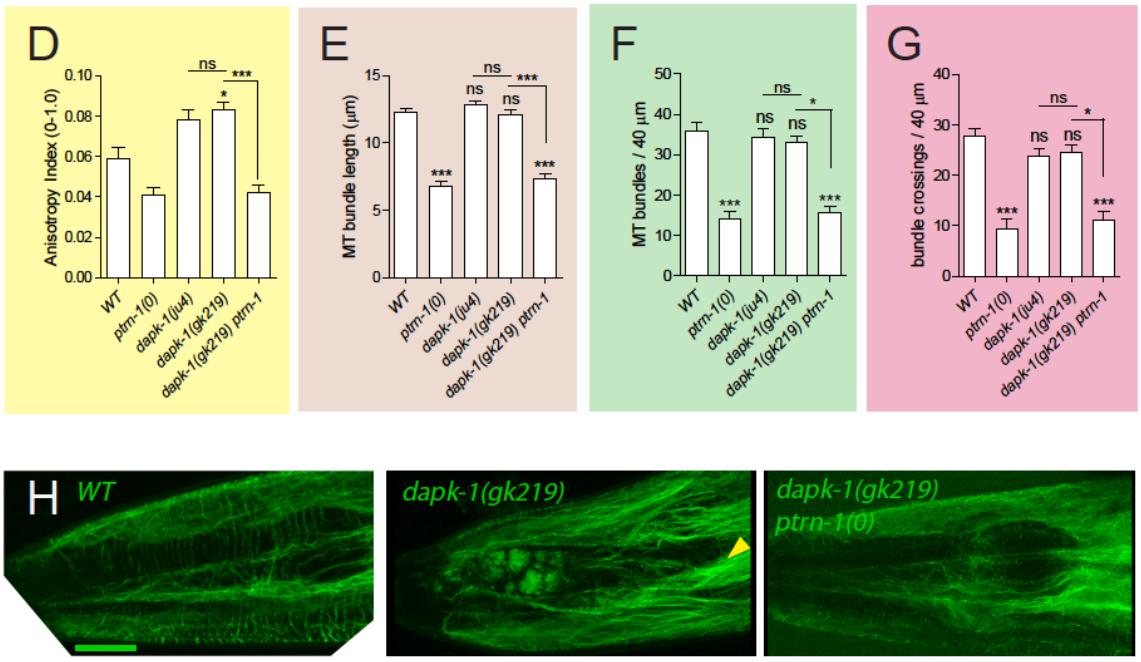

Figure 4.8. Epidermal MTs in wild type and *dapk-1* mutants, continued

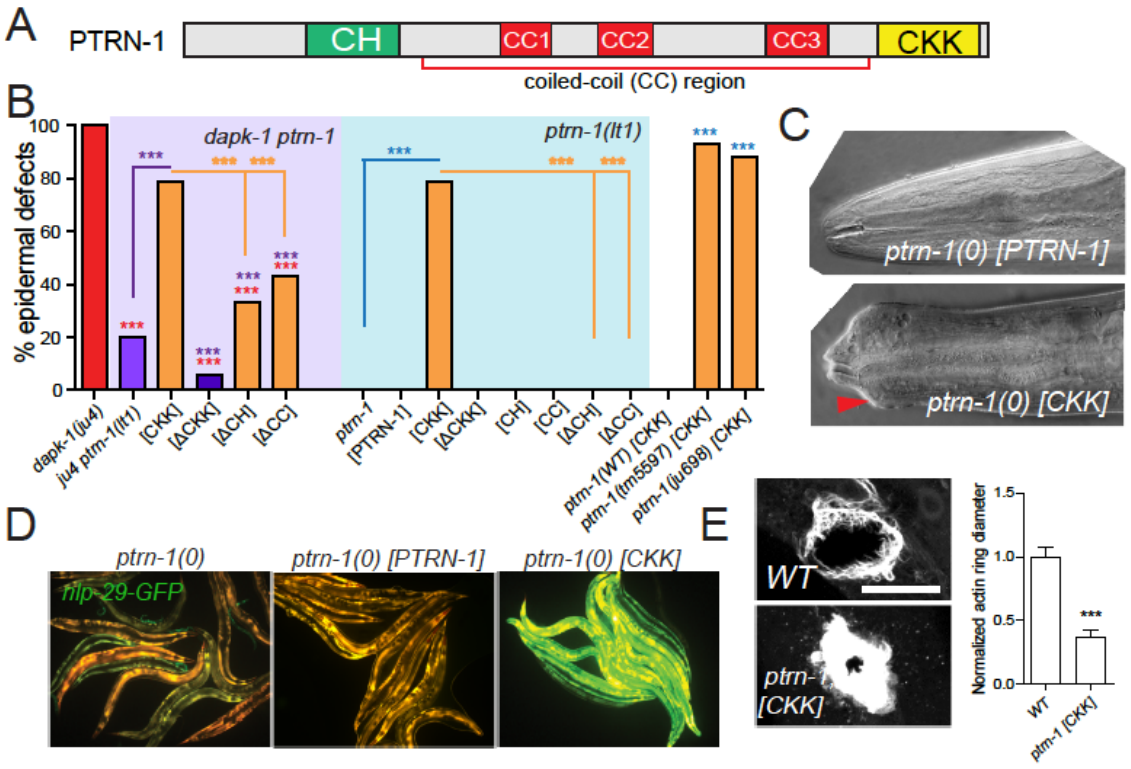

Figure 4.9. The CKK domain of PTRN-1 is required and sufficient to cause *dapk-1*-like defects in epidermal morphology

A, PTRN-1 domain organization. B, Quantitation of epidermal defects in animals expressing different truncations of GFP::PTRN-1. N>100. Fisher's exact test; ***p<0.001. C, Representative DIC images of heads of animals expressing full length PTRN-1 or the CKK domain alone (*dpy-7* promoter, *juEx6697* and *juEx6695*), in *ptrn-1(lt1)*. D, Over-expression of the CKK domain is sufficient to induce P*nlp-29*-GFP expression in *ptrn-1(0)* mutants (*frIs7*; *juEx7385*) and E, speed up wound closure (*juIs352*; *juEx6825*). N>15, t-test; ***p<0.001. F, Localization of full length GFP::PTRN-1 in the larval epidermis *(juEx6697)*. White arrowhead points to a thick filament in the midbody lateral epidermis. PTRN-1 also localizes to puncta (blue arrow) and thin filaments (red arrowhead). All scale bars, 10 µm. G. Localization of GFP-tagged PTRN-1 fragments in larval epidermis. H, Colocalization of PTRN-1 CKK domain and MTs in anterior larval epidermis. Genotype: *ptrn-1(lt1)*; *juEx6825* (P*dpy-7*-mKate2::CKK); *ltSi570* (P*dpy-7*-GFP::TBB-2). Asterisk indicates region devoid of MTs.

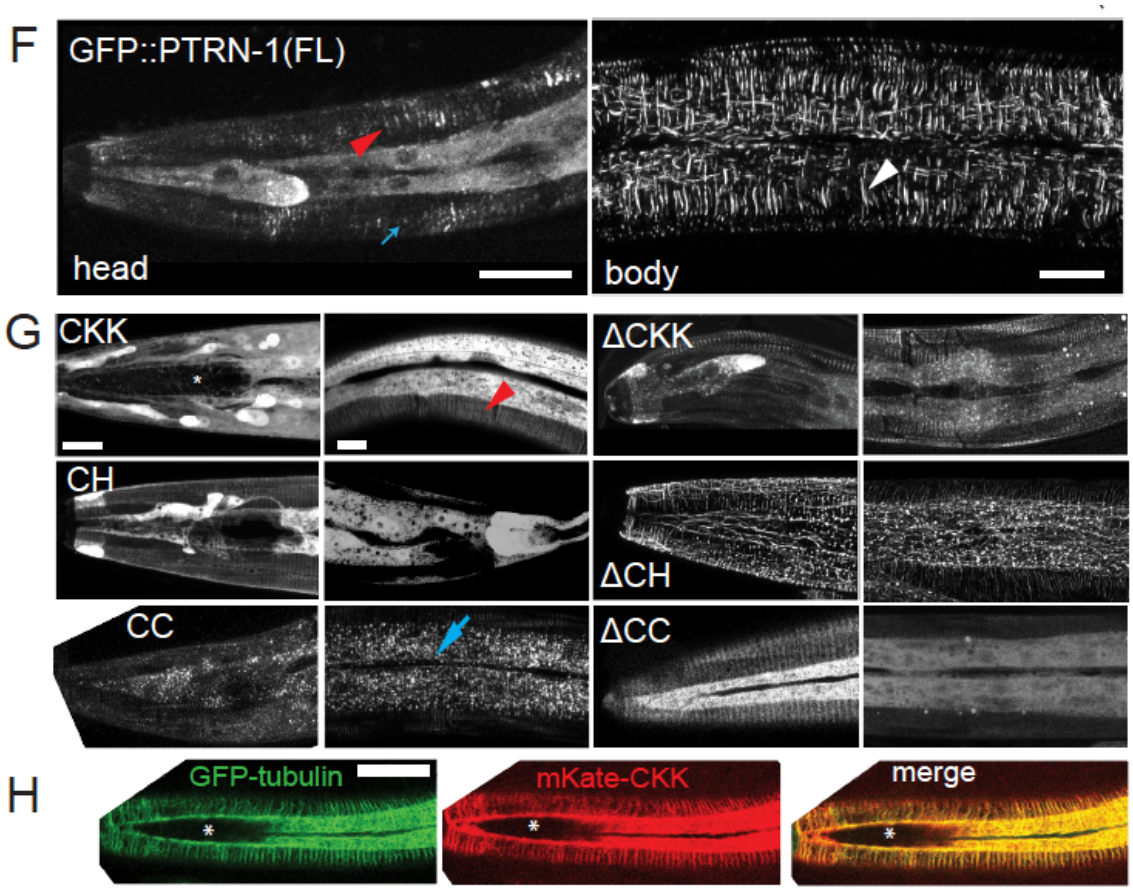

Figure 4.9. The CKK domain of PTRN-1 is required and sufficient to cause *dapk-1*-like defects in epidermal morphology, continued

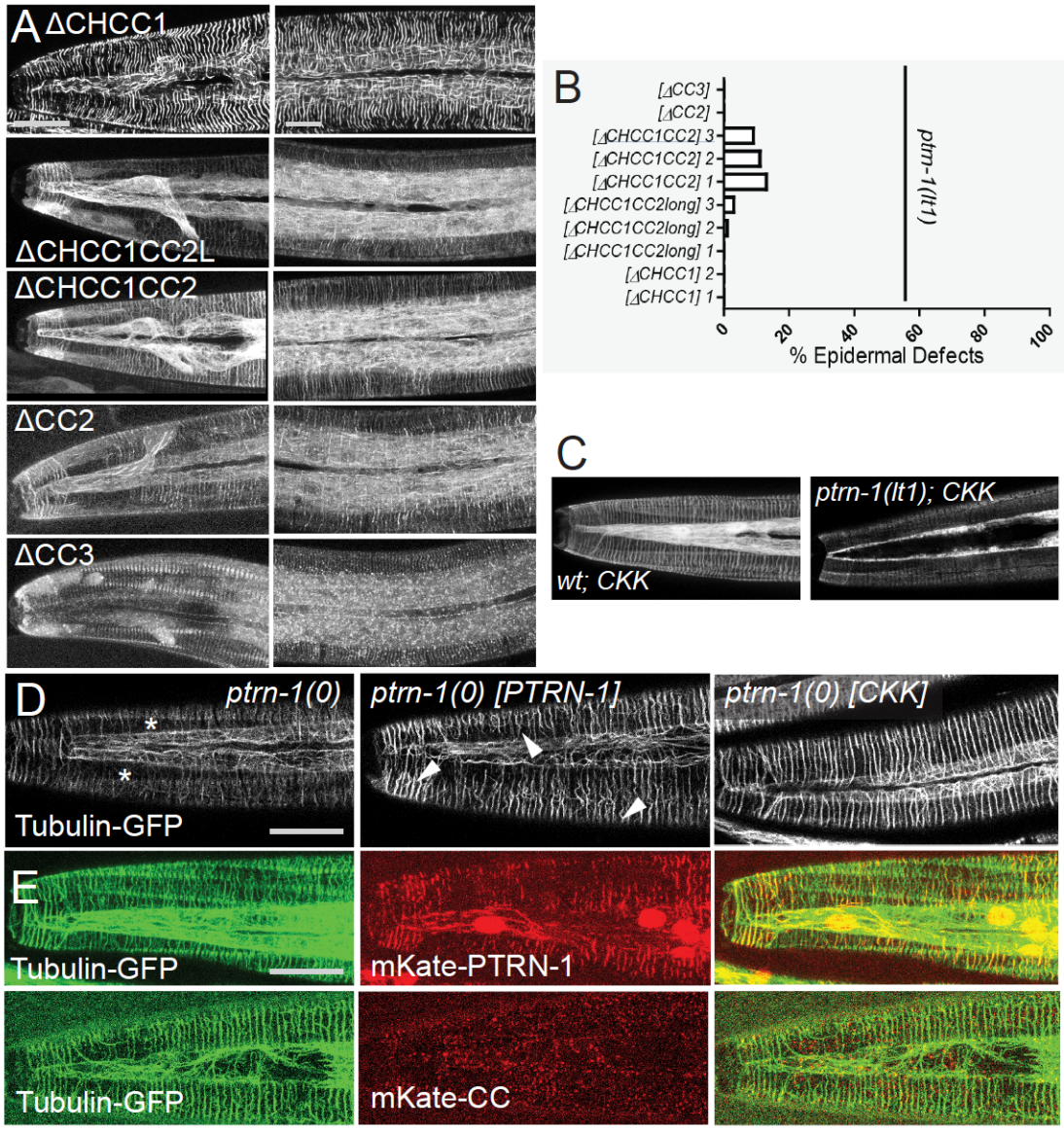

Figure 4.10. Structure-function analyses of PTRN-1

A. Localization of GFP-tagged fragments of the PTRN-1 coiled coil (CC) domain, in the head (left) and anterior lateral epidermis (right). Scale bars, 10 μm. B. Quantitation of epidermal defects of transgenic animals expressing fragments of the CC domain. C. The CKK domain localizes strongly to filaments in *ptrn-1(+)* but not so strongly in *ptrn-1(0)* backgrounds. D. Expression of the CKK domain, but not of full-length PTRN-1, causes MT bundles to straighten (marker: *ltSi570*). E. Full length PTRN-1 and the CC domain co-localize with MTs (P*dpy-7*-mKate2::PTRN-1, *juEx6762*; P*dpy-7*-mKate2::CC, *juEx6822*).

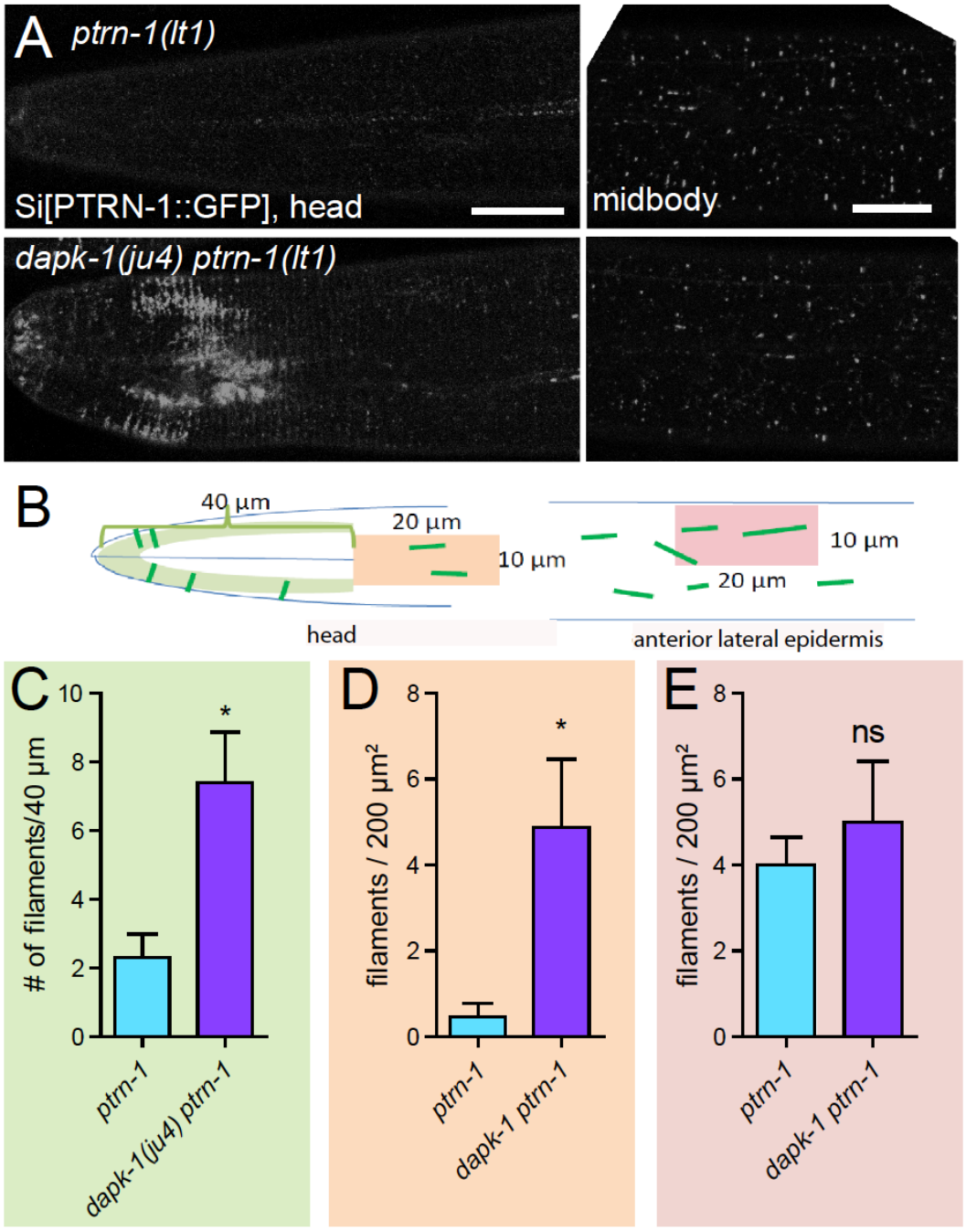

Figure 4.11. *dapk-1(ju4)* mutants display aberrant PTRN-1 localization

A. Localization of PTRN-1::GFP expressed from single-copy insertion in L4 stage anterior epidermis (left) and midbody lateral epidermis (right); transgene P*dpy-7*-PTRN-1::GFP, *ltSi541*, in *ptrn-1(0)* or *dapk-1(ju4) ptrn-1(0)* background. Scale bars, 10 µm. B. Schematic showing ROIs analyzed in the anterior epidermis. C-E. Quantitation of PTRN-1 localization in ROIs indicated in B. Experiments performed at 25°C. N>8 animals per genotype. Bars indicate mean ± SEM. Student's t-test; *p<0.05.

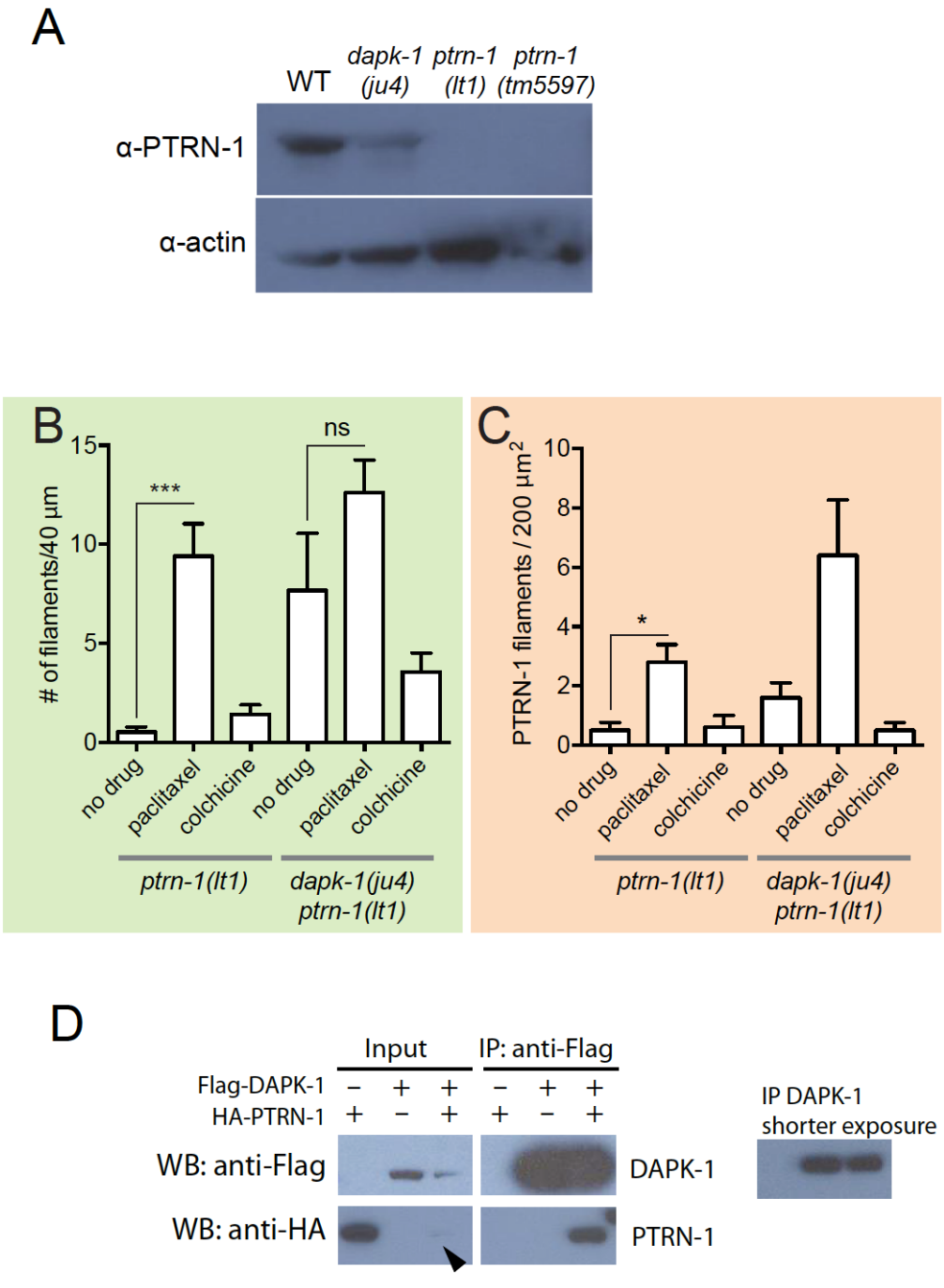

Figure 4.12. PTRN-1 localization is sensitive to MT polymerization and *dapk-1*

A. PTRN-1 is not overexpressed in *dapk-1(ju4)* animals; western blot using anti-CePTRN-1. Control, anti-actin. B,C. The number of PTRN-1 filaments in the head and lateral epidermis is sensitive to MT polymerization. Paclitaxel increases the number of PTRN-1 filaments, and colchicine decreases the number of PTRN-1 filaments in *dapk-1(ju4)* mutants. Color code according to the ROIs in Figure 11B. Mean ± SEM, N > 8 animals per genotype. Kruskal-Wallis and Dunn's post test; *p<0.05; ***p<0.001. D. Co-immunoprecipitation (Co-IP) of DAPK-1 and PTRN-1 in HEK293T cells.

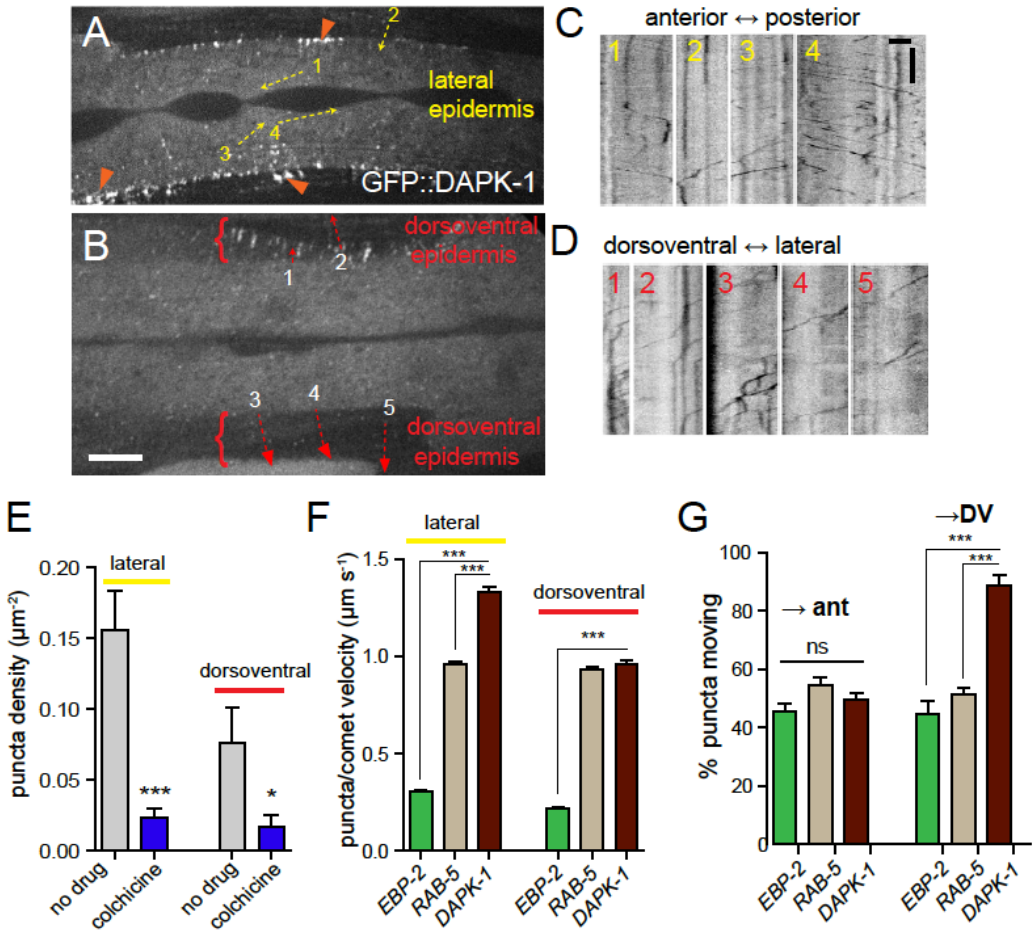

Figure 4.13. DAPK-1 undergoes MT-dependent transport in the epidermis

A, B. Representative images of GFP::DAPK-1 puncta in larval epidermis (P*dpy-7*-GFP::DAPK-1, *juEx1774*), showing lateral and dorsoventral regions, respectively. Dotted arrows indicate line scans used to generate kymographs in C,D. Orange arrowheads indicate clusters of GFP::DAPK-1 puncta at the boundary of the dorsoventral epidermis. Scale bars, 10 µm. C. Kymographs of puncta in lateral epidermis (movie frame in A); inverted grayscale; x axis scale, 10 µm; y axis scale, 10 s. D. Kymographs of puncta in dorsoventral epidermis (movie frame in B). E. Density of motile GFP::DAPK-1 puncta in adult anterior lateral epidermis, with or without colchicine treatment (*cat-4*; P*col-19*-GFP::DAPK-1 *juEx4781*). N>20. F. GFP::DAPK-1 puncta move faster than RAB-5 puncta or EBP-2 comets in the lateral epidermis (P*col-19*-GFP::DAPK-1, *juEx4781*). n>100. Bar charts show mean ± SEM. Statistics, Kruskal-Wallis test and Dunn's post test; *p<0.1, ***p<0.001. G. Directionality of puncta or comet motion. Approximately equal numbers of RAB-5 and EBP-2 comets move in each direction; only DAPK-1 displays a significant bias in the dorsoventral epidermis. H. Reduced dynein/*dhc-1* function slows GFP::DAPK-1 puncta; loss of *ptrn-1* or mutation in *unc-116*/kinesin-1 has no effect; n>100. I. *ptrn-1(0)* mutants have reduced DAPK-1 puncta in the dorsoventral epidermis. J. DAPK-1 puncta directionality is unaffected in *ptrn-1(0)* or *dhc-1* mutants.

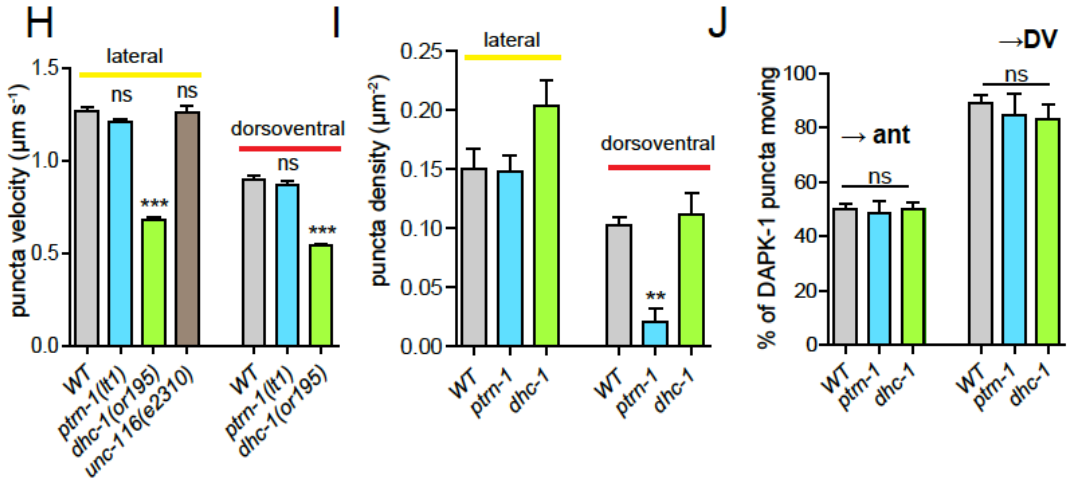

Figure 4.13. DAPK-1 undergoes MT-dependent transport in the epidermis, continued

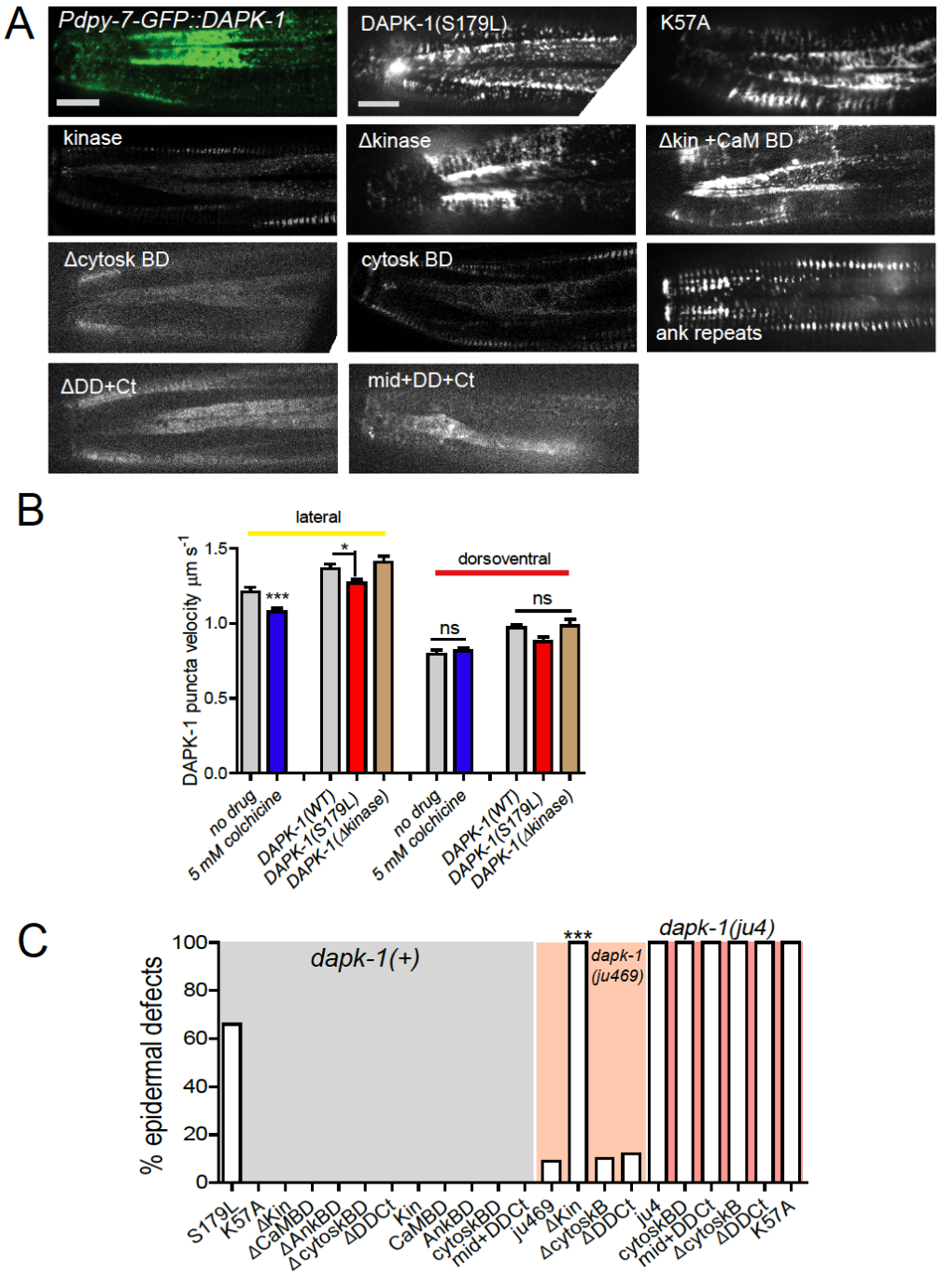

Figure 4.14. Structure function analysis of DAPK-1

A. Representative images of GFP-tagged DAPK-1 protein fragments and their localization in the lateral epidermis in the head. B. Velocity of DAPK-1 puncta, with or without colchicine treatment (*cat-4*; P*col-19*-GFP::DAPK-1 *juEx4781*). n>20. Velocity of mutant DAPK-1. C. Quantitation of Mor induction or enhancement of different DAPK-1 fragments. N>100. Fisher's exact test; ***p<0.001.

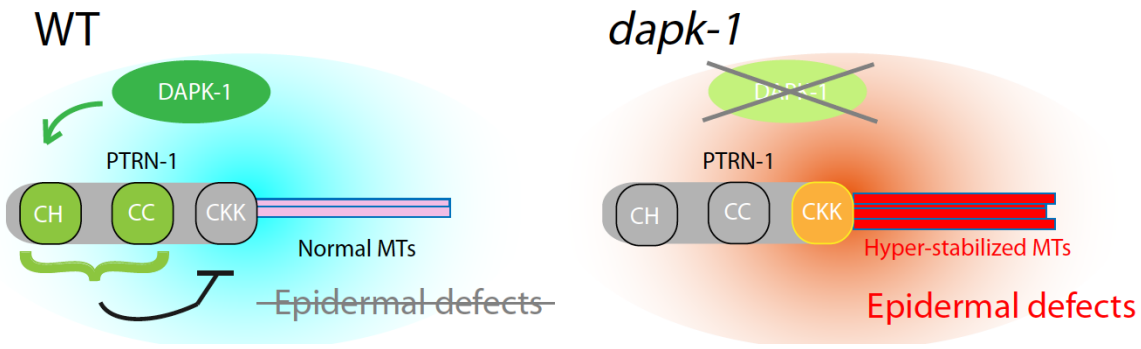

Figure 4.15. Model for DAPK-1-mediated regulation of epidermal MTs via PTRN-1

See Discussion for details.

Table 4.1 Suppressors and enhancers of *dapk-1* morphological defects

Gene	Alleles and sequence change	Mammalian orthologs
A. Suppressors (forward screen)		
ptrn-1	*ju698*	CAMSAP/Patronin
	**lt1*	
	tm5597	
dhc-1	*ju697,*	Dynein heavy chain
	**or195*ts	
dapk-1	*ju1143*	(intragenic)
	ju1145	
B. Suppressors (candidates)		
unc-116	*e2310*	Kinesin-1
sma-1	*e30*	Beta-heavy spectrin
C. Enhancers		
klp-7	*tm2143*	Kinesin-13
mei-1	*or642ts*	p60 katanin
spas-1	*tm683*	Spastin
cat-4	*tm773*	GTP cyclohydrolase I
F47G4.5	*ok2667*	P80 katanin
D. No interaction		
ebp-1	*tm1357*	Plus-end binding protein
ebp-2	*gk756*	Plus-end binding protein
ccpp-1	*ok1821*	Cytosolic Carboxypeptidase
ccpp-6	*ok382*	Cytosolic Carboxypeptidase
mcrs-1	*tm3681*	Microspherule Protein 1
efa-6	*tm3124*	EFA6
ttll-5	*tm3360*	Tubulin tyrosine ligase-like
ttll-11	*tm4059*	Tubulin tyrosine ligase-like
ttll-12	*tm4957*	Tubulin tyrosine ligase-like
unc-70	*e524*	β-Spectrin
dylt-2	*gk762*	Dynein light chain
dnc-1	*or404*ts	p150 dynactin
nud-1	*ok552*	NDE1/NDEL1
nud-2	*ok949*	NDE1/NDEL1
unc-14	*e57*	kinesin-1 adaptor
tbg-1	*t1465*	γ-tubulin
ptl-1	*ok621*	tau
pinn-1	*tm2235*	Pin1
par-1	*zu310*ts	MARK

Suppressors indicated * were tested for suppression of *dapk-1(ju4)* and *dapk-1(gk219)*. Enhancers were tested with *dapk-1(gk219)*. Genes in section D were mostly tested for interaction with *dapk-1(ju4)*. *dapk-1 tbg-1* double mutants were extremely sick, and a stable strain could not be obtained; n > 100 animals scored per genotype.

Table 4.2 PTRN-1 structure-function analysis

	Localization			Function		
Protein Fragment	**Puncta**	**Thick filaments**	**Thin filaments**	**Restore Mor**	**Induce Mor**	**Co-loc with MTs**
Full length	x	x	x	yes	no	yes
CH	-	-	-	no	no	no
CC	x	-	-	no	no	yes
CKK	-	-	x	yes	yes	yes
ΔCKK	x	-	-	no	no	yes
ΔCH	x	x	-	yes	no	ND
ΔCC	-	-	x	yes	no	ND
ΔCHCC1	?	x	-	ND	no	ND
ΔCHCC1CC2	-	-	x	ND	slightly	ND
ΔCC2	?	x*	x	ND	no	ND
ΔCC3	x	-	-	ND	no	ND

Notes: *: Thick filaments present, but fewer compared to PTRN-1 full length or ΔCH. ?: unclear. ND: Not Determined.

Table 4.3 DAPK-1 structure-function analysis

Protein Fragment	**Puncta?**	**Motile?**	**Rescues Mor***	**Induces Mor****	**Enhances Mor*****	**Lethal in *dapk-1(ju4)***
Full Length	yes	yes	yes	no	no	no
Δ Kinase	yes	yes	no	no	yes	yes
Δ Kinase +CaM Bind Domain (BD)	yes	yes	no	no	yes	yes
Δ Cytoskeletal BD	no	no	no	no	no	no
Δ Death Domain + C terminus	no	no	no	no	no	no
Kinase only	some	no	no	no	ND	ND
CaM BD only	no	no	no	no	ND	ND
Ankyrin Domain only	some	no	no	no	no	no
Cytoskeletal BD only	some	no	no	no	no	no
Mid+DD+Ct	no	no	no	no	no	no
S179L *dapk-1(ju4)*	yes	yes	no	yes	yes	yes
K57A (kinase dead)	yes	yes	no	no	no	no

Notes: *: In *dapk-1(ju4)*. **: In WT background. ***: In *dapk-1(ju469)*.

Table 4.4 Dynamics parameters in the epidermis

Type of Dynamics	**Transgene**	**Velocity (mean ± SEM) µm s^{-1}**		**Directionality**	
		Lateral	Dorso-ventral	Lateral	Dorso-ventral
MT plus-end growth	P*col-19*-EBP-2::GFP	0.30 ± 0.00	0.22 ± 0.007	A→P P→A	Lat→DV DV→Lat
Early endosome transport	P*dpy-7*-GFP::RAB-5	0.96 ± 0.014	0.93 ± 0.014	A→P P→A	Lat→DV DV→Lat
DAPK-1	P*dpy-7*-GFP::DAPK-1	1.33 ± 0.028	0.96 ± 0.021	A→P P→A	Lat→DV
DAPK-1	P*col-19*-GFP::DAPK-1	1.26 ± 0.02	0.90 ± 0.017	A→P P→A	Lat→DV

Notes: A→P: Anterior to Posterior. P→A: Vice versa. Lat→DV: Lateral to dorsoventral epidermis. DV→Lat: *vice versa*.

Table 4.5 New strains and genotypes

Strain	DNA construct/allele descript	New Transgene/ allele	Genetic background
CZ15506			*dapk-1(ju4); ptrn-1(ju698)*
CZ17509			*dapk-1(ju4); ptrn-1(lt1)*
CZ18000			*dapk-1(ju4); PTRN-1::mcherry (ltSi183); ptrn-1(ju698)*
CZ18102			*ptrn-1(ju698)*
CZ15505			*dapk-1(ju4) dhc-1(ju697)*
CZ18060			*dapk-1(ju4) dhc-1(or195)*
CZ19321			*dapk-1(ju4) dhc-1(or195); orIs17*
CZ23031			*dapk-1(gk219) dhc-1(or195)*
CZ18570			*dapk-1(gk219) ptrn-1(lt1)*
CZ18444			*dapk-1(ju4); klp-7(tm2143)*
CZ18445			*dapk-1(ju4); klp-7(tm2143); ptrn-1(ju698)*
CZ18920			*dapk-1(gk219); klp-7(tm2143)*
CZ19322			*dapk-1(ju4) dhc-1(ju697); orIs17*
CZ21884			*dapk-1(ju4); unc-116(e2310)*
CZ21866			*dapk-1(gk219); unc-116(e2310)*
CZ21889			*dapk-1(ju4); dhc-1(ju697); klp-7(tm2143)*
CZ18563			*dapk-1(ju4); dylt-2 (gk762)*
CZ20536			*dapk-1(ju4); dnc-1(or404)*
CZ18569			*dapk-1(ju4); efa-6 (tm3124)*
CZ18832			*dapk-1(ju4); mcrs-1(tm3861)*
CZ18829			*dapk-1(ju4); ttll-5(tm3360)*
CZ19320			*dapk-1(ju4); unc-14 (e57)*
CZ20542			*dapk-1(ju4) ; unc-70(e524)*
CZ19908			*dapk-1(gk219); mei-1(or642)*
CZ21860			*dapk-1(gk219); spas-1(tm683)*
CZ21861			*dapk-1(gk219); sma-1(e30)*
CZ21862			*dapk-1(gk219); ebp-2(gk756)*
CZ21863			*dapk-1(gk219); F47G4.5(ok2667)*
CZ21864			*dapk-1(gk219); unc-51(ky347)*
CZ21865			*dapk-1(gk219); efa-6(tm3124)*
CZ20883			*dapk-1(ju4); ebp-1(tm1357)*
CZ21189			*dapk-1(ju4); ebp-2(gk756)*
CZ21881			*dapk-1(ju4); sma-1(e30)*
CZ21883			*dapk-1(ju4); unc-51 (ky347)*

Table 4.5 New strains and genotypes, continued

CZ24640	*dapk-1(23402 bp deletion, 682 bp upstream of gene, 143 bp downstream of gene)*	*ju1936*	
CZ24641	*dapk-1(22922 bp deletion, 205bp up, 140bp down)*	*ju1937*	
CZ24642	*dapk-1 (22920 bp deletion, 202 bp up, 141 bp down)*	*ju1938*	
CZ20165	*dapk-1(C/T Q608*)*	*ju1143*	*dapk-1(ju4) o/c1*
CZ20166	*dapk-1(C/T R48*)*	*ju1145*	*dapk-1(ju4) o/c1*
CZ19770	*unc-33(G/A E527K)*	*ju1149*	*dapk-1(ju4) o/c2*
CZ19878			*frIs7; ptrn-1(lt1)*
CZ19905			*dapk-1(ju4) dhc-1(or195); fris7*
CZ19907			*dapk-1(ju4) dhc-1(ju697); fris7*
CZ20171			*dhc-1(or195); fris7*
CZ17965			*frIs7; ptrn-1(tm5597)*
CZ17999			*dapk-1(ju4); frIs7; ptrn-1(tm5597)*
CZ17964			*dapk-1(ju4); frIs7; ptrn-1(ju698)*
CZ21890			*dapk-1(ju4); klp-7 (tm2143); frIs7; ju698*
CZ20170			*klp-7(tm2143); fris7*
CZ21874			*unc-116 (e2310); frIs7*
CZ21886			*dapk-1(ju4); unc-116 (e2310); frIs7*
CZ21878			*frIs7; sma-1 (e30)*
CZ21885			*dapk-1(ju4); frIs7; sma-1 (e30)*
CZ24105			*dhc-1(or195); frIs7; ptrn-1(lt1)*
CZ23253			*dapk-1(ju4) dhc-1(or195); frIs7; ptrn-1(lt1)*
CZ24124	[P*dpy-7*-mKate2-PTRN-1]	*juEx7387*	*frIs7; ptrn-1(lt1)*
CZ24122	[P*dpy-7*-mKate2-PTRN(CKK)]	*juEx7385*	*frIs7; ptrn-1(lt1)*
CZ21897			*Pdpy-7-GFP-tbb-2 (ltSi570) dapk-1(ju4); ptrn-1(lt1)*
CZ21894			*dapk-1(ju4) ltSi570*
CZ22742			*ltSi570; cat-4(tm773)*
CZ18919			*Pcol-19-GFP-moesin (juIs352); ptrn-1(lt1)*
CZ18921			*juIs352 dapk-1(ju4); ptrn-1(lt1)*
CZ19904	[P*dpy-7*-PTRN-1::GFP]	*juEx6036*	*dapk-1(ju4); ptrn-1(lt1)*
CZ22136	[P*dpy-7*-GFP::PTRN-1]	*juEx6697*	*ptrn-1(lt1)*

Table 4.5 New strains and genotypes, continued

CZ22725		*juEx6697*	*dapk-1(ju4)*
CZ22726		*juEx6697*	*dapk-1(ju4); ptrn-1(lt1)*
CZ22134	[P*dpy-7*-GFP::CKK]	*juEx6695*	*ptrn-1(lt1)*
CZ22160		*juEx6695*	WT
CZ22161		*juEx6695*	*ptrn-1(ju698)*
CZ22162		*juEx6695*	*ptrn-1(tm5597)*
CZ22138	[Pdpy-7-GFP::PTRN-1(ΔCKK)]	*juEx6699*	*ptrn-1(lt1)*
CZ19383	[P*dpy-7*-GFP::PTRN-1(CKK)]	*juEx5853*	*dapk-1(ju4); ptrn-1(lt1)*
CZ22147	[P*dpy-7*-GFP::PTRN-1(CH)]	*juEx6704*	*dapk-1(ju4); ptrn-1(lt1)*
CZ22146	[P*dpy-7*-GFP::PTRN-1(CC)]	*juEx6703*	*dapk-1(ju4); ptrn-1(lt1)*
CZ23024		*juEx6699*	*dapk-1(ju4); ptrn-1(lt1); juEx6826*
CZ22257	[P*dpy-7*-GFP::ΔCH]	*juEx6736*	*ptrn-1(lt1)*
CZ22273	[Pdpy-7-GFP::PTRN-1(ΔCHCC1)]	*juEx6752*	*ptrn-1(lt1)*
CZ22276	[P*dpy-7*-GFP::PTRN-1(ΔCHCC1CC2longer)]	*juEx6755*	*ptrn-1(lt1)*
CZ22277	[P*dpy-7*-GFP::PTRN-1(ΔCHCC1CC2)]	*juEx6756*	*ptrn-1(lt1)*
CZ22280	[P*col-19*-GFP-PTRN-1(CKK)]	*juEx6759*	*ptrn-1(lt1)*
CZ22465	[P*dpy-7*-GFP::PTRN-1(ΔCC2)	*juEx6817*	*ptrn-1(lt1)*
CZ22466	[P*dpy-7*-GFP::PTRN-1(ΔCC3)]	*juEx6818*	*ptrn-1(lt1)*
CZ22467	[P*dpy-7*-GFP::PTRN-1(ΔCC)]	*juEx6819*	*ptrn-1(lt1)*
CZ23030		*juEx6819*	*WT*
CZ22145	[P*dpy-7*-GFP::ΔCC1]	*juEx6702*	*ptrn-1(lt1)*
CZ8985	[P*dpy-7*-GFP::DAPK-1(FL)]	*juEx1774*	*dapk-1(ju4)*
CZ22260	[P*dpy-7*-GFP::DAPK-1(ΔDDΔCt)]	*juEx6739*	
CZ23014		*juEx6739*	*dapk-1(ju4)*
CZ22262	[P*dpy-7*-GFP::DAPK-1(mid+DD+Ct)]	*juEx6742*	
CZ23256		*juEx6742*	*dapk-1(ju469)*
CZ23257		*juEx6742*	*dapk-1(ju4)*
CZ22265	[P*dpy-7*-GFP::DAPK-1(ΔKinase)]	*juEx6744*	
CZ23012		*juEx6744*	*dapk-1(ju469)*
CZ23061		*juEx6744*	*dapk-1(ju4)*
CZ22269	[P*dpy-7*-GFP::DAPK-1(ΔCalmB)]	*juEx6748*	
CZ23011		*juEx6748*	*dapk-1(ju469)*

Table 4.5 New strains and genotypes, continued

Unable to freeze		*juEx6748*	*dapk-1(ju4)*
CZ22476	[P*dpy-7*-GFP::DAPK-1(CalmB only)]	*juEx6828*	
CZ22267	[Pdpy-7-GFP::DAPK-1(ΔcytoskB)]	*juEx6746*	
CZ23013		*juEx6746*	*dapk-1(ju4)*
CZ22723	[P*dpy-7*-GFP::DAPK-1(cytoskB)]	*juEx6924*	
CZ23254		*juEx6924*	*dapk-1(ju469)*
CZ23255		*juEx6924*	*dapk-1(ju4)*
CZ22482	[P*dpy-7*-GFP::DAPK-1(ANK only)]	*juEx6834*	
CZ22717	[*Pdpy-7*-GFP::DAPK-1(Kinase only)]	*juEx6918*	
CZ23019	[P*dpy-7*-GFP::DAPK-1(K57A)]	*juEx7011*	
CZ23025		*juEx7011*	*dapk-1(ju4)*
CZ23022	[P*dpy-7*-GFP::DAPK-1(S179L)]	*juEx7013*	
CZ16503	[P*col-19*-GFP::DAPK-1]	*juEx4781*	*WT*
CZ22123		*juEx4781*	*dhc-1(or195)*
CZ17886		*juEx4781*	*dapk-1(ju4)*
CZ18915		*juEx4781*	*ptrn-1(lt1)*
CZ22727		*juEx4781*	*cat-4(tm773)*
CZ22291		*juEx4781*	*unc-116(e2310)*
CZ9336	[P*dpy-7*-GFP::RAB-5]	*juEx1921*	WT
CZ21789	[P*col-19*-GFP::TBB-2]	*juSi239*	
CZ23247		*juSi239*	*dapk-1(ju4) ptrn-1(lt1)*
CZ23248		*juSi239*	*dapk-1(ju4)*
CZ23249		*juSi239*	*ptrn-1(lt1)*
CZ24779		*juSi239*	*dapk-1(gk219)*
CZ24778		*juSi239*	*dapk-1(gk219) ptrn-1(lt1)*
CZ23018	[P*dpy-7*-PTRN-1::GFP]	*ltSi541*	*dapk-1(ju4); ptrn-1(lt1)*
CZ22739	[P*dpy-7*-mKate2::PTRN-1]	*juEx6820*	*ltSi570; ptrn-1(lt1)*
CZ23015	[P*dpy-7*-mKate2::PTRN-1(CKK)]	*juEx6826*	*ltSi570; ptrn-1(lt1)*
CZ22736	[P*dpy-7*-mKate2::PTRN-1(CC)	*juEx6822*	*ltSi570*
CZ14453	[P*col-19*-EBP-2::GFP]	*juEx3762*	*WT*
CZ18902		*juEx3762*	*ptrn-1(lt1)*
CZ18903		*juEx3762*	*dapk-1(ju4)*
CZ24151		*juEx3762*	*dapk-1(ju4); ptrn-1(lt1)*

Table 4.6 New plasmids

Name	Plasmid #	Construction
P*dpy-7*-GFP::PTRN-1	pCZGY2467	LR recombination with pCZGY2409 (PTRN-1 +stop pCR8) and pCZGY2096 (P*dpy-7*-GFP-gw)
P*dpy-7*-PTRN-1	pCZGY2468	LR recombination with pCZGY2409 (PTRN-1 +stop pCR8) and pCZGY146 (P*dpy-7*-gw)
P*dpy-7*-PTRN-1::GFP	pCZGY2469	LR recombination with pCZGY2410 (PTRN-1 -stop pCR8) and pCZGY1598 (P*dpy-7*-gw-GFP)
P*dpy-7*-GFP::PTRN-1(CH)	pCZGY2452	LR recombination with pCZGY2411 (PTRN-1(CH) pCR8) and pCZGY2096 (P*dpy-7*-GFP-gw)
P*dpy-7*-GFP:: PTRN-1(CKK)	pCZGY2453	LR recombination with pCZGY2413 (PTRN-1(CKK) pCR8) and pCZGY2096
P*dpy-7*-GFP::PTRN-1(ΔCH)	pCZGY2454	LR recombination with pCZGY2414 (PTRN-1(ΔCH) pCR8) and pCZGY2096 (P*dpy-7*-GFP-gw)
P*dpy-7*-GFP:: PTRN-1(ΔCKK)	pCZGY2455	LR recombination with pCZGY2415 (PTRN-1(ΔCKK) pCR8) and pCZGY2096 (P*dpy-7*-GFP-gw)
P*dpy-7*-GFP::PTRN-1(CC)	pCZGY2456	LR recombination with pCZGY2412 (PTRN-1(CC) pCR8) and pCZGY2096 (P*dpy-7*-GFP-gw). aa301-969.
P*dpy-7*-GFP::PTRN-1(ΔCC1)	pCZGY2466	LR recombination with pCZGY2442 (PTRN-1(ΔCC1)) and pCZGY2096 (P*dpy-7*-GFP-gw). Delete aa 402-452.
P*dpy-7*-GFP::PTRN-1(ΔCHCC1)	pCZGY2778	Gibson Cloning. Template: pCZGY246. Delete aa 1-452.
P*dpy-7*-GFP::PTRN-1(ΔCHCC1CC2longer)	pCZGY2779	Gibson Cloning. Template: pCZGY246. Delete aa 1-615.
P*dpy-7*-GFP::PTRN-1(ΔCHCC1CC2)	pCZGY2780	Gibson Cloning. Template: pCZGY246. Delete aa 1-777.
P*dpy-7*-GFP::PTRN-1(ΔCC2)	pCZGY2781	Gibson Cloning. Template: pCZGY246. Delete aa 473-615.
P*dpy-7*-GFP::PTRN-1(ΔCC3)	pCZGY2782	Gibson Cloning. Template: pCZGY246. Delete aa 786-969.
P*dpy-7*-GFP::PTRN-1(ΔCC)	pCZGY2783	Gibson Cloning. Template: pCZGY246. Delete aa 301-947.
P*col-19*-GFP::PTRN-1(CKK)	pCZGY2448	LR recombination with pCZGY2413 (PTRN-1(CKK) pCR8) and pCZGY2097 (P*col-19*-GFP-gw)
DAPK-1(ΔDDΔCt)pCR8	pCZGY2784	Gibson Cloning. Template: pCZGY440 (DAPK-1 pCR8). Delete aa 1300-1426.
DAPK-1(mid+DD+Ct) pCR8	pCZGY2785	Gibson Cloning. Template: pCZGY440 (DAPK-1 pCR8). aa 845-1426.
DAPK-1(ΔKinase) pCR8	pCZGY2786	Gibson Cloning. Template: pCZGY440 (DAPK-1 pCR8). Delete aa 1-275

Table 4.6 New plasmids, continued

DAPK-1(ΔcytoskB) pCR8	pCZGY2787	Gibson Cloning. Template: pCZGY440 (DAPK-1 pCR8). Delete aa 649-844.
DAPK-1(ΔCalmB)] pCR8	pCZGY2788	Gibson Cloning. Template: pCZGY440 (DAPK-1 pCR8). Delete aa 288-320.
DAPK-1(Kin+CalmB) pCR8	pCZGY2789	Gibson Cloning. Template: pCZGY440 (DAPK-1 pCR8). aa 1-320.
DAPK-1(ANK only) pCR8	pCZGY2790	Gibson Cloning. Template: pCZGY440 (DAPK-1 pCR8). aa 373-637.
DAPK-1(cytoskB) pCR8	pCZGY2791	Gibson Cloning. Template: pCZGY440 (DAPK-1 pCR8). aa 649-844.
DAPK-1(Kinase only) pCR8	pCZGY2792	Gibson Cloning. Template: pCZGY440 (DAPK-1 pCR8). aa 1-275.
P*dpy-7*-GFP-DAPK-1(ΔDDΔCt)	pCZGY2793	LR recombination with pCZGY2784 (DAPK-1(ΔDDΔCt) pCR8) and pCZGY2096 (P*dpy-7*-GFP-gw)
P*dpy-7*-GFP-DAPK-1(mid+DD+Ct)	pCZGY2794	LR recombination with pCZGY2785 (DAPK-1(mid+DD+Ct pCR8) and pCZGY2096 (P*dpy-7*-GFP-gw)
P*dpy-7*-GFP-DAPK-1(ΔKinase)	pCZGY2795	LR recombination with pCZGY2786 (DAPK-1(Δkinase pCR8) and pCZGY2096 (P*dpy-7*-GFP-gw)
P*dpy-7*-GFP-DAPK-1(ΔcytoskB)	pCZGY2796	LR recombination with pCZGY2787 (DAPK-1(ΔcytoskB) pCR8) and pCZGY2096 (P*dpy-7*-GFP-gw)
P*dpy-7*-GFP-DAPK-1(ΔCaMBD)	pCZGY2797	LR recombination with pCZGY2788 (DAPK-1(ΔCaMBD) pCR8) and pCZGY2096 (P*dpy-7*-GFP-gw)
P*dpy-7*-GFP-DAPK-1(Kin+CaMBD)	pCZGY2798	LR recombination with pCZGY2789 (DAPK-1(Kin+CaMBD pCR8) and pCZGY2096 (P*dpy-7*-GFP-gw)
P*dpy-7*-GFP-DAPK-1(ANK only)	pCZGY2799	LR recombination with pCZGY2790 (DAPK-1(ANK pCR8) and pCZGY2096 (P*dpy-7*-GFP-gw)
P*dpy-7*-GFP-DAPK-1(cytoskB)	pCZGY2800	LR recombination with pCZGY2791 (DAPK-1(cytoskBD) pCR8) and pCZGY2096 (P*dpy-7*-GFP-gw)
P*dpy-7*-GFP-DAPK-1(Kinase only)	pCZGY2801	LR recombination with pCZGY2792 (DAPK-1(kinase) pCR8) and pCZGY2096 (P*dpy-7*-GFP-gw)
P*dpy-7*-GFP::DAPK-1(K57A)	pCZGY2802	Gibson cloning. Template: pCZGY501 (P*dpy-7*-GFP-DAPK-1).
P*dpy-7*-GFP::DAPK-1(S179L)	pCZGY2803	LR recombination with (DAPK-1(S179L) pCR8) and pCZGY2096 (P*dpy-7*-GFP-gw)
P*dpy-7*-mKate2::PTRN-1	pCZGY2804	Gibson Cloning. Template: pCZGY246.
P*dpy-7*-mKate2::PTRN-1(CC)	pCZGY2805	Gibson Cloning. Template: pCZGY246.

Table 4.6 New plasmids, continued

P*dpy-7*-mKate2::PTRN-1(CKK)	pCZGY2806	Gibson Cloning. Template: pCZGY246.
PCMV-Flag-DAPK-1	pCZGY3111	LR reaction with pCZGY440 (DAPK-1 cDNA pCR8) and pCZGY57 (PCMV-Flag-gw).
PCMV-HA-PTRN-1	pCZGY3112	LR reaction with pCZGY2409 (PTRN-1 cDNA pCR8) and pCZGY58 (PCMV-HA-gw).

4.7 References

Akhmanova, A., and Hoogenraad, C.C. (2015). Microtubule minus-end-targeting proteins. Current biology : CB *25*, R162-171.

Baines, A.J., Bignone, P.A., King, M.D., Maggs, A.M., Bennett, P.M., Pinder, J.C., and Phillips, G.W. (2009). The CKK domain (DUF1781) binds microtubules and defines the CAMSAP/ssp4 family of animal proteins. Mol Biol Evol *26*, 2005-2014.

Bialik, S., and Kimchi, A. (2006). The death-associated protein kinases: structure, function, and beyond. Annu Rev Biochem *75*, 189-210.

Boudaoud, A., Burian, A., Borowska-Wykret, D., Uyttewaal, M., Wrzalik, R., Kwiatkowska, D., and Hamant, O. (2014). FibrilTool, an ImageJ plug-in to quantify fibrillar structures in raw microscopy images. Nat Protoc *9*, 457-463.

Chakilam, S., Gandesiri, M., Rau, T.T., Agaimy, A., Vijayalakshmi, M., Ivanovska, J., Wirtz, R.M., Schulze-Luehrmann, J., Benderska, N., Wittkopf, N.,Chellappan, A., Ruemmele, P., Vieth, M., Rave-Frank, M., Christiansen, H., Hartmann, A., Neufert, C., Atreya, R., Becker, C., Steinberg, P., Schneider-Stock, R. (2013). Death-associated protein kinase controls STAT3 activity in intestinal epithelial cells. Am J Pathol *182*, 1005-1020.

Chuang, M., Goncharov, A., Wang, S., Oegema, K., Jin, Y., and Chisholm, A.D. (2014). The microtubule minus-end-binding protein patronin/PTRN-1 is required for axon regeneration in *C. elegans*. Cell Rep *9*, 874-883.

Chuang, Y.T., Fang, L.W., Lin-Feng, M.H., Chen, R.H., and Lai, M.Z. (2008). The tumor suppressor death-associated protein kinase targets to TCR-stimulated NF-kappa B activation. J Immunol *180*, 3238-3249.

Chuang, Y.T., Lin, Y.C., Lin, K.H., Chou, T.F., Kuo, W.C., Yang, K.T., Wu, P.R., Chen, R.H., Kimchi, A., and Lai, M.Z. (2010). Tumor suppressor death-associated protein kinase is required for full IL-1beta production. Blood *117*, 960-970.

Cohen, O., Feinstein, E., and Kimchi, A. (1997). DAP-kinase is a Ca2+/calmodulin-dependent, cytoskeletal-associated protein kinase, with cell death-inducing functions that depend on its catalytic activity. EMBO J *16*, 998-1008.

Cohen, O., Inbal, B., Kissil, J.L., Raveh, T., Berissi, H., Spivak-Kroizaman, T., Feinstein, E., and Kimchi, A. (1999). DAP-kinase participates in TNF-alpha- and Fas-induced apoptosis and its function requires the death domain. The Journal of cell biology *146*, 141-148.

Couillault, C., Pujol, N., Reboul, J., Sabatier, L., Guichou, J.F., Kohara, Y., and Ewbank, J.J. (2004). TLR-independent control of innate immunity in Caenorhabditis elegans by the TIR domain adaptor protein TIR-1, an ortholog of human SARM. Nat Immunol *5*, 488-494.

Del Rosario, J.S., Feldmann, K.G., Ahmed, T., Amjad, U., Ko, B., An, J., Mahmud, T., Salama, M., Mei, S., Asemota, D., Mano, I. (2015). Death Associated Protein Kinase (DAPK) -mediated neurodegenerative mechanisms in nematode excitotoxicity. BMC Neurosci *16*, 25.

Dierking, K., Polanowska, J., Omi, S., Engelmann, I., Gut, M., Lembo, F., Ewbank, J.J., and Pujol, N. (2011). Unusual regulation of a STAT protein by an SLC6 family transporter in C. elegans epidermal innate immunity. Cell Host Microbe *9*, 425-435.

Engelmann, I., and Pujol, N. (2010). Innate immunity in *C. elegans*. Adv Exp Med Biol *708*, 105-121.

Gonczy, P., Pichler, S., Kirkham, M., and Hyman, A.A. (1999). Cytoplasmic dynein is required for distinct aspects of MTOC positioning, including centrosome separation, in the one cell stage *Caenorhabditis elegans* embryo. The Journal of cell biology *147*, 135-150.

Goodwin, S.S., and Vale, R.D. (2010). Patronin regulates the microtubule network by protecting microtubule minus ends. Cell *143*, 263-274.

Jiang, K., Hua, S., Mohan, R., Grigoriev, I., Yau, K.W., Liu, Q., Katrukha, E.A., Altelaar, A.F., Heck, A.J., Hoogenraad, C.C., Akhmanova, A. (2014). Microtubule minus-end stabilization by polymerization-driven CAMSAP deposition. Dev Cell *28*, 295-309.

Kang, C., and Avery, L. (2009). Death-associated protein kinase (DAPK) and signal transduction: fine-tuning of autophagy in *Caenorhabditis elegans* homeostasis. FEBS J *277*, 66-73.

Kim, B.M., You, M.H., Chen, C.H., Lee, S., Hong, Y., Kimchi, A., Zhou, X.Z., and Lee, T.H. (2014). Death-associated protein kinase 1 has a critical role in aberrant tau protein regulation and function. Cell Death Dis *5*, e1237.

Kim, E., Sun, L., Gabel, C.V., and Fang-Yen, C. (2013). Long-term imaging of *Caenorhabditis elegans* using nanoparticle-mediated immobilization. PLoS One *8*, e53419.

Lin, Y., Stevens, C., and Hupp, T. (2007). Identification of a dominant negative functional domain on DAPK-1 that degrades DAPK-1 protein and stimulates TNFR-1-mediated apoptosis. J Biol Chem *282*, 16792-16802.

Loer, C.M., Calvo, A.C., Watschinger, K., Werner-Felmayer, G., O'Rourke, D., Stroud, D., Tong, A., Gotenstein, J.R., Chisholm, A.D., Hodgkin, J., Werner, E.R., Martinez, A.

(2015). Cuticle integrity and biogenic amine synthesis in *Caenorhabditis elegans* require the cofactor tetrahydrobiopterin (BH4). Genetics *200*, 237-253.

Mukhopadhyay, R., Ray, P.S., Arif, A., Brady, A.K., Kinter, M., and Fox, P.L. (2008). DAPK-ZIPK-L13a axis constitutes a negative-feedback module regulating inflammatory gene expression. Mol Cell *32*, 371-382.

Priess, J.R., and Hirsh, D.I. (1986). *Caenorhabditis elegans* morphogenesis: the role of the cytoskeleton in elongation of the embryo. Developmental biology *117*, 156-173.

Pujol, N., Cypowyj, S., Ziegler, K., Millet, A., Astrain, A., Goncharov, A., Jin, Y., Chisholm, A.D., and Ewbank, J.J. (2008). Distinct innate immune responses to infection and wounding in the *C. elegans* epidermis. Current biology : CB *18*, 481-489.

Quintin, S., Wang, S., Pontabry, J., Bender, A., Robin, F., Hyenne, V., Landmann, F., Gally, C., Oegema, K., and Labouesse, M. (2016). Non-centrosomal epidermal microtubules act in parallel to LET-502/ROCK to promote *C. elegans* elongation. Development *143*, 160-173.

Richardson, C.E., Spilker, K.A., Cueva, J.G., Perrino, J., Goodman, M.B., and Shen, K. (2014). PTRN-1, a microtubule minus end-binding CAMSAP homolog, promotes microtubule function in *Caenorhabditis elegans* neurons. Elife *3*, e01498.

Shiloh, R., Bialik, S., and Kimchi, A. (2013). The DAPK family: a structure-function analysis. Apoptosis *19*, 286-297.

Starr, D.A. (2011). Watching nuclei move: Insights into how kinesin-1 and dynein function together. Bioarchitecture *1*, 9-13.

Tong, A., Lynn, G., Ngo, V., Wong, D., Moseley, S.L., Ewbank, J.J., Goncharov, A., Wu, Y.C., Pujol, N., and Chisholm, A.D. (2009). Negative regulation of Caenorhabditis elegans epidermal damage responses by death-associated protein kinase. Proc Natl Acad Sci U S A *106*, 1457-1461.

Tu, W., Xu, X., Peng, L., Zhong, X., Zhang, W., Soundarapandian, M.M., Balel, C., Wang, M., Jia, N., Lew, F., Chan, S. L., Chen, Y., Lu, Y. (2010). DAPK1 interaction with NMDA receptor NR2B subunits mediates brain damage in stroke. Cell *140*, 222-234.

Wang, S., Wu, D., Quintin, S., Green, R.A., Cheerambathur, D.K., Ochoa, S.D., Desai, A., and Oegema, K. (2015). NOCA-1 functions with gamma-tubulin and in parallel to Patronin to assemble non-centrosomal microtubule arrays in C. elegans. Elife *4*, e08649.

Wu, P.R., Tsai, P.I., Chen, G.C., Chou, H.J., Huang, Y.P., Chen, Y.H., Lin, M.Y., Kimchi, A., Chien, C.T., and Chen, R.H. (2011). DAPK activates MARK1/2 to regulate

microtubule assembly, neuronal differentiation, and tau toxicity. Cell Death Differ *18*, 1507-1520.

Xu, S., and Chisholm, A.D. (2011). A Galphaq-Ca(2)(+) signaling pathway promotes actin-mediated epidermal wound closure in C. elegans. Current biology : CB *21*, 1960-1967.

Zhang, J., Hu, M.M., Shu, H.B., and Li, S. (2014). Death-associated protein kinase 1 is an IRF3/7-interacting protein that is involved in the cellular antiviral immune response. Cell Mol Immunol *11*, 245-252.

Zhang, Y., Li, W., Li, L., Li, Y., Fu, R., Zhu, Y., Li, J., Zhou, Y., Xiong, S., and Zhang, H. (2015). Structural damage in the *C. elegans* epidermis causes release of STA-2 and induction of an innate immune response. Immunity *42*, 309-320.

Chapter 5

Conclusions and Discussion

The majority of MTs in differentiated polarized cells are non-centrosomal; what these MTs do during and after the development of these mature, non-mitotic cells, and how these MTs are regulated, are large questions currently being addressed in the MT field. The work presented in this dissertation addresses a critical issue: what regulates the changes that occur to the non-centrosomal MT arrays when these mature cells, or the tissue that they compose of, encounter stress and physical damage? Here we focus on the minus end-binding protein CAMSAPs to understand non-centrosomal MT regulation in the *C. elegans* epidermis and neurons. Specifically, we study axon regeneration after laser axotomy, and the constitutively active wound response mutant *dapk-1* as in vivo models of tissue repair. Although our study does not definitively show that PTRN-1 is regulating specifically the non-centrosomal MTs, considering that CAMSAPs have been shown to bind to and regulate non-centrosomal MTs dynamics and architecture in various tissues and organisms (Jiang et al., 2014; Meng et al., 2008; Tanaka et al., 2012; Toya et al., 2016; Yau et al., 2014), our work very likely reveals the roles of non-centrosomal MTs in these tissues upon injury.

5.1 PTRN-1 and axon regeneration

A major question about axonal MTs, both in uninjured and regenerating axons, is what regulates the minus ends of these MTs? We indirectly answer this question by studying PTRN-1, the *C. elegans* member of the known minus end-binding protein CAMSAP family. In Chapter 3, I show that PTRN-1 is required for axon regeneration. PTRN-1's normal role is to maintain stable MTs, both in the uninjured and injured axons. The genetics suggests that, like Patronin in fly embryos (Wang et al., 2013), PTRN-1 promotes MT stability by blocking the MT depolymerizing enzyme Kinesin-13 from destabilizing MT ends. Additionally, the CKK domain is necessary and sufficient for PTRN-1 function in both maintaining normal MT dynamics and enabling efficient axonal regrowth.

Loss of CAMSAP2 in primary mouse hippocampal neurons results in severe defects in development, such as decreased dendritic branching and loss of axon specification (Yau et al., 2014). However, *C. elegans* neurons are different from mammalian neurons in that their development is largely unaffected by loss of *ptrn-1* function (Marcette et al., 2014; Richardson et al., 2014). Interestingly though, subjecting *ptrn-1* mutants to a three day treatment of colchicine caused ectopic branching of motor and touch neurons (Richardson et al., 2014). We do not see these phenotypes in *ptrn-1* mutants after laser axotomy, perhaps due to the fact that the physical damage to MTs was acute and local, instead of chronic and global. However, the defects in regrowth from this MT injury assay suggest that PTRN-1 plays an important role in neurons under stress. Whether CAMSAP2 in mammalian neurons plays an even more important role in axonal regrowth compared to its role in development remains to be seen.

5.2 PTRN-1 in epidermal development and wound response

In Chapter 4, the role of PTRN-1 in epidermal development and wound response was investigated. Several lines of evidence suggest PTRN-1 acts under the regulation of Death Associated Protein Kinase DAPK-1 to regulate MT arrays in the epidermis. First, PTRN-1 is required for the formation of epidermal morphology defects in *dapk-1* mutants. Unlike other suppressors, mutations in *ptrn-1* suppressed the wound response phenotypes in *dapk-1* mutants as well as the developmental defects. Even more striking, over-expressing only the CKK domain induced the Mor phenotype constitutively active injury responses, as long as there was no functional full-length PTRN-1 present. The CKK domain likely caused these defects by increasing stable MTs, since chronic taxol treatment induced *dapk-1*-like phenotypes. Furthermore, the CKK domain appears to be negatively regulated by the remaining PTRN-1 domains. Finally, since DAPK-1 is a kinase, and has already been shown to regulate tens of other proteins in various pathways (Bialik and Kimchi, 2014), we hypothesize that DAPK-1 is regulating PTRN-1, directly or indirectly, through the CH and CC domain to inhibit over-activity of the CKK domain.

One alternative hypothesis is that PTRN-1 is not under DAPK-1 regulation; instead, the CKK domain can induce the Mor phenotype in *ptrn-1* mutants because the epidermal MTs in the mutants are more susceptible to hyper-stabilization. Indeed, taxol treatment caused higher incidence of Mor phenotype in these mutants compared to WT. However, over-expression of the CKK domain in the dynein heavy chain/*dhc-1* or *dhc-1 ptrn-1* mutants could not induce Mor defects (not shown), while taxol treatment in *dhc-1* mutants could. More over-expression experiments in other MT mutants may be needed to

show that the CKK domain only induces *dapk1-1*-like defects if *ptrn-1* is lost, and not in any other mutants with easily hyper-stabilized MTs.

If DAPK-1 indeed is regulating PTRN-1 activity, one likely mechanism of regulation is phosphorylation. Expression of kinase-dead DAPK-1 in *dapk-1* mutants cannot rescue the epidermal defects, suggesting *dapk-1*'s kinase activity is essential for normal function. In vitro kinase assays will need to be performed to see whether DAPK-1 directly phosphorylates PTRN-1. If the results turn out negative, then DAPK-1 may perhaps phosphorylate a factor upstream of PTRN-1, or regulate PTRN-1 through one of its many other protein-protein interaction domains (Shiloh et al., 2014). We show through co-immunoprecipitation that DAPK-1 and PTRN-1 are able to physically interact with each other; testing the interaction between dissected domains may elucidate how DAPK-1 regulates PTRN-1 activity.

Though PTRN-1 is an important player in regulating epidermal morphology in *dapk-1* mutant background, *ptrn-1* mutants themselves do not appear to exhibit any cuticle or epidermal defects (Wang et al., 2015). In fact, the mutants look superficially WT (Marcette et al., 2014; Richardson et al., 2014). By contrast, CAMSAP3 knockout mice displayed growth defects, with 15% of them dying before postnatal day (P) 30 (Toya et al., 2016). Structural defects could also be seen in the small intestine (Toya et al., 2016). This discrepancy in viability and development between the CAMSAPs in the two species may be explained by functional redundancy in *C. elegans*. The ninein/*noca-1* and γ-tubulin/*tbg-1* together work separately from and in parallel with *ptrn-1* to regulate the epidermal MT array, and only double mutants in these two pathways will exhibit leaky cuticles and lethality (Wang et al., 2015). *dapk-1* seems to be suppressed only by

loss of *ptrn-1*, and not by loss of *tbg-1*, suggesting DAPK-1 is regulating MTs through specifically the PTRN-1-controlled pathway. In fact, though many suppressors of the *dapk-1* Mor phenotype was seen, only *ptrn-1* suppressed the innate immune response phenotype, again indicating the specificity of DAPK-1 in regulating PTRN-1.

The study presented here is one of the first reports of CAMSAP being regulated by a kinase to control MT stability. Further work needs to be done to elucidate the mechanism of PTRN-'s regulation by DAPK-1 in the epidermis.

5.3 Comparison between PTRN-1's roles in tissue repair in the neurons and in the epidermis

Though PTRN-1 is dispensible for development in both tissues under normal laboratory conditions, changes in MT architecture and dynamics were still observed in neurons and in the epidermis of *ptrn-1* mutants. Ultrastructural serial reconstruction of the PLM touch neuron revealed that there are fewer MTs in the *ptrn-1* touch neuron axon. Fewer GFP-*tbb-2* filaments were observed in the head epidermis as well. Additionally, EBP-2 analysis in *ptrn-1* mutants show that, although comets in the neurons were increased while in the lateral epidermis comet number remained wild type, the velocity of the comets in both tissues was increased. These results show that, in both the neurons and epidermis, loss of *ptrn-1* leads to fewer MTs and increased MT dynamics, consistent with the role of CAMSAPs in promoting MT stability.

These changes in the non-centrosomal MT arrays are not necessary for non-injured tissues in *C. elegans*. However, once the tissue is damaged, PTRN-1 plays a

critical role in repair. *ptrn-1* mutants exhibit larger actin rings around the wound site compared to WT after sterile needle injury, suggesting they are impaired in epidermal wound repair. The inability to repair is also seen after laser axotomy of the neurons. As loss of *ptrn-1* leads to loss of MT stability, this suggests that stable MTs are needed for injury repair in both tissues. These results fit with the current dogma that stable MTs are needed for axon regeneration; stable MTs are needed for growth cone formation (Bradke et al., 2012)), and the application of MT stabilizing drugs taxol or epithilone B enhances regeneration CNS neurons ((Hellal et al., 2011) (Baas and Ahmad, 2013) (Brunden et al., 2010); (Zhang et al., 2012)). How MTs play a role in *C. elegans* epidermal wound healing will have to be addressed in the future by visualizing MT dynamics after wounding and pharmacological assays. Prior research in the *Xenopus* embryo showed that a balance in MT dynamics is important, with both over-stabilization or destabilization by drug treatment impairing wound closure (Mandato and Bement, 2003). This balance may also be critical for epidermal wound closure in *C. elegans*, and PTRN-1 is required to achieve this balance.

Whether DAPK-1 is regulating PTRN-1 in neurons remains to be seen. If such is the case, the mechanism of PTRN-1 regulation can be further studied through the suppressor screen on the epidermal defects in *dapk-1* mutants. Many other modifiers of *dapk-1* have been discovered so far, and the screen is not saturated by any means. Some of these modifiers may be players in the DAPK-1-PTRN-1 pathway involved in not only epidermal development and wound response, but also in axon regeneration. In this way, further screening and study on the discovered modifiers can, in the future, shed light on

the cytoskeletal regulation and other molecular processes important in epidermal and neuronal tissue repair.

5.4 References

Baas, P.W., and Ahmad, F.J. (2013). Beyond taxol: microtubule-based treatment of disease and injury of the nervous system. Brain *136*, 2937-2951.

Bialik, S., and Kimchi, A. (2014). The DAP-kinase interactome. Apoptosis *19*, 316-328.

Bradke, F., Fawcett, J.W., and Spira, M.E. (2012). Assembly of a new growth cone after axotomy: the precursor to axon regeneration. Nat Rev Neurosci *13*, 183-193.

Brunden, K.R., Zhang, B., Carroll, J., Yao, Y., Potuzak, J.S., Hogan, A.M., Iba, M., James, M.J., Xie, S.X., Ballatore, C., Smith, A. B., 3rd, Lee, V. M., Trojanowski, J. Q. (2010). Epothilone D improves microtubule density, axonal integrity, and cognition in a transgenic mouse model of tauopathy. J Neurosci *30*, 13861-13866.

Hellal, F., Hurtado, A., Ruschel, J., Flynn, K.C., Laskowski, C.J., Umlauf, M., Kapitein, L.C., Strikis, D., Lemmon, V., Bixby, J.,Hoogenraad, C. C., Bradke, F. (2011). Microtubule stabilization reduces scarring and causes axon regeneration after spinal cord injury. Science *331*, 928-931.

Jiang, K., Hua, S., Mohan, R., Grigoriev, I., Yau, K.W., Liu, Q., Katrukha, E.A., Altelaar, A.F., Heck, A.J., Hoogenraad, C.C., Akhmanova, A. (2014). Microtubule minus-end stabilization by polymerization-driven CAMSAP deposition. Dev Cell *28*, 295-309.

Mandato, C.A., and Bement, W.M. (2003). Actomyosin transports microtubules and microtubules control actomyosin recruitment during Xenopus oocyte wound healing. Curr Biol *13*, 1096-1105.

Marcette, J.D., Chen, J.J., and Nonet, M.L. (2014). The Caenorhabditis elegans microtubule minus-end binding homolog PTRN-1 stabilizes synapses and neurites. Elife *3*, e01637.

Meng, W., Mushika, Y., Ichii, T., and Takeichi, M. (2008). Anchorage of microtubule minus ends to adherens junctions regulates epithelial cell-cell contacts. Cell *135*, 948-959.

Richardson, C.E., Spilker, K.A., Cueva, J.G., Perrino, J., Goodman, M.B., and Shen, K. (2014). PTRN-1, a microtubule minus end-binding CAMSAP homolog, promotes microtubule function in Caenorhabditis elegans neurons. Elife *3*, e01498.

Shiloh, R., Bialik, S., and Kimchi, A. (2014). The DAPK family: a structure-function analysis. Apoptosis *19*, 286-297.

Tanaka, N., Meng, W., Nagae, S., and Takeichi, M. (2012). Nezha/CAMSAP3 and CAMSAP2 cooperate in epithelial-specific organization of noncentrosomal microtubules. Proc Natl Acad Sci U S A *109*, 20029-20034.

Toya, M., Kobayashi, S., Kawasaki, M., Shioi, G., Kaneko, M., Ishiuchi, T., Misaki, K., Meng, W., and Takeichi, M. (2016). CAMSAP3 orients the apical-to-basal polarity of microtubule arrays in epithelial cells. Proc Natl Acad Sci U S A *113*, 332-337.

Wang, H., Brust-Mascher, I., Civelekoglu-Scholey, G., and Scholey, J.M. (2013). Patronin mediates a switch from kinesin-13-dependent poleward flux to anaphase B spindle elongation. J Cell Biol *203*, 35-46.

Wang, S., Wu, D., Quintin, S., Green, R.A., Cheerambathur, D.K., Ochoa, S.D., Desai, A., and Oegema, K. (2015). NOCA-1 functions with gamma-tubulin and in parallel to Patronin to assemble non-centrosomal microtubule arrays in C. elegans. Elife *4*, e08649.

Yau, K.W., van Beuningen, S.F., Cunha-Ferreira, I., Cloin, B.M., van Battum, E.Y., Will, L., Schatzle, P., Tas, R.P., van Krugten, J., Katrukha, E.A.,Jiang, K., Wulf, P. S., Mikhaylova, M., Harterink, M., Pasterkamp, R. J., Akhmanova, A., Kapitein, L. C., Hoogenraad, C. C.. (2014). Microtubule minus-end binding protein CAMSAP2 controls axon specification and dendrite development. Neuron *82*, 1058-1073.

Zhang, B., Carroll, J., Trojanowski, J.Q., Yao, Y., Iba, M., Potuzak, J.S., Hogan, A.M., Xie, S.X., Ballatore, C., Smith, A.B., 3rd, Lee, V. M., Brunden, K. R. (2012). The microtubule-stabilizing agent, epothilone D, reduces axonal dysfunction, neurotoxicity, cognitive deficits, and Alzheimer-like pathology in an interventional study with aged tau transgenic mice. J Neurosci *32*, 3601-3611.